Juel-4349

Jülich Center for Hadron Phyics (JCHP)
Institut für Kernphysik (IKP)
COSY

WASA-at-COSY: Hints for a novel resonance

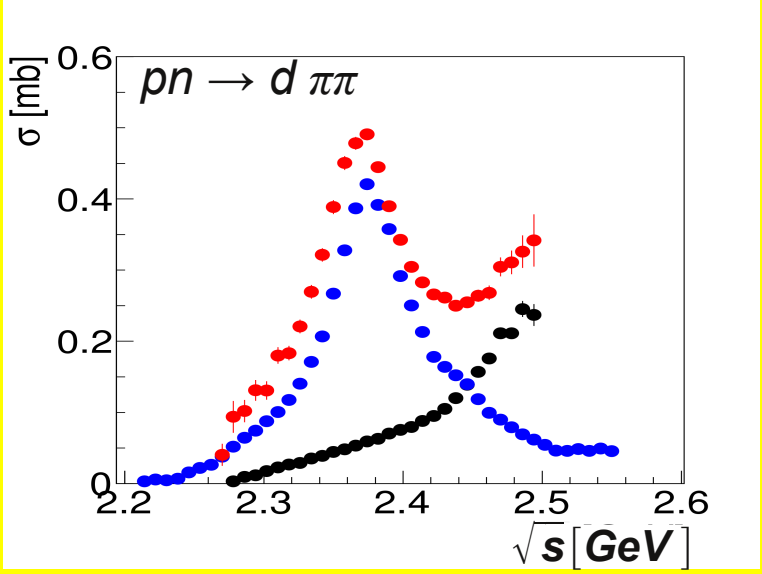

Annual Report 2011

JÜLICH
FORSCHUNGSZENTRUM

Annual Report 2011

Jülich Center for Hadron Physics / Institut für Kernphysik / COSY

Cover picture:
Isospin decomposition of the double-pionic fusion to deuterium, from an experiment by the WASA-at-COSY collaboration. Only the isoscalar component (blue data points) exhibits a resonance-like structure pointing to the existence of a new, unconventional $I = 0$, $J^P = 3^+$ resonance in the two-baryon system. The isovector component is shown by the black data points, whereas the mixed situation is represented by the red data points.

Preface

A main focus of the Institut für Kernphysik (IKP) of Forschungszentrum Jülich (FZJ) is the design and construction of the High Energy Storage Ring (HESR) for the Facility for Antiproton and Ion Reseach (FAIR), which is being built at Helmholtzzentrum für Schwerionenforschung (GSI), Darmstadt. A corresponding contract between the FAIR company and FZJ has been signed in 2011 and 65 M€ have been assigned for this purpose. An international consortium comprising IKP as the leading institution, the Zentralinstitut für Technologie (ZAT) of FZJ, the GSI, the Helmholtzinstitut Mainz (HIM) and the National Institute for R&D in Electrical Engineering (ICPE-CA), Bucharest, will build the HESR in the years up to 2018 and commission it afterwards. IKP is also contributing to the design and construction of the PANDA detector at HESR: after the decision of the PANDA collaboration to use a straw-tube tracker (STT) as the central tracking detector, a cooperation of IKP, Frascati, Pavia and Ferrara (Italy), Cracow (Poland) and Bucharest (Romania) will build the STT and later install it in PANDA. IKP is making essential contributions to the Micro-Vertex-Detector(MVD), as well as conceiving a day-one experiment for PANDA, and is involved in the PANDA pellet target development, together with IHEP (Moscow). In 2011 the Technical Design Reports have been finalized and approved by PANDA to be submitted to FAIR for these three detectors components (MVD, STT, target).

IKP is also pursuing a feasibility study which aims at a search for electric dipole moments (EDM) of charged particles in storage rings. For this purpose, the JEDI-collaboration (Jülich Electric Dipole moment Investigations) has been formed as a study group together with RWTH Aachen, Ferrara (Italy), BNL, Cornell and Indiana (USA), and HEPI-TSU (Georgia) to (i) perform test measurements at COSY (together with colleagues from the BNL-EDM collaboration), (ii) devise a precursor experiment for pEDM and dEDM using COSY, and (iii) design a dedicated EDM storage ring for a high-precision search with a sensitivity up to 10^{-29} e cm.

The cooler and storage ring COSY has been continuously used for hadron physics experiments with three major detector systems (ANKE and WASA inside COSY, TOF at the extracted COSY beam), and in the past year the following highlights have been obtained:

- Evidence for a new isoscalar resonance in double-pionic fusion of a proton and a neutron to deuterium and two neutral pions has been found by the WASA-at-COSY collaboration (see also cover picture). The structure in the excitation function is located about 80 MeV below the $\Delta\Delta$-maximum and has a width of approximately 70 MeV; from differential distributions, quantum numbers $I(J^P) = 0(3^+)$ have been deduced.

- The mass of the η-meson has been determined in the reaction deuteron (beam) plus proton (target) to ^{3}He and the η-meson at the COSY-ANKE spectrometer. The result, $m_\eta = (547.689 \pm 0.007 \pm 0.040)$ MeV/c^2, is in excellent agreement with other recent measurements.

- The transparency ratio for ϕ-meson production in proton-nucleus (C, Cu, Ag, and Au) has been studied by the COSY-ANKE collaboration, first averaged over the accessible ϕ-momentum region, and later also as a function of ϕ-momentum. Indications for a significant momentum dependence and an effective ϕN absorption cross section have been deduced.

- In preparation for the spin-filtering tests with protons at COSY by the PAX collaboration, the COSY accelerator crew has reproducibly achieved beam lifetimes of the order of 8000 seconds.

Highlights from theory include:

- The "Hoyle state", an excitation of ^{12}C, predicted by Fred Hoyle in 1954 as a crucial intermediate state in the astrophysical production of carbon, has been obtained for the first time in an ab-initio lattice calculation based on two- and three-nucleon interactions, which are derived in chiral effective field theory. The spatial structure is consistent with a bent chain of α-particles.
- Bound states moving in a finite periodic volume have been investigated. Due to their spatial extension, they receive an energy correction which is topological in origin and universal in character. The topological volume corrections contain information about the number and mass of the constituents of the bound states. These results have broad applications to lattice calculations involving nucleons, nuclei, hadronic molecules, and cold atoms.
- The slope parameters α and α' of the decay of the η and η' meson, respectively, into two pions and a photon have been shown to be identical, if only the leading term in the expansion in the number of colors is kept. This finding is corroborated by a model independent analysis of the corresponding decays, yielding $\alpha = 1.96 \pm 0.27 \pm 0.02$ GeV^{-1} and $\alpha' = 1.80 \pm 0.49 \pm 0.04$ GeV^{-1}.

Along with the current physics program at COSY a major part of machine operation was scheduled for beam dynamic studies, HESR component tests and FAIR related activities. COSY also contributed its expertise in the context of EU projects and assisted the research of in- and outside users for instance by performing irradiations at the cyclotron and at external detector areas.

A method for precise absolute luminosity determinations based on the energy losses due to the electromagnetic interaction during repeated passages of the beam through a thin target has been developed by IKP-4 and the ANKE collaboration and tested in elastic proton-proton scattering.

The 485. WE-Heraeus Seminar *Search for Electric Dipole Moments at Storage Rings* organized by IKP with Hans Ströher and Frank Rathmann as chairmen brought together the experts in this field to assess the current status of this research field.

At this prominent place, I would like to thank our colleagues in the ZAT, ZEL and JSC and our national and international collaboration partners for their activities and support.

Jülich, April 2012 Rudolf Maier

Contents

1 Physics at COSY 1

2 COSY Operation and Developments .. 17

3 Theoretical Investigations 21

4 Developments for the HESR 27

5 The PANDA Experiment at FAIR 33

6 Further Experimental Activities 39

Appendix

A Councils 43

B Publications 44

C Talks and Colloquia 50

D Diploma and Ph.D. Theses 58

E Awards & Offers for Professorships ... 60

F Funded Projects 61

G JCHP-FFE Projects 62

H Conferences (co-)organized by the IKP 64

I Teaching Positions 66

J Personnel 67

K Further Contributions 70

1 Physics at COSY

1.1 Overview

The cooler synchrotron and storage ring COSY delivers unpolarized and polarized beams of protons and deuterons with momenta up to 3.7 GeV/c for three internal experiments — ANKE, PAX and WASA — and one experiment — TOF — at an external target position. All detection systems are operated by large international collaborations.

- **ANKE** (Apparatus for Studies of Nucleon and Kaon Ejectiles) is a large acceptance forward magnetic spectrometer at an internal target station in the COSY ring. The central dipole is movable to adjust the momenta of the detected particles independent of the beam momentum. Using deuterium cluster targets, reactions on the neutron are tagged by detecting the low-energy recoil proton in silicon strip detectors in vacuum next to the target. In addition, a polarized internal target with a storage cell can be used.
- **PAX** (Polarized Antiproton EXperiment) is the test set-up to investigate spin filtering as a method to produce polarized beams. It uses an atomic beam source, an openable storage cell an a Breit-Rabi polarimeter in a low-β section of COSY.
- **TOF** (Time Of Flight) is a non-magnetic spectrometer combining excellent tracking capabilities with large acceptance and full azimuthal symmetry allowing to measure complete Dalitz plots. TOF is optimized for final states with strangeness. With the new straw tube tracking system (STT), TOF has a significantly improved mass resolution and reconstruction efficiency.
- **WASA** (Wide Angle Shower Apparatus), an internal 4π spectrometer for neutral and charged particles, is operated at the internal COSY beam. WASA comprises an electro-magnetic calorimeter, a very thin superconducting solenoid, inner and forward trigger and tracking detectors, and a frozen-pellet target.

The unique COSY capabilities are also used by the Storage-Ring EDM (srEDM) collaboration to investigate spin-manipulations as preparation to build (a) dedicated storage ring(s) to search for electric dipole moments of light ions (p, d, ^{3}He).

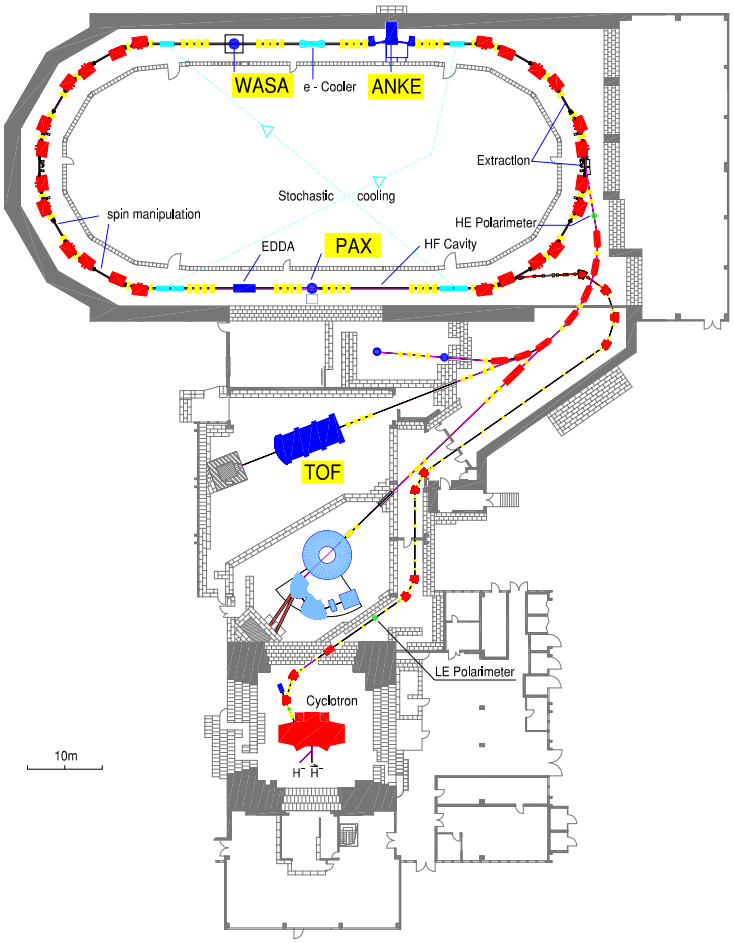

1.2 Major Physics Results at COSY

1.2.1 ABC effect and resonance structure in the basic double-pionic fusion

Two-pion production in nucleon-nucleon collisions gives access to the study of the mutual excitation of two nucleons. Of particular interest is the question, whether this intermediate baryon-baryon system exhibits features, which go beyond those of the individual baryons.

Already more than fifty years ago Abashian, Booth and Crowe observed a peculiar phenomenon in the two-pion production leading to the fusion of p and d to ^{3}He, namely a huge low-mass enhancement in the $\pi\pi$-invariant mass spectrum. Subsequently this phenomenon was found also in other fusion reactions — if associated with the production of an isoscalar pion pair. In lack of any consistent explanation the effect was later-on named ABC effect after the initials of the first authors.

In an effort to study the ABC phenomenon in more detail and the two-pion production process in general a program has been set up to investigate all two-pion production channels in the collision of two nucleons by exclusive and kinematically complete measurements at CELSIUS and COSY by use of the WASA and TOF detector setups. That way the pp-induced, *i.e. isovector* two-pion production has been extensively studied from threshold up to T_p = 1.4 GeV. As a result it was shown that the data are quantitatively understood by t-channel (π- and σ-exchange) nucleon excitation and decay. In the near-threshold region the excitation of the Roper resonance is the leading process. At energies $T_p > 1$ GeV the Roper contributions are fading away and the reaction gets characterized by the mutual excitation of the nucleons into the Δ resonance. This situation provides the unique opportunity to study the intermediate $\Delta\Delta$ system in very detail.

For studying the *isoscalar* two-pion production process the $pn \to d\pi^0\pi^0$ reaction is unique, since it is the only two-pion production channel, which is purely isoscalar. In contrast to the small low-mass enhancement observed in the $M_{\pi^0\pi^0}$ distributions of the $pp \to pp\pi^0\pi^0$ reaction, which is well accounted for by the t-channel $\Delta\Delta$ process, we find a huge low-mass enhancement in the *isoscalar* $pn \to d\pi^0\pi^0$ reaction, *i.e.* the phenomenon known as ABC effect. This enormeous enhancement cannot be accounted by the conventional t-channel $\Delta\Delta$ process. Moreover — as reported previously in *Physical Review Letters* ***106*** *(2011) 202302* as well as in popular scientic journals like *Spektrum der Wissenschaft* and *CERN Courier* — we find this ABC effect to be correlated with a narrow resonance-like structure in the total cross section of the $pn \to d\pi^0\pi^0$ reaction peaking at an energy 80 MeV below the mass of two Δs with a width of only 70 MeV, *i.e.* three to four times smaller than the width expected for the t-channel $\Delta\Delta$ process. From the angular distributions we impose $I(J^P) = 0(3^+)$ for this resonance structure.

In order to pin down the origin of this resonance structure, we started to investigate *all* reaction channels, which this envisaged resonance can decay into. These are the reactions $pn \to d\pi^+\pi^-$, $pn \to pp\pi^0\pi^-$, $pn \to pn\pi^0\pi^0$, $pn \to pn\pi^+\pi^-$, $NN \to NN\pi$ (isoscalar part) and pn scattering. Some of these reactions have still to be measured at WASA, for others data are already available and are being analysed. Preliminary results are shown in Fig. 1 from a WASA run with proton beam on a deuteron pellet target at T_p = 1.2 GeV providing quasifree reaction data over the resonance region for the channels $pd \to d\pi^+\pi^- + p_{spectator}$, $pd \to d\pi^0\pi^0 + p_{spectator}$ and $pd \to d\pi^+\pi^0 + n_{spectator}$. In that way it allows the isospin decomposition of the $pn \to d\pi^+\pi^-$ reaction into isoscalar ($I = 0$) and isovector ($I = 1$) components. As seen in Fig. 1 there is good agreement with previous bubble chamber data (open symbols) for the $pn \to d\pi^+\pi^-$ and $pp \to d\pi^+\pi^0$ reactions. As expected the resonance structure shows up only in the isoscalar part.

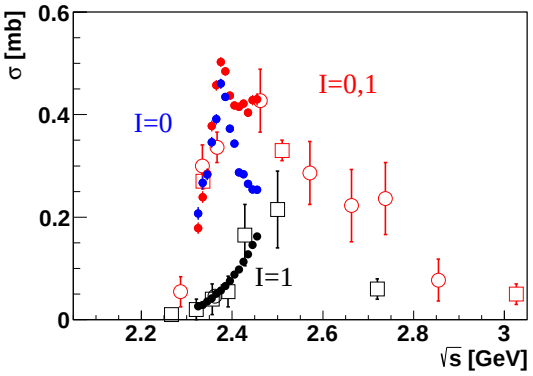

Fig. 1: Total cross section of the $pn \to d\pi^+\pi^-$ reaction (red symbols) in dependence of the center-of-mass energy $\sqrt{s}$ and its decomposition into isoscalar ($I = 0$, blue symbols) and isovector ($I = 1$, black symbols) contributions. The isoscalar part corresponds to just twice the $pn \to d\pi^0\pi^0$ cross section and the isovector part to half of the $pp \to d\pi^+\pi^0$ cross section. The open symbols represent previous bubble chamber measurements of the $pn \to d\pi^+\pi^-$ (I. Bar-Nir *et al.*, *Nucl. Phys.* **B 54** (1973) 17, A. Abdivaliev *et al.*, *Sov. J. Nucl. Phys.* **29**(1979) 796) and $pp \to d\pi^+\pi^0$ reactions (F. Shimizu *et al.*, *Nucl. Phys.* **A 386** (1982) 571, J. Bystricky *et al.*, *J. Physique* **48** (1987) 1901). The filled symbols show our preliminary results.

First preliminary results are also already available for the $pn \to pp\pi^0\pi^-$ channel in the energy region of interest. Since here the isovector pion pair has to be in relative p-wave, any low-mass enhancement in the $\pi^0\pi^-$-invariant mass spectrum (ABC effect) is *a priori* strongly suppressed. As a consequence the decay of the new envisaged resonance into this channel has to be suppressed as well. And that is indeed, what we observe.

1.2.2 Charge Symmetry Breaking: Single π^0 production in dd collisions with WASA-at-COSY

Charge symmetry is a special case of isospin symmetry, and thus a fundamental symmetry of QCD. As isospin symmetry it is broken by the different masses of the up and down quarks and by electromagnetic interaction, but it has the advantage, that the relative π-mass difference, which is of electromagnetic origin, does not contribute. Thus, in order to access the quark mass difference it is advised to look at charge symmetry breaking observables. Triggered by high-precision experiments at IUCF ($dd \to {}^4\mathrm{He}\pi^0$, Stephenson *et al.*) and TRIUMPF ($pn \to d\pi^0$, Opper *et al.*) an international collaboration has been formed aiming at a consistent description of the data within chiral perturbation theory. In course of the ongoing analysis a set of essential observables has been identified, which are now being addressed with WASA-at-COSY. The final goal of this program is to quantify the contribution of higher partial waves in the charge symmetry breaking reaction $dd \to {}^4\mathrm{He}\pi^0$.

In a first step the focus was on an exclusive measurement of the reaction $dd \to {}^3\mathrm{He}n\pi^0$ at $p_d = 1.2\,\mathrm{GeV/c}$ studying the relevance of initial and final state interaction as well as providing a testing ground for χPT calculations of this closely related charge symmetry conserving case. In order to provide quantitative results the data have been compared to a quasi-free reaction model based on existing data for the two-body reaction $dp \to {}^3\mathrm{He}\pi^0$ and a partial-wave expansion for the three-body reaction, both added incoherently. The ${}^3\mathrm{He}n\pi^0$ final state is described by the two Jacobi momenta $\vec{q}$ and $\vec{p}$, where $\vec{q}$ is the π^0 momentum in the overall c.m. frame and $\vec{p}$ the relative momentum in the ${}^3\mathrm{He}n$ subsystem.

The relative angular momenta for the partial wave expansion were defined accordingly: one in the global π^0-$({}^3\mathrm{He}n)$ system and one within the ${}^3\mathrm{He}n$ subsystem (in the following described by a lower and a upper case letter, respectively). The analysis has been limited to $l + L \leq 1$. Taking into account all possible spin configurations this results in 18 possible low level amplitudes. After combining amplitudes with the same signature in final state four possible contributions can be identified: sS, sP, pS and $sP - pS$ interferences. They can be described by seven real coefficients (four complex numbers minus one overall phase), see Table 1.

Table 1: Possible configurations of the $({}^3\mathrm{He}n)\pi^0$ final state and definition of the fit parameters addressing different aspects of the reaction dynamics.

Configuration	Fit parameter	
sS	A_0	
pS sP	A_1 (angular A_3 independent)	A_2 (angular A_4 dependent)
$sP - pS$ interference	A_5 (helicity dependent)	A_6 (helicity independent)
$pd \to {}^3\mathrm{He}\pi^0$ q.f.	A_7	

The kinematics of the final state can be fully described by four independent variables: $\cos\theta_q$, $\cos\theta_p$ (the polar angles of $\vec{q}$ and $\vec{p}$), $M_{{}^3\mathrm{He}n}$ and $\Delta\varphi$ (the angle between the projections of $\vec{q}$ and $\vec{p}$ onto the xy-plane). All four distributions were fitted simultanously.

For the total cross section a value of $\sigma_{\mathrm{tot,prelim.}} = (3.98 \pm 0.01_{\mathrm{stat}} \pm 0.49_{\mathrm{sys}})\,\mu\mathrm{b}$ has been extracted. The contribution from the quasi-free reaction mechanism is about $1/3$ of the total cross section and is consistent with the value one gets from folding the cross section for $pd \to {}^3\mathrm{He}\pi^0$ with the deuteron wave function. Contributions from higher partial waves are illustrated in Fig. 2: while the effect of p-waves in the angular distributions is significant, the restriction to at most one p-wave is already sufficient to provide a consistent description of the data. The probablity of a p-wave in the overall c.m. system and in the ${}^3\mathrm{He}n$ subsystem is of similar size.

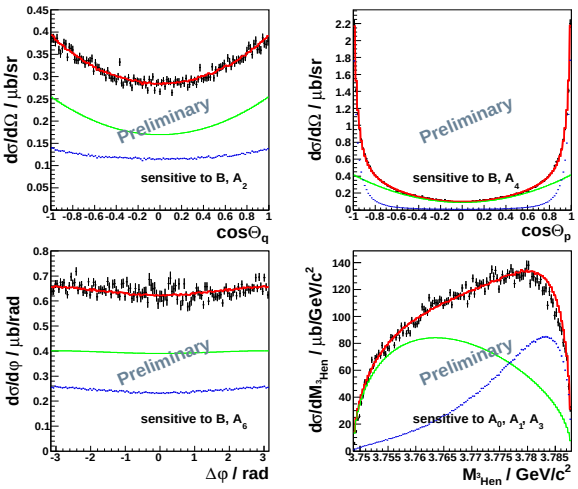

Fig. 2: Differential cross sections in $\cos\theta_q$, $\cos\theta_p$, $\Delta\varphi$ and $M_{{}^3\mathrm{He}n}$: quasi-free (blue), three-body partial-wave fit (green), full model (red). The parameter B is a linear combination of A_0, A_1 and A_3.

For the partial wave analysis the standard approximation for the momentum dependence of $|M|^2 \propto q^{2l+1}\,p^{2L+1}$ was used. Deviations from this assumption was studied by repeating the fit for various subranges in $M_{{}^3\mathrm{He}n}$ (corresponding to intervals in q and p). All but one coefficient remained constant. Only A_4 (representing the p-wave contribution in the ${}^3\mathrm{He}n$ system) showed a significant momentum dependence: compared to the default scaling A_4 has larger values for small relative momenta. A quantitative analysis of this effect is in progress.

A corresponding publication is in preparation.

In a subsequent run first data for the charge-symmetry breaking reaction $dd \to {}^4\mathrm{He}\pi^0$ at $p_d = 1.2\,\mathrm{GeV/c}$ have already been taken. A preliminary analysis indicates a cross section lower than estimated from extrapolating the IUCF result. For a high-statistics run aiming at contributions from higher partial waves also other options are currently being discussed like exploiting the reaction $dd \to dd\pi^0$ or going higher in energy closer to the pole of the Δ resonance and the $2\pi^0$ threshold.

1.2.3 Nucleon-nucleon scattering studies at ANKE

One of the major priorities of the ANKE collaboration is to contribute to the understanding of the nucleon-nucleon (NN) interaction. NN data are necessary ingredients, not only for the understanding of nuclear forces, but also for the description of meson production and other nuclear reactions at intermediate energies. Therefore it is incumbent on any facility that can make significant and new contributions in this field to do so. This was the underlying philosophy of very successful COSY-EDDA collaboration.

***pp*-elastic scattering** The complete investigation of the NN interaction needs precise elastic scattering data as input to a phase-shift analysis (PSA), from which scattering amplitudes at fixed angles can be reconstructed. Detailed experiments have been carried out for the pp system up to about 3.0 GeV. The EDDA collaboration has produced very extensive and important data on $pp \to pp$ differential cross sections and various single and spin-correlation observables, which have allowed the construction of reliable isospin $I = 1$ phase shifts up to at least 2 GeV. Despite the enormous work undertaken by this group, there is a hole in the data base near the forward direction above 1.0 GeV. As a consequence, there are severe problems with the small angle SAID predictions above 2.5 GeV.

The ANKE spectrometer can provide precise measurements of the differential cross-section and spin observables in the energy range 1.0 to 2.8 GeV for centre-of-mass angles $5^\circ < \theta_{cm} < 30^\circ$. One of the main tools here is the independent and accurate determination of the absolute luminosity. The technique relies on measuring the energy losses due to the electromagnetic interactions of the beam as it repeatedly passes through the target by studying the shift of the revolution frequency using the Schottky spectrum (see Sect.2).

The experiment was performed using an unpolarised proton beam at eight different beam energies, $T_p = 1.0, 1.6, 1.8, 2.0, 2.2, 2.4, 2.6, 2.8$ GeV, interacting with a hydrogen cluster-jet target. pp elastic scattering was identified by detecting one or both of the scattered protons in either the FD or STT system in ANKE. Detecting both protons provides valuable cross-checks between the two detection systems and significantly improves the accuracy and reliability of the measurements.

The target density was determined for each cycle and the corresponding integrated luminosity evaluated. Numerical results for typical cycles are listed in Table 2. The total accuracy of the luminosity determination was roughly 2%.

Table 2: Results of the target density and luminosity measurements for several cycles.

Cycle	df/dt	Target Density	Integr. Luminosity
1	0.152	$2.75 \cdot 10^{14}$ cm^{-2}	$1.67 \cdot 10^{33}$ cm^{-2}
2	0.151	$2.74 \cdot 10^{14}$ cm^{-2}	$1.76 \cdot 10^{33}$ cm^{-2}
3	0.154	$2.79 \cdot 10^{14}$ cm^{-2}	$1.81 \cdot 10^{33}$ cm^{-2}
4	0.149	$2.70 \cdot 10^{14}$ cm^{-2}	$1.68 \cdot 10^{33}$ cm^{-2}

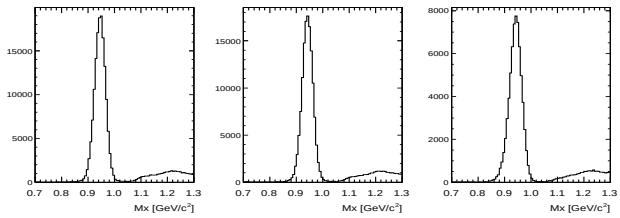

Fig. 3: Missing mass spectra for the $pp \to pX$ reaction at 2.0 GeV for different angular bins (13°–14°, 20°–21°, 27°–28° from left to right). The proton peak can be cleanly separated from inelastic reactions.

After determining the luminosity it is possible to measure the elastic pp differential cross section. Currently only data from the Forward Detector system, where the forwardly scattered fast particles are detected, have been analysed. The reaction identification was done using the missing-mass technique, which is illustrated in Fig. 3 at $T_p = 2.0$ GeV for different angular bins. There is a clear proton peak with minimal background, which is well separated from pion production reactions. Preliminary differential cross section results are presented in Fig. 4 together with the SAID prediction.

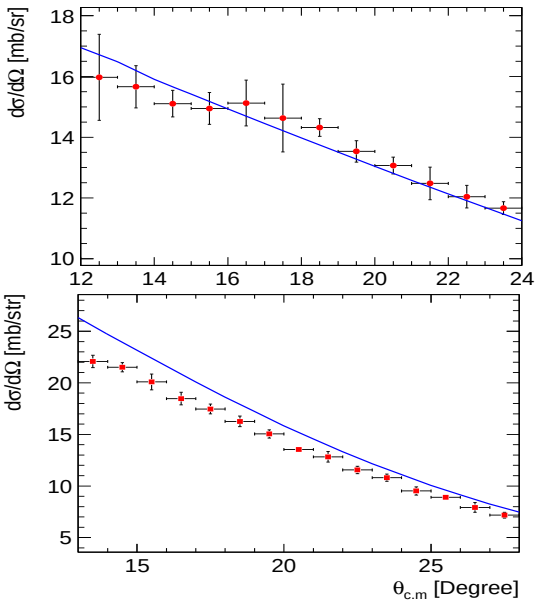

Fig. 4: Preliminary laboratory differential cross section for elastic pp-scattering at 1.0 (upper panel) and 2.0 GeV (lower). The curves show SAID 2007 predictions.

These first results show that ANKE is capable of providing robust pp elastic scattering data in the energy region of $T_p = 1.0 - 2.8$ GeV for angular range $\theta_{c.m.} = 5 - 30^\circ$. Further analysis is in progress and final results with total errors of better than 5% are expected.

***Δ* excitation in the $\vec{n}p \to \vec{p}\Delta^0$ reaction**

Deuteron charge-exchange break-up $\vec{d}p \to \{pp\}n$, where the final $\{pp\}$ diproton system is at very low excitation energy and hence in the $^1S_0$ state, is a powerful tool to probe the spin-flip terms in the proton-neutron charge-exchange reaction.

It was emphasised many years ago that quasi-free (p,n) or (n,p) reactions on the deuteron can act, in suitable kinematic regions, as a spin filter that selects the spin-dependent contributions to the np elastic cross section. Theory suggests that much information on the np charge-exchange amplitudes could be extracted by studying the deuteron charge-exchange break-up reaction, $\vec{d}p \to \{pp\}X$. Two channels are of interest here: $X = n$ and $X = \Delta^0$. In impulse approximation these reactions can be considered as $np \to pn$ or $np \to p\Delta^0$ scattering with a spectator proton. This approach was implemented in detail for the neutron channel (Fig. 5) and predicts analysing powers, spin-correlation coefficients, and cross sections for this reaction. In the $^1S_0$ limit, the $\vec{d}\vec{p} \to \{pp\}_s n$ reaction observables are directly related to the np spin-dependent amplitudes [D.V. Bugg and C. Wilkin, *Nucl. Phys.* A **467** (1987) 575].

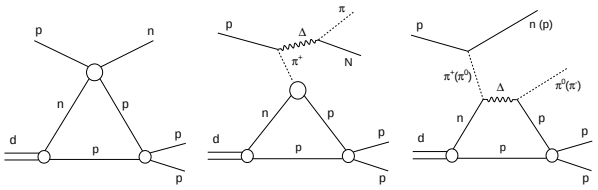

Fig. 5: Deuteron charge-exchange break-up diagram for the neutron channel (left), the simplest implementation of direct Δ^0 production channel (centre), and Δ excitation in the incident deuteron (right).

Recent measurements with the ANKE spectrometer at 1.6, 1.8, and 2.3 GeV have extended this study into the pion-production regime in order to investigate the excitation of the $\Delta(1232)$ isobar in the $dp \to \{pp\}\Delta^0$ reaction. It was demonstrated many years ago at Saclay that at $T_d = 2.0$ GeV the Δ can be excited in the $dp \to \{pp\}\Delta^0$ charge-exchange reaction [C. Ellegaard *et al. Phys. Lett.* B **231** (1989) 365]. Within the framework of direct Δ^0 production shown in Fig. 5 (centre), such measurements would correspond to a spin transfer from the initial neutron to the final proton in the $np \to \Delta^0 p$ reaction, and this would provide valuable information about the spin structure in the excitation of the Δ isobar. However, the simple one-pion-exchange model for the $pn \to p\Delta^0$ amplitude gives the wrong shape for the cross section at low M_x, as is seen in Fig. 6.

The same problem was observed in the pioneering Saclay experiments. It is very analogous to the search for the excitation of the $I = 1/2$ Roper resonance in inclusive $dp \to dX$ or $\alpha p \to \alpha X$ reactions [P. Fernández de Córdoba *et al.*, *Nucl. Phys.* A **586** (1995) 586]. The dominant (physics) background at low M_x is here connected with the possibility of exciting the $\Delta(1232)$ inside the projectile d or α. This means that the pion and nucleon that make up the state X are produced at different vertices. The corresponding diagram for the $dp \to \{pp\}_s X$ reaction is shown in Fig. 5 (right).

The two mass regions, where different mechanisms are dominant, are also reflected in the tensor analysing powers shown in Fig. 7. Here the sum and difference of

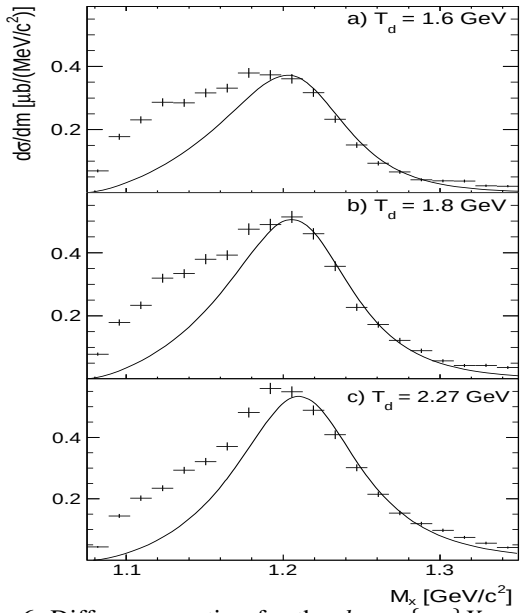

Fig. 6: Diff. cross section for the $dp \to \{pp\}X$ reaction for $M_x > M_N + M_\pi$ at three beam energies. Curves correspond to one-pion-exchange predictions.

deuteron Cartesian tensor analysing powers A_{xx} and A_{yy} are presented as functions of the missing mass M_x. The minimum in $A_{xx} + A_{yy}$ comes at $M_x \approx 1.15$ GeV/c^2, which is precisely where there is the biggest discrepancy in the cross section predictions in Fig. 6. It is also interesting to note that the values of $A_{xx} + A_{yy}$ are remarkably stable and seem to show a universal behaviour, independent of beam energy. Hence, whatever the mechanism is driving the reaction, it seems to be similar at all energies. Theoretical calculations are currently in progress.

The Δ^0 production will also be studied in the near future in the $p\vec{d} \to \{pp\}\Delta^0$ channel at energies up to $T_p = 2.88$ GeV by using a polarised deuterium target.

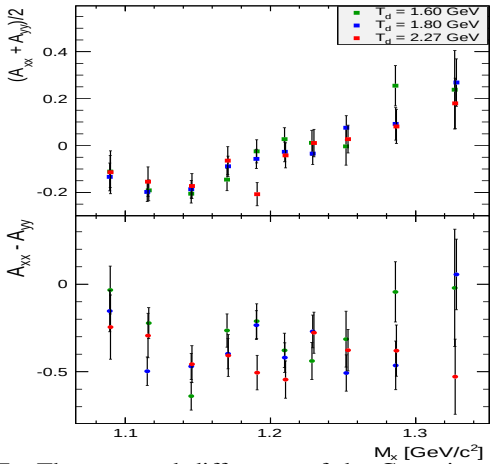

Fig. 7: The sum and difference of the Cartesian tensor analysing powers for the $dp \to \{pp\}X$ reaction for $M_x > M_N + M_\pi$ at three beam energies.

1.2.4 Near-threshold pion production at ANKE

An experimental programme to study near-threshold pion production in the $pp \to \{pp\}_s\pi^0$ and $pn \to \{pp\}_s\pi^-$ reactions is underway at ANKE-COSY. The final proton pair $\{pp\}_s$ is selected to be in the $^1S_0$ state by making a cut on the diproton excitation energy $E_{pp} < 3$. The combined study of these reactions is motivated by the extension of Chiral Perturbation Theory (χPT) to pion production in NN collisions [T.D. Cohen *et al*, *Phys. Rev.* C **53** (1996) 2661; C. Hanhart, *Phys. Rept.* **397** (2004) 155]. Measurements of $d\sigma/d\Omega$, A_y^p and the spin-correlation coefficients A_{xx} and $A_{x,z}$ for both reactions will provide a non-trivial test of χPT predictions, and lead to the isolation of the strength parameter d of the four-nucleon-pion contact interaction in χPT.

As a first step of the programme, measurements with a polarized proton beam incident on unpolarized hydrogen and deuterium cluster targets were performed in 2009 at a beam energy of $T_p = 353$ MeV [T. Tsirkov *et al*, nucl–ex/1112.3799, S. Dymov *et al*, nucl–ex/1112.3808]. Through a careful use of the Watson theorem, an amplitude analysis of the combined data sets (global fit performed by IKP-theory group) has been achieved and these have allowed the determination of the partial waves up to $\ell_\pi = 2$.

The beam polarization and luminosity were determined by detecting simultaneously the $\vec{p}p \to d\pi^+$ and $\vec{p}p \to pp$ processes, for which the cross section and analyzing power are known with high precision at this energy. In the case of the pn-experiment, the quasi-free $\vec{p}n \to d\pi^0$ process was used. Excellent conditions of the polarized proton beam (polarization $P \approx 67\%$) and the cluster target (high density) allowed us to achieve the desired statistical precision.

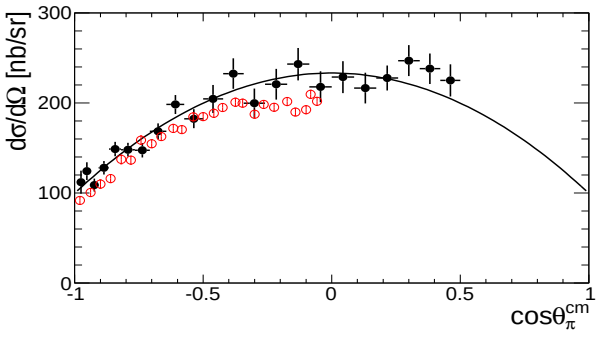

Fig. 8: Differential cross section for the $pp \to \{pp\}_s\pi^0$ reaction at 353 MeV as a function of the cosine of the pion centre-of-mass (c.m.) angle. The solid (black) circles represent the ANKE measurements. Open (red) circles are CELSIUS data. The curve is a global fit to our data on π^0 and π^- production.

Figures 8 and 9 show the results obtained for the $\vec{p}p \to \{pp\}_s\pi^0$ reaction. The ANKE cross section is compared to the CELSIUS data at 360 MeV [R. Bilger *et al*, *Nucl. Phys.* A **693** (2001) 633]. If one considers only pion waves with $\ell_\pi \leq 2$, a non-zero value of the analyzing power in this process must arise from the interference between the s and d waves. The strong signal observed here shows the importance of this interference.

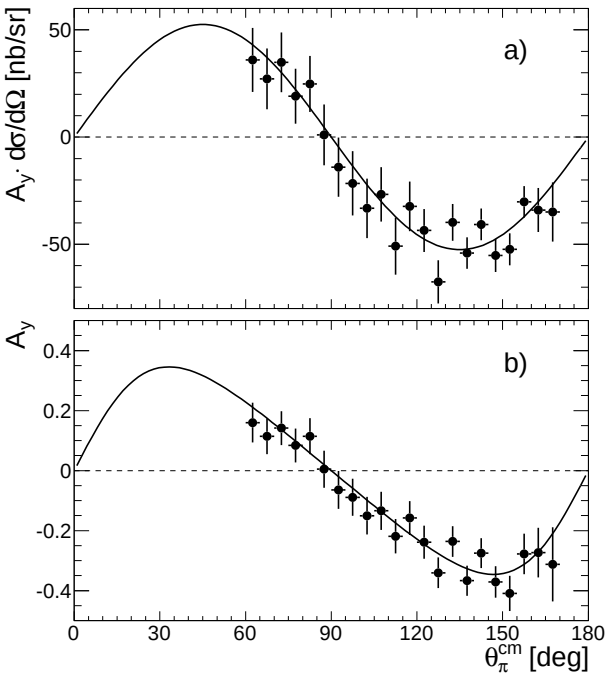

Fig. 9: (a) The product of the measured analyzing power and differential cross section for the $pp \to \{pp\}_s\pi^0$ reaction. The curve represents the global fit results. (b) Measured values of A_y for the $pp \to \{pp\}_s\pi^0$ reaction. The line represents the quotient of the global fit in panel-a and the fit to the cross section.

The differential cross section measured for the quasi-free $pn \to \{pp\}_s\pi^-$ reaction is shown in Fig. 10 compared with the TRIUMF data [F. Duncan *et al*, *Rev. Lett.* **80** (1998) 4390] and pion absorption data [H. Hahn *et al*, *Phys. Rev.* C **53** (1996) 1074]. Whereas the TRIUMF results only cover the central region of pion angles, the current data extend over the whole angular domain. The two data sets are consistent in the backward hemisphere but the TRIUMF measurements show no indication of the rise at forward angles that is seen at ANKE. The forward/backward peaking is in complete contrast to the results found for π^0 production and is an indication of the dominance of the $I = 0$ p-wave amplitudes.

The results for the $pn \to \{pp\}_s\pi^-$ analyzing power are displayed in Fig. 11, with $A_y\, d\sigma/d\Omega$ being shown in panel a and A_y in panel b. The agreement with the TRIUMF A_y data [Hahn H *et al*, *Phys. Rev. Lett.* **82** (1999) 2258] is reasonable and both show the strong and rather asymmetric fluctuation in the central region of angles.

Some of the biggest uncertainties in the global amplitude analysis arise from the normalisations in the $pp \to \{pp\}_s\pi^0$ and $pn \to \{pp\}_s\pi^-$ data, which affect primarily the s- and p-wave production, respectively. The relative normalisation can be determined independently

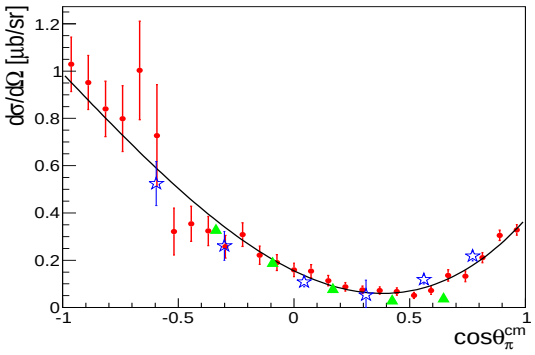

Fig. 10: Unpolarized differential cross section for the quasi-free $pn \to \{pp\}_s\pi^-$ reaction at $\approx$ 353 MeV. The ANKE data are shown by red circles and the TRIUMF results by green triangles. The arbitrarily scaled TRIUMF cross sections extracted from $\pi^-{}^3\mathrm{He} \to pnp_{\mathrm{sp}}$ data are also included (blue stars). The curve is the result of the global fit to the ANKE data.

through a measurement of the transverse spin correlation parameter $A_{x,x}$ for the $pn \to \{pp\}_s\pi^-$ reaction. Such a measurement was done at ANKE in 2011 by using the vector polarized deuteron beam and the hydrogen Polarized Internal Target of ANKE equipped with a long storage cell. The preliminary results of the measurement are shown in Fig. 12. These will provide an independent determination of the contact interaction term d.

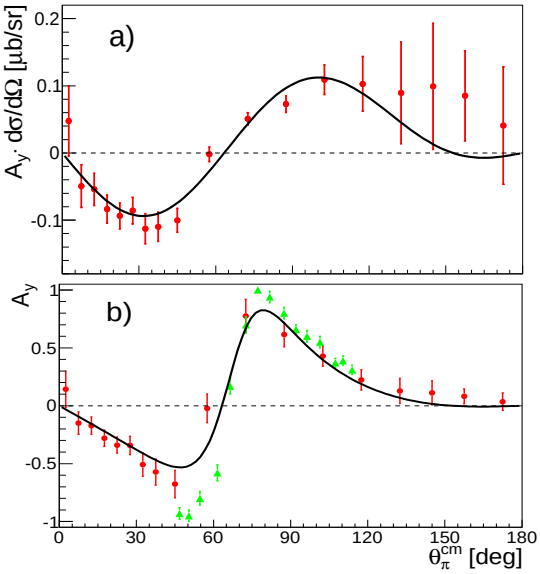

Fig. 11: (a) The product of the measured analyzing power and differential cross section for the quasi-free $pn \to \{pp\}_s\pi^-$ reaction at 353 MeV. The curve represents the global fit results. (b) Measured values of A_y for the $pn \to \{pp\}_s\pi^-$ reaction showing both the ANKE (circles) and TRIUMF data (triangles). The line represent the quotient of the fit in panel-a and that to the cross section.

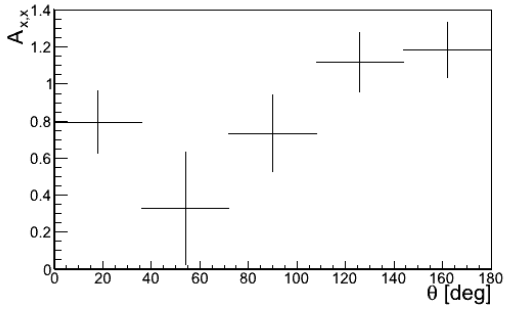

Fig. 12: Preliminary results on the spin-correlation coefficient $A_{x,x}$ for the $pn \to \{pp\}_s\pi^-$ reaction at 353 MeV.

A next step in the pion production study could be to measure the spin-correlation parameter $A_{x,z}$. This will provide additional restrictions on the partial wave analysis and provide a check on the assumptions made. This experiment would require the installation of a Siberian snake in COSY at the (so-called) 'PAX low-β' section.

1.2.5 η meson mass determination with ANKE at COSY

Recent measurements of the η meson mass performed at different experimental facilities (CERN-NA48, COSY-GEM, CESR-CLEO, DAΦNE-KLOE, MAMI-Crystal Ball) have resulted in very precise data but which differ by up to eight standard deviations, *i.e.*, 0.5 MeV/c^2. In order to clarify this situation, a high precision measurement has been realised at COSY using the ANKE spectrometer.

The value of the η mass can be obtained by determining the threshold of the two-body $dp \to {}^3\mathrm{He}\,\eta$ production reaction and then applying purely kinematics. For this purpose twelve data points at fixed excess energies in the range of $Q = 1 - 12$ MeV were investigated. The final state momentum p_f of the ^{3}He-particles in the centre-of-mass (CM) frame

$$p_f(s) = \frac{\sqrt{\left[s - (m_{^3\mathrm{He}} + m_\eta)^2\right]\left[s - (m_{^3\mathrm{He}} - m_\eta)^2\right]}}{2\sqrt{s}}, \quad (1)$$

measured with the ANKE spectrometer, depends very sensitively on the η mass and the total energy $\sqrt{s}$. The latter is completely defined in a fixed target experiment by the masses of the initial particles and the deuteron beam momentum p_d. The precise determination of the production threshold requires that both the final state momenta of the ^{3}He-particles and the corresponding deuteron beam momenta have to be measured with highest accuracy.

The beam momentum was determined using a method developed at an electron-positron machine in Novosibirsk [Ya.S. Derbenev *et al.*, Part. Accel. **10** (1980) 177] based on the spin dynamics of a polarised beam. The spin precession frequency of a relativistic particle is disturbed

by an artificial spin resonance induced by a horizontal rf-magnetic field of a solenoid leading to a depolarisation of the polarised accelerator beam. The depolarising resonance frequency f_r depends on the kinematical γ-factor (i.e. the beam momentum $p = m\sqrt{\gamma^2 - 1}$) and the beam revolution frequency f_0 via the resonance condition $f_r = (k + \gamma G) f_0$, where k is an integer and G the gyromagnetic anomaly of the beam particle. By measuring these two frequencies the beam momentum of a polarised beam can be determined with a precision better than $\Delta p/p < 10^{-4}$. This method was used at COSY with a vector polarised deuteron beam and the momenta in the threshold range of 3.1 - 3.2 GeV/c were determined with an accuracy of $\Delta p/p < 6 \times 10^{-5}$, i.e., to 170 keV/$c$ [P. Goslawski *et al.*, Phys. Rev. ST Accel. Beams **13** (2010) 022803].

The correct value of the final state momenta of the ^{3}He-nuclei can only be extracted provided that there is (*a*) a clean identification of the $dp \to {}^3\mathrm{He}\,\eta$ reaction and (*b*) a precise detector calibration. The fact that ANKE has full geometrical acceptance for the $dp \to {}^3\mathrm{He}\,\eta$ reaction up to $Q = 15$ MeV allows us to verify and improve the detector calibration by studying the kinematics of this two-body reaction. For a fixed total energy the ^{3}He momenta are distributed on a momentum sphere in the CM frame with constant radius $p_f = (p_x^2 + p_y^2 + p_z^2)^{1/2}$. This can be visualised by plotting the transverse versus the longitudinal reconstructed momentum, as shown in Fig. 13a. A centered momentum locus with a fixed radius p_f is expected, as indicated by the dashed line.

The main tool to verify the spectrometer calibration is the requirement that the momentum sphere be completely symmetric in p_x, p_y and p_z, i.e., that the final state momentum p_f should be constant in all directions. Through a careful investigation of the dependence of p_f on the cosine of the polar angle ϑ and the azimuthal angle ϕ, the shape of the momentum "sphere" can be studied in more detail. Deviations from a symmetric shape will indicate the need for improvements of the calibration. In order to implement this the ^{3}He η signal has to be extracted free of background.

The ^{3}He can be identified at ANKE using the energy loss and time of flight information and this largely suppresses the protons and deuterons. The residual background originates mainly from multipion production. This contribution can be subtracted using data taken below the η threshold but analysed as if they were taken above [T. Mersmann *et al.*, Phys. Rev. Lett. **98** (2007) 242301]. This technique was applied to the final state momentum spectra shown in Fig. 13b for different $\cos\vartheta$ bins. The dependence of p_f on ϕ can be similarly studied. The background-free ^{3}He η distributions in $\cos\vartheta$ and ϕ allow one to extract the mean final state momenta for individual $\cos\vartheta$ and ϕ bins, as shown in Fig. 14.

In contrast to Monte Carlo simulations of p_f without momentum smearing, the data show a dependence on both $\cos\vartheta$ and ϕ. This is a kinematic effect caused by the different momentum resolutions of the ANKE detector in

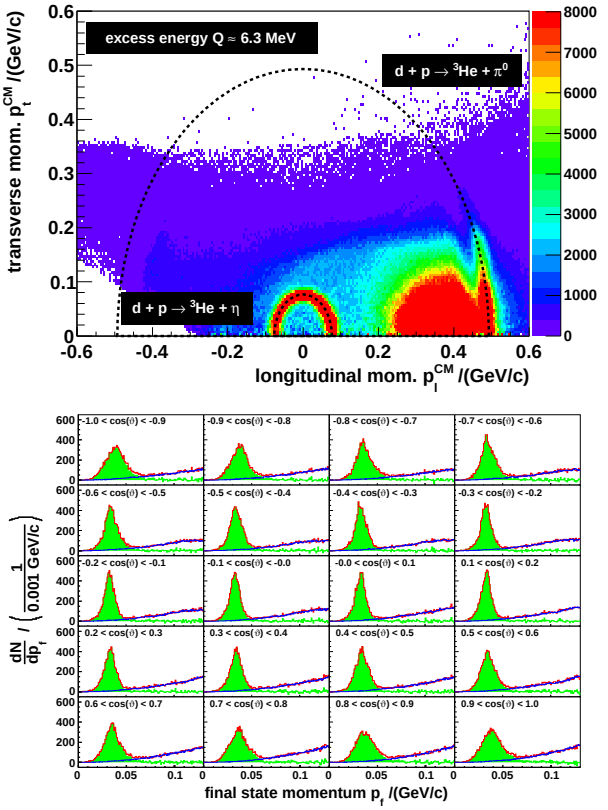

Fig. 13: **a)** The momentum loci for the ^{3}He η and ^{3}He π^0 channels. ANKE covers the full solid angle for η production near threshold whereas for the ^{3}He π^0 final state only fast ^{3}He-nuclei are detected at small angles. **b)** Final state momentum p_f (red) in different $\cos\vartheta$ bins at an excess energy of $Q \approx 1$ MeV, the background description (blue), and the extracted ^{3}He η signal (green).

the x, y, and z directions. Assuming that p_x, p_y and p_z distributions are gaussian distributed with different widths, it is possible to reproduce the data in Fig. 14. These plots are of the highest importance for determining the final state momentum for the following three reasons.

1. Improvement of the calibration. Asymmetric shapes in $\cos\vartheta$ and ϕ caused by an "unpolished" calibration can be corrected by minor changes of the ANKE calibration parameters. These changes are so small that they have no impact on typical calibration quantities, such as the missing masses of different reactions. This means that, by studying the $\cos\vartheta$ and ϕ dependence, the accuracy of the different calibration parameter can be significantly improved.

2. Extraction of the correct momentum resolution in (p_x, p_y, p_z). Assuming gaussian distributions with different widths, we found for ANKE that $(\sigma_x, \sigma_y, \sigma_z) = (3.2, 7.8, 16.4)$ MeV/c.

3. Correction of the reconstructed final state momentum. Because of the finite momentum resolution,

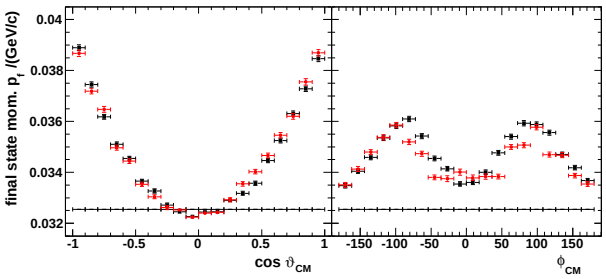

Fig. 14: Dependence of the final state momentum on $\cos\vartheta$ and ϕ for data (red circles), Monte Carlo simulations without momentum smearing (horizontal black lines), and with momentum smearing (black squares).

the extracted average over all $\cos\vartheta$ and ϕ bins (see Fig. 14 red circles) is larger than the original one (black line). This has to be considered when determining the twelve final state momenta.

The final state momentum analysis is still in progress but already the twelve momenta in the range of 30–100 MeV/c have been determined with a precision better than 400 keV/c. Fitting the $p_f = p_f(p_d, m_\eta)$ dependence, as shown in Fig. 15, the η mass is preliminarily determined to be

$$m_\eta = (547.869 \pm 0.007 \pm 0.040)\ \mathrm{MeV}/c^2. \qquad (2)$$

The accuracy, which will be achieved at ANKE, will be competitive with the precision achieved at other recent experiments that studied the decay of the meson.

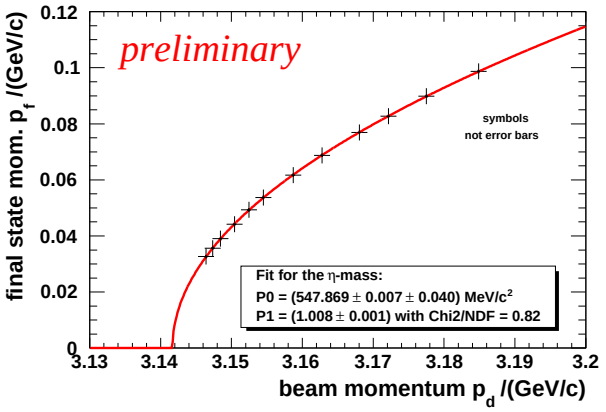

Fig. 15: Determination of the η mass by fitting the dependence of p_f on p_d.

1.2.6 FSI and polarization observables in the process $\vec{p}p \to pK^+\Lambda$

An important part of the actual COSY-TOF physics program is the study of the hyperon nucleon interaction in the production reaction $\vec{p}p \to pK^+\Lambda$. With a method, proposed by Gasparyan et al., it should be possible to extract the spin triplet $p\Lambda$ scattering length with the polarized COSY beam.

While the first beam time of the program was carried out in September 2010, the kinematic reconstruction of the $pK^+\Lambda$ final state with the new Straw Tube Tracker has been completed during 2011. Studies of Monte Carlo simulated events have shown that the resolution of the invariant mass is $\approx 1\,\mathrm{MeV}/c^2$ at a reconstruction efficiency of 20 %. This is an improvement of a factor of 4 as compared to the old COSY-TOF detector setup.

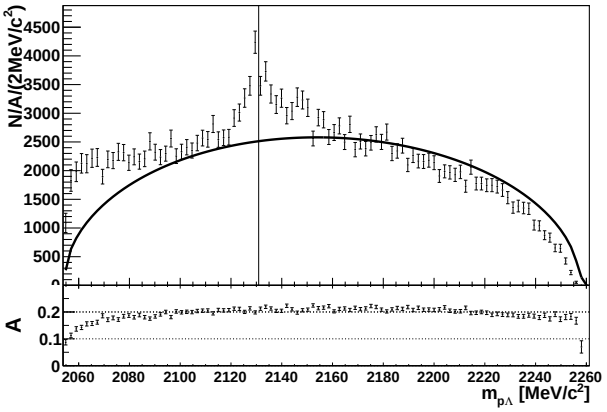

Fig. 16: The $m_p\Lambda$ invariant mass spectrum. The number of measured events (N) is scaled with the detector acceptance (A)

Figure 16 shows the reconstructed $p\Lambda$ invariant mass ($m_{p\Lambda}$) spectrum with 42 000 events that were collected during 1 week beam time at 2.95 GeV/c with a stable beam polarization of 61.0 ± 1.8 %. The ratio of measured events and the detector acceptance is given. The latter is shown below the spectrum and it is noteworthy that it is nearly constant over the whole $m_{p\Lambda}$ range.

In comparison to the arbitrarily scaled phase space (black curve) a cusp structure is visible exactly at the $pK^+\Sigma^0$ threshold (vertical line). Because of the high resolution, a detailed analysis of the cusp position and shape will give insight to the $p\Lambda - p\Sigma^0$ coupled channel effect that gives rise to the cusp structure.

So far the analysis was focused on the final state interaction that can be seen close to the threshold. From the ratio of the corrected data to the phase space distribution we could extract the effective $p\Lambda$ scattering length to be $a = -1.28 \pm 0.11 \pm 0.3$ fm. The two given errors are experimental and from the extraction method, respectively. Therefore, we demonstrate that the reconstruction precision of the new experimental setup is capable to perform the measurement.

The method of the spin triplet extraction depends on a precise measurement of the K^+ analyzing power (A_N) as a function of the $p\Lambda$ invariant mass in the region of the FSI. This works because with a partial wave analysis A_N can be decomposed into a symmetric part from S and P wave interference and an asymmetric part from S and D wave interference. When one considers a $p\Lambda$ system in

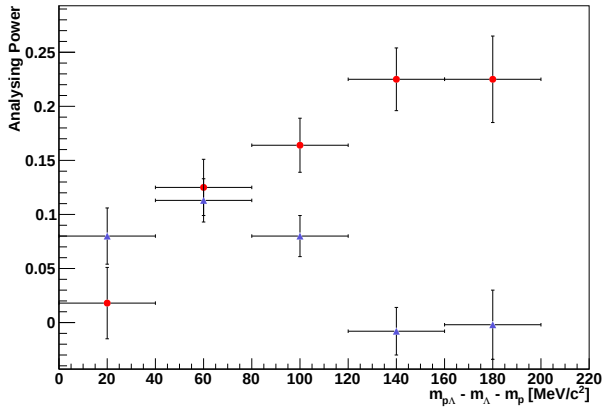

Fig. 17: The coefficients of the symmetric (red) and asymmetric (blue) part of the K^+ analyzing power.

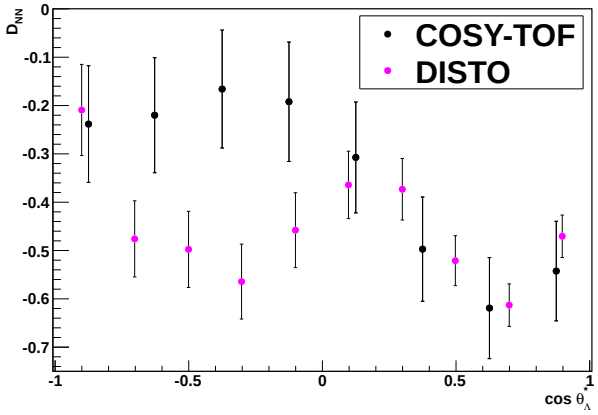

Fig. 18: The spin transfer coefficient D_{NN} as a function of the azimuthal angle of the Λ in the CMS. The COSY-TOF result (black) is compared to the earlier DISTO measurement (magenta).

the final state that has no internal angular momentum, for small $m_{p\Lambda}$, one can show that for $p\Lambda$ spin singlet scattering the K^+ cannot be in P wave. Therefore, the symmetric part of A_N is proportional to the spin triplet scattering amplitude.

In Figure 17 the coefficients for the symmetric part (red) an asymmetric part are shown. Unfortunately, in the interesting region close to the threshold the symmetric part of the analyzing power becomes much smaller than 25% which was expected from measurements of the reaction $pp \to d\pi^+$ with the exact same selection rules. Therefore with the data collected so far the extraction of the spin triplet scattering length is impossible.

However, it is very important to find an explanation for this behavior. The presented result is compatible with the absence of spin triplet ($^1S_3$) scattering. But also the P wave amplitudes of $^1S_3$ scattering could be individually 0 or interfere to 0. Furthermore, the analyzing power depends only on the imaginary part of the interference and a phase cancellation is possible. The viability of the latter explanations depends on the upper limit one can find for the symmetric part of the analyzing power. Therefore, the collection of more data is needed.

Another part of the physics program is the study of the production mechanism. For example, the polarized COSY beam together with the self analyzing decay of the Λ that is produced with polarization in the reaction permits the measurement of the spin transfer coefficient D_{NN}. This quantity is given in Figure 18 (black). Because the actual analysis contradicts an earlier test measurement with the old detector setup the result is preliminary. However, in comparison with an earlier measurement from the DISTO experiment the results agree for the forward Λs.

In the framework of the Laget model one expects $D_{NN} = +1$ for pure π exchange and $D_{NN} = -1$ for pure K^+ exchange. Therefore, both experiments suggest a dominant K^+ exchange in the production process. The experiments differ for backward Λs. However, in the Laget Model the ceasing D_{NN} to $\cos\theta^*_\Lambda = -1$ is well explained by a connection of the Λ to the unpolarized target proton in that case and to the polarized beam proton in case of $\cos\theta^*_\Lambda = +1$. Because of these discrepances it is important to improve on the statistical accuracy of the COSY-TOF measurement also in this area.

1.2.7 Production of K^+K^- pairs in proton-proton collisions at 2.83 GeV

The $pp \to ppK^+K^-$ reaction was measured at ANKE at excess energies with respect to the ϕ threshold of $\varepsilon_\phi = 18.5, 34.5, 76$ MeV [Y. Maeda *et al.*, Phys. Rev. C **77** (2008) 015204]. Though the ϕ meson was well identified, the statistics at the higher energies did not permit the study of higher partial waves. High statistics data are now available at $\varepsilon_\phi = 76$ MeV which can be compared to DISTO results at $\varepsilon_\phi = 83$ MeV [F. Balestra *et al.*, Phys. Rev. C **63** (2001) 024004].

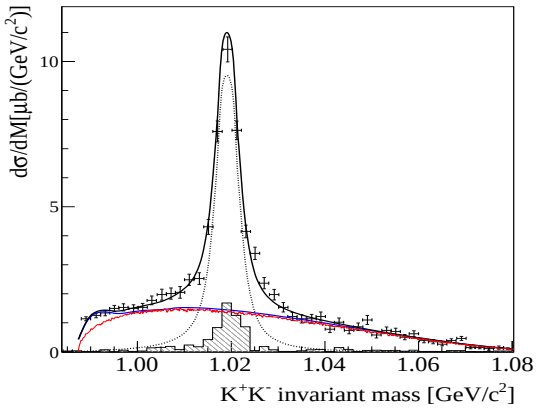

Fig. 19: The $pp \to ppK^+K^-$ differential cross section in terms of the K^+K^- invariant mass. The solid line is the sum of ϕ (dotted histogram) and non-ϕ contributions (red is phase space and blue FSI parametrization).

To deduce the $pp \to ppK^+K^-$ cross section, shown

in Fig. 19 in terms of the K^+K^- invariant mass, parametrizations of both ϕ and non-ϕ contributions have to be fitted to different differential spectra in order to make acceptance estimates. For the ϕ this was done on the basis of a truncated partial wave decomposition whereas for the non-ϕ our earlier ansatz as the product of final state interactions (FSI) in the K^-p, pp, and K^+K^- systems was employed. Using the same parameters that fitted the $\varepsilon_\phi = 18.5$ MeV data, the strong distortions in the non-ϕ spectra are well reproduced as seen, for example, in Fig. 20 for the ratio of the Kpp mass distributions.

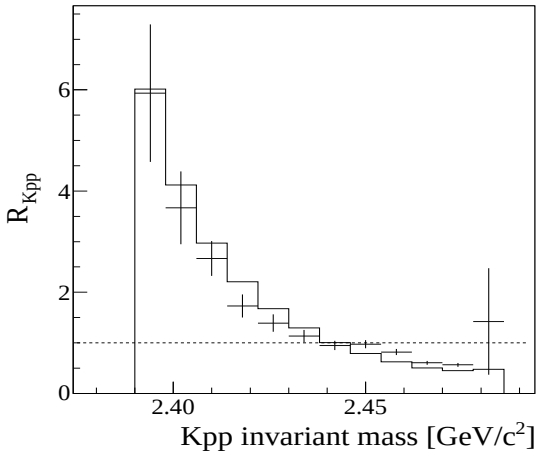

Fig. 20: Ratio of the $pp \to ppK^+K^-$ cross sections in terms of the K^-pp and K^+pp invariant masses. The histogram is the prediction in the FSI model.

Having reliable parametrizations of the background under the ϕ peak in Fig. 19, the differential distributions for the $pp \to pp\phi$ reaction could be safely extracted. As already noted by DISTO, the non-isotropy in the different angular distributions shown in Fig. 21 shows the presence of different partial waves. For example, the departure from a $\sin^2\theta$ dependence (dashed line) in the ϕ decay angle requires p-wave ϕ production, whereas the deviations from isotropy in the angle between the proton in the pp rest frame and the ϕ direction (the helicity angle) indicate the importance of P-waves in both the pp and $\phi\{pp\}$ systems. Higher partial waves are also necessary to explain the momentum distributions of the proton in the pp rest frame and the ϕ in the c.m. system.

The truncated partial wave description of the $pp \to pp\phi$ spectra show that the contribution from purely S-wave final states represents only a small fraction of the total cross section at $\varepsilon_\phi = 76$ MeV. This explains why there is no evidence for the S-wave pp final state interaction in either these or the DISTO data. However, in order to explain the energy dependence of the $pp \to pp\phi$ total cross section seems to require a low mass ϕp enhancement.

Further evidence is found for structure in the K^+K^- invariant mass distribution at the $K^0\bar{K}^0$ threshold [A. Dzyuba *et al.*, Phys. Lett. B **668** (2008) 315] and this region will also be investigated in data already taken below the ϕ threshold.

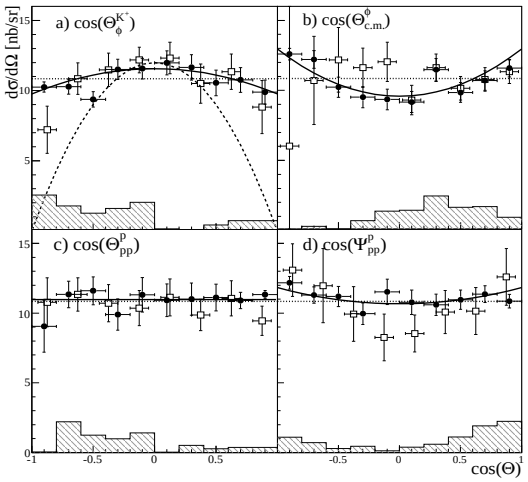

Fig. 21: Angular distributions for the $pp \to pp\phi$ reaction compared with the scaled DISTO data (open squares). The solid curves show fits to the ANKE results for (a) The ϕ decay angle, (b) The ϕ c.m. angle, (c) The proton Jackson angle, and (d) The proton helicity angle.

1.2.8 Momentum dependence of the ϕ-meson nuclear transparency

The production of the ϕ meson in proton collisions with C, Cu, Al, and Au targets has been studied at 2.83 GeV by measuring at ANKE the K^+K^- decay in the angular cone $\theta_\phi < 8^\circ$. The analysis of such data yields information on the behaviour of the ϕ in a nuclear environment.

The nuclear transparency ratios is defined as $R = (12/A)(\sigma^A/\sigma^C)$, where σ^A is the inclusive cross sections for ϕ production in pA collisions. The comparison of the values of R, averaged over the ϕ momentum range 0.6–1.6 GeV/c, with model calculations yields an in-medium ϕ width of $33-50$ MeV/c^2 in the nuclear rest frame at normal nuclear density [A. Polyanskiy *et al.*, Phys. Lett. B **695** (2011) 74].

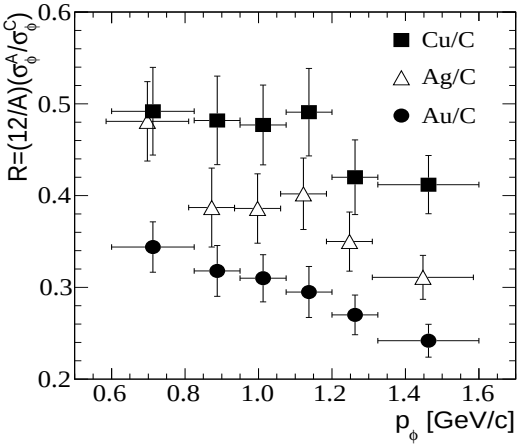

Fig. 22: Momentum dependence of the transparency ratio R, normalized to C, for Cu, Ag, and Au targets.

The data have now been put into six bins of ϕ momen-

tum and Fig. 22 shows the momentum dependence of the measured transparency ratios for different nuclei. In order to extract information on the in-medium ϕ width, a reaction model is essential and three approaches have been considered.

Model 1: The Valencia eikonal approximation uses the predicted ϕ self-energy for both 1- and 2-step production processes, with nucleon and Δ intermediate states.

Model 2: Paryev developed the spectral function technique for ϕ production in both the primary proton-nucleon and secondary pion-nucleon channels.

Model 3: The Rossendorf BUU transport calculation includes a variety of secondary ϕ production processes. In contrast to Models 1 and 2, where ϕ absorption is governed by its width, Γ_ϕ, Model 3 describes it in terms of an effective in-medium ϕN cross section $\sigma_{\phi N}$ that is related to Γ_ϕ in the low-density limit.

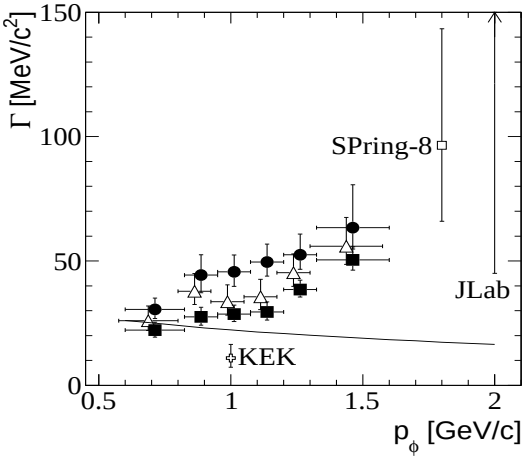

Fig. 23: In-medium ϕ width in the nuclear rest frame as a function of its momentum. The points were evaluated by comparing the data of Fig. 22 with model calculations (1 –full squares, 2 – full circles, 3 – open triangles).

The in-medium ϕ width in the nuclear rest frame at normal nuclear density obtained in these models is shown in Fig. 23. Similar behaviour is seen for all three approaches and the differences come mainly from the descriptions of secondary production processes. The ϕ width extracted is not in disagreement with the Spring-8 and JLab results that were determined at slightly higher momentum but it exceeds the Valencia prediction (solid line).

In order to understand further the model calculations, the double differential cross sections for ϕ production have been evaluated within the ANKE acceptance window for different momentum bins. The experimental results for the four target nuclei are compared in Fig. 24 with the predictions of the Paryev and BUU calculations that used the extracted central values of the ϕ width shown in Fig. 23 as input.

The BUU calculation describes rather well the data at high momenta, where direct ϕ production dominates, but both models strongly underestimate ϕ production at low momenta. This suggests that some process, whose contribution to ϕ production increases for low ϕ momenta and with the size of the nucleus, is not included in the three models.

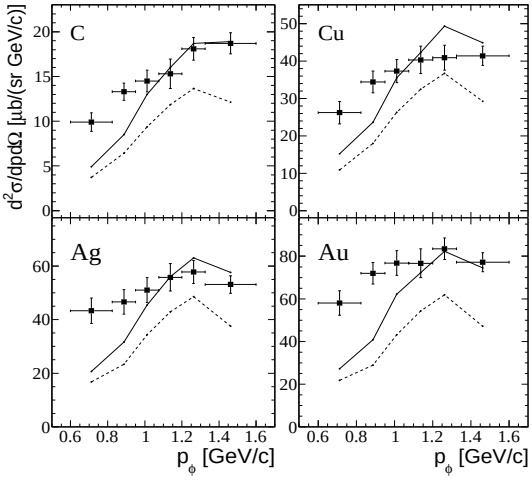

Fig. 24: Inclusive double-differential cross sections for ϕ production on C, Cu, Ag, and Au targets, as functions of the ϕ momentum, compared with the predictions of model 2 (dashed) and model 3 (solid lines).

1.3 Developments for the Experimental Facilities

1.3.1 Piezoelectric nozzle units for pellet targets

Up to now the WASA-at-COSY experiment, formerly used at the CELSIUS ring in Uppsala, is the only internal beam experiment which uses a pellet target as internal target. One major focus of the experimental program here are studies on symmetry breaking effects by the investigation of rare and forbidden meson decays. To achieve the required high luminosities for these measurements, a high performance and reliable operation of the pellet target is mandatory. Therefore, detailed investigations and optimizations of the pellet generator are of highest interest. Furthermore, since e.g. also the future 4π experiment $\overline{\text{P}}$ANDA, which will be operated at the antiproton ring HESR at FAIR/Darmstadt, considers to use both cluster jets as well as pellet streams as targets, further progress of the pellet beam technology is of high relevance.

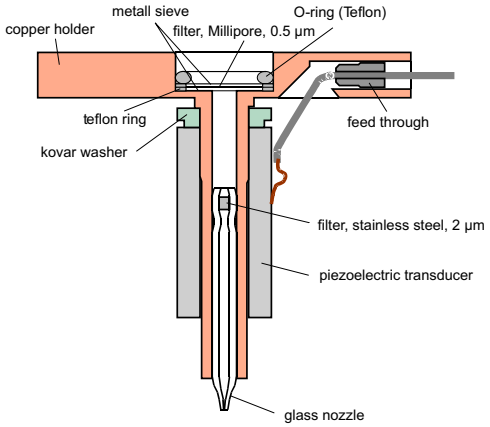

Fig. 25: Sketch of a nozzle holder unit.

Main part of the pellet generator at COSY is a compact nozzle holder unit, which is equipped with a glass nozzle with an opening of $\sim$13 μm. A sketch of such a unit is shown in Fig. 25. Cold liquefied hydrogen or deuterium is pressed through this nozzle into vacuum. Due to mechanical excitation of the nozzle by means of a piezoelectric transducer, this liquid is split into a regular stream of droplets which freeze and form the pellets. One major limitation of the nozzle life time is the irreversible blocking by microscopic particles which can still happen in spite of the usage of filters. To counter this a nozzle production line has been established at the ZAT of the FZ Jülich in 2007 which includes several cleaning and quality checks. By this nozzle blocking could be reduced significantly. Another reason for the need of nozzle exchanges is the fact that in case of some of the piezoelectric nozzle holder units it was not possible to find efficient droplet/pellet working points. Therefore, to further increase the uptime of the pellet target during experimental measurements, a test station for complete nozzle holders has been established at the University of Münster. By this additional quality and reliability checks of nozzle units can be performed before the installation at the pellet target generator. Currently these tests are performed in two independent stages: In the first step endurance tests of the complete nozzle units in vacuum are performed. Here nitrogen gas at room temperature and at gas input pressures similar to the operation at COSY, i.e. $\sim$ 1 bar, is fed to the glass nozzle and the gas flow as well as the gas input and vacuum pressures are monitored. Since the glass nozzles contain micrometer filters, with these measurements the influence of the gas flow on irreversible nozzle blocking by particles inside the nozzle can be tested. After passing this step, the piezoelectric transducer is switched on and operated with frequencies similar to those used for the pellet generation. In both steps the effective nozzle opening diameter can be reconstructed by the observed gas flows and pressures. By this a nozzle blocking can directly be observed by monitoring this number. Moreover, the time dependence of a possible reduction of the effective nozzle diameter directly gives valuable information on the blocking mechanisms.

In first measurements several nozzles have been tested with this setup. One of these nozzles was used for one week without the operation of the piezoelectric transducer and after that for one week with the piezo switched on. As the nozzle did not block during these tests it was installed into the WASA-at-COSY pellet target where it was operated successfully for two weeks without blocking until it had to be dismounted for maintenance reasons. Further systematic tests of more nozzles will be performed in 2012.

In addition to the already available two stages of the nozzle test station two possible further steps are under discussion. One next step could allow for cooling down of the system in order to test the temperature changes which can cause material stress of the nozzle units. In a last step hydrogen droplets could be generated using helium as the background gas under the same condition under which the pellet target is operated. By this the influence of a mechanically vibrating liquid on the production and transport of blocking particles can be tested.

The rate of the produced pellets and therefore the performance of the target is mainly influenced by the oscillation of the piezoelectric transducer. Therefore, a further device has been set up to perform careful studies on the properties of the transducers, which are used for the different available nozzle units.

Electrically a piezoelectric transducer can be described in first order as a damped resonant circuit (see Fig. 26). In case of the used piezos the following resonance frequencies are expected for the different mechanical oscillation modes:

Table 3: Expected resonance frequencies of the piezoelectric transducers.

oscillation mode	frequency / kHz
longitudinal mode	55.0 ± 0.2
thickness mode	583 ± 18
radial mode	99.5 ± 1.1

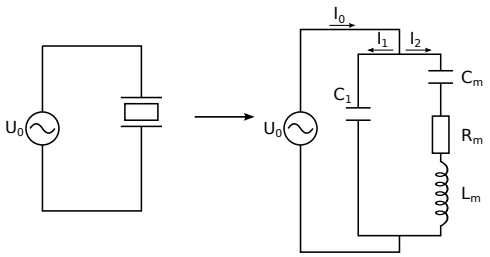

Fig. 26: Piezoelectric transudcer described by an electrical equivalent circuit in first order.

An important quality check for the nozzle holders is the verification of the proper functioning of the installed piezos and the observation of the expected mechanical vibrations induced by the transducers. For measuring these resonances two methods are used. The first one is an electric measurement of the impedance of the piezoelectric transducers as a function of the external oscillator frequency, coupled to the piezos and the second one is an acoustic measurement via a microphone. In the latter case the amplitude of the mechanical vibration of the piezo, and thus of the glass nozzle, can be measured as a function of the driving frequency. With both methods the predicted resonance at $f = 55.0 \pm 0.2$ kHz of the longitudinal mode can be seen as well as the first harmonic of this mode at about 110 kHz (see Figs. 27 and 28). The resonance of the radial mode is hardly visible. Additionally to the predicted one, a resonance at about 30 kHz has been observed which is only present when the piezo is connected to the holder. It is important to note, that this resonance is not observed for nozzle holder units which were already installed into the pellet target and had to be dismounted because it was not possible to find a good working point for target operation. Thus, these oscillation measurements allow for important checks of the proper functioning of the piezo crystals as well as of the mechanical coupling to the nozzle units. Therefore all nozzle holder units will be checked via this method before installation into the pellet target, which reduces the number of needed nozzle exchanges during target operation.

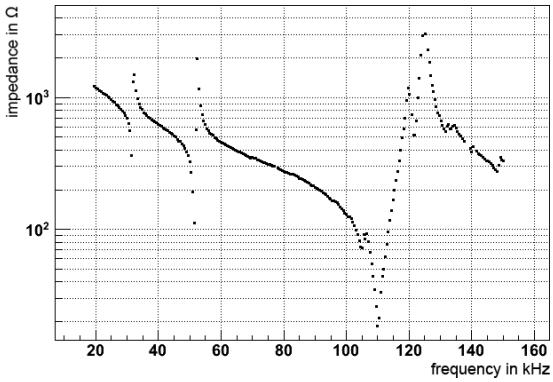

Fig. 27: Impedance measurement of a piezoelectric transducer installed in a nozzle holder unit.

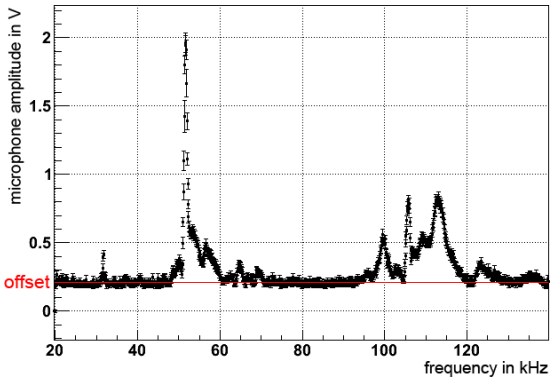

Fig. 28: Acoustic measurement of a complete nozzle holder unit via a microphone. Mechanical vibrations are only observed at certain resonance frequencies corresponding to possible working points of the pellet generator.

During the operation of the pellet target it has been observed that the working frequency for optimum pellet beams has to be changed if the nozzle temperature is varied. This behavior can be explained by the temperature dependence of the mechanical properties of the piezoelectric transducers and by this the expected shift for a certain temperature change can be calculated. To confirm this, impedance measurements have been done for different temperatures and compared to the theoretical predictions (see Fig. 29).

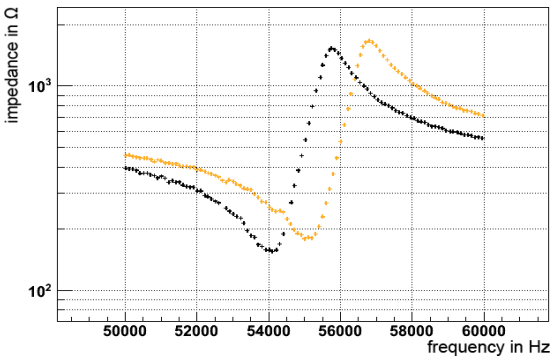

Fig. 29: Impedance measurement of a piezo holder unit for frequencies around 55 kHz at room temperature (18°C, black) and at −5°C (orange). The resonance is shifted by ∼ 1100 Hz which is compatible with the theoretical expectations.

The pellet target is typically operated at nozzle temperatures of about 15 K. Due to this a shift of about 18 kHz towards higher frequencies is expected for the piezo resonances at 55kHz and at 110 kHz, which have been observed in measurements at room temperature. This is in very good agreement with experiment where frequencies in the order of 70 kHz and 128 kHz typically result in nice droplet streams and highest pellet rates. This also holds for frequencies of ∼ 30 kHz which is compatible with the observed resonance of the piezo holder unit.

1.3.2 Spin Filtering at COSY — First Results

The PAX-Collaboration is investigating spin dependent attenuation as a method to produce polarized antiproton beams. In 1993 this method has been shown to work with protons at the FILTEX in Heidelberg. During spin filtering a stored beam suffers spin dependent attenuation by multiple traversing of a polarized internal gas target. More particles of one state than the other are scattered out of the ring acceptance and a polarized beam remains. The theoretical prediction for the difference σ_1 of the two spin dependent cross sections $\sigma_1 = \sigma_{\uparrow\uparrow} - \sigma_{\uparrow\downarrow}$ in pp scattering is plotted versus the kinetic beam energy in Fig. 30.

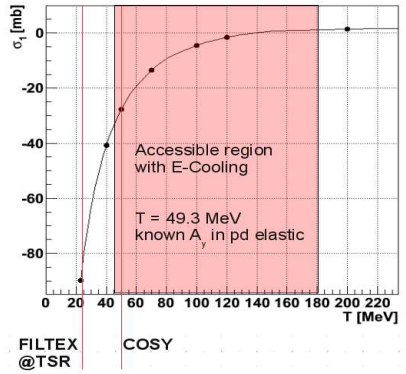

Fig. 30: Theoretical calculations for the spin dependent cross-section $\sigma_1 = \sigma_{\uparrow\uparrow} - \sigma_{\uparrow\downarrow}$.

Experimental Setup In autumn 2011, a spin filtering experiment was performed at Jülich-COSY using a stored proton beam at $T_p = 49.3\,\mathrm{MeV}$. The polarized target and its polarimeter (G. Ciullo et al., J. Phys.: Conf.Ser. **295**, 012150 (2011)) performed smoothly during the whole data taking period. In particular, the density in the target cell was measured through the observed beam deceleration induced by the target gas detected by the Schottky signal and resulted in a value larger than $5 \cdot 10^{13}$ atoms/cm^2 for one injected hyperfine state from the ABS. This value is consistent with expectations calculated from the known ABS flux ($3 \cdot 10^{16}$ atoms/s) and the known conductance of the storage cell. During data taking, the target polarization was continuously monitored by the Breit-Rabi polarimeter and the Target Gas Analyzer, and the value was found to be $Q_y = 0.72 \pm 0.04$ and constant in time. The magnetic field coils mounted at the chamber provided the vertical weak holding field ($B \approx 10\,\mathrm{G}$), required to define the quantization axis for the target polarization. The use of compensation coils in front and behind the main holding field coils allowed for an almost perfect compensation of the beam displacement: when powering the holding field coils no transverse displacement of the beam position could be detected by beam position monitors.

During the 2011 summer shutdown, a new NEG pumping system, designed and constructed in the FZJ mechanical workshops, has been installed below the PAX target chamber and put into operation. The pump has been realized by an array of 10 NEG cartridges. During the activation of the cartridges at a temperature up to 450 °C, a mechanical shutter separating the pump from the chamber was closed (see Fig. 31). In this way, the temperature in the target chamber was limited to less than about 80 °C. By means of a calibrated H_2 gas inlet a pumping of 12000 l/s has been measured, according to design specifications. The use of the pump during COSY operation allowed to achieve a target chamber pressure in the 10^{-10} mbar range without gas load from the ABS and about 10^{-7} mbar with H gas injected from the ABS in one hyperfine state ($3 \cdot 10^{16}$ H atoms/s).

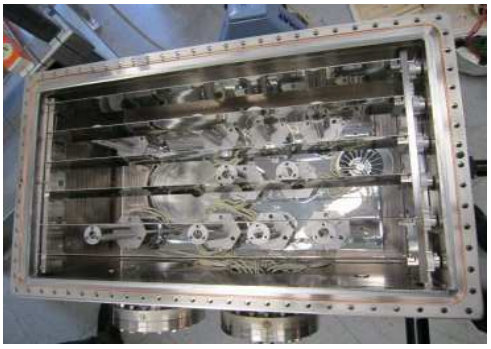

Fig. 31: The NEG pump with the NEG cartridges mounted on the bottom of the chamber; the opened mechanical shutter is clearly visible.

The newly installed NEG pump below the target chamber together with the activation of the neighbouring NEG coated tubes (produced at CERN) provided excellent vacuum conditions in the COSY ring. The combination of the good vacuum and the effect of the low-β section at the PAX interaction point produced a situation in which almost no effect on the beam lifetime could be detected after injection of the polarized gas in the storage cell of the chamber. The same vacuum configuration is planned to be installed at CERN.

The polarization lifetime of the COSY beam has been measured prior to the spin-filtering experiments. The measurement has been performed by injecting a polarized proton beam into COSY and comparing the polarization at the beginning of a fill and after the beam was stored in the ring for 5000 s. The polarization loss during this time amounted to about 5 %, resulting in a polarization lifetime of $(2.0 \cdot 10^5 \pm 5 \cdot 10^4)\,\mathrm{s}$, confirming the prediction that no depolarizing resonances are present in the neighbourhood of the chosen machine tunes. In view of the polarization build-up experiment, the beam polarization lifetime can be considered as infinite. In order to reduce systematic errors, spin-flips of the beam polarization have been introduced at every measurement cycle. The spin-flipper employs a resonant RF-solenoid and is part of the standard equipment of the COSY ring. Before the measurement, the spin-flipper has been tuned to the proper working conditions and its efficiency has been measured in dedicated runs to be $\varepsilon_{SF} = 0.9887 \pm 0.001$.

The beam polarization has been measured by means of the polarimeter at the ANKE interaction point in the op-

posite straight section of COSY. Beam polarimetry has been accomplished by making use of the analyzing power in proton-deuteron elastic scattering. For this purpose two three-layer silicon detectors have been employed to detect elastically scattered particles in the interaction of the stored proton beam and the ANKE deuterium cluster target. Silicon layers of 70, 300, and 5000 μm thickness have been used for the realization of each telescope. The telescopes were symmetrically placed with respect to the target and longitudinally positioned in order to optimize the figure of merit (FOM $= \mathrm{d}\sigma/\mathrm{d}\Omega\, A_y^2$) of the reaction. The energy of the experiment has been chosen to be 49.3 MeV, since at this energy a precise determination of the beam polarization is possible, because accurate analyzing power data are available. Elastically scattered deuterons and protons were clearly identified by the deposited energy in the different layers (see Fig. 32). Due to the low energy of the reaction, no background for deuterons is expected, while some (small) background coming from deuteron breakup is expected for protons.

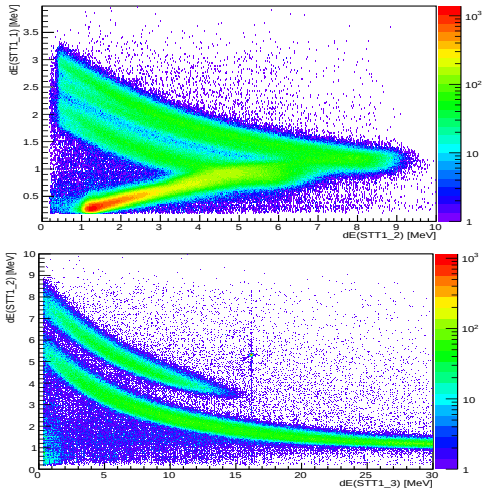

Fig. 32: Proton and deuteron identification using the silicon telescope system. Upper panel: deposited energy in the second *vs* first layer. Lower panel: deposited energy in the third *vs* the second layer.

Spin-filtering measurements The sequence of operations in a spin-filtering cycle is as follows (see Fig. 33):

- The unpolarized proton beam is injected in the COSY ring at 45 MeV. The beam is cooled and accelerated to 49.3 MeV for the measurement. As mentioned already, this energy has been chosen because of the existing data of the analyzing power. The typical number of particles injected and accelerated for every cycle was $(5\ldots12)\cdot10^9$;
- At this point the spin-filtering cycle starts. Polarized gas is injected into the storage cell at the PAX interaction point and the holding field coils are powered. The typical duration of a spin-filtering cycle was 2 beam lifetimes, corresponding to a total spin-filtering time of 16000 s.
- At the end of the spin-filtering period, the PAX polarized target was switched off, and the ANKE deuterium cluster target and the data acquisition of the beam polarimeter were started. During the beam polarization measurement the beam polarization has been reversed twice by using the spin-flipper. This allows the determination of the induced beam polarization for every cycle, thereby reducing systematic errors. The total duration of the polarization measurement was 18500 s;
- Spin-filtering cycles have been repeated for different directions of the target holding fields.

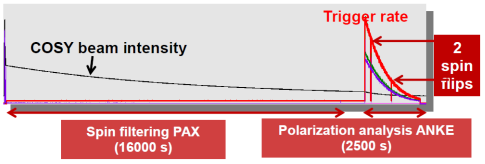

Fig. 33: Picture taken from an online monitor of the COSY control room representing a spin-filtering cycle. At the end of the cycle the trigger rate can be noticed together with the two points in time where the spin flipper was activated.

In order to provide a zero polarization calibration of the detector, a series of cycles without spin-filtering has been carried out in addition. To be as close as possible to the experimental conditions of a standard filtering cycle, the zero-measurement cycle reflected exactly the same sequence of operations, differing only in the number of injected particles ($< 1\cdot10^9$) and the duration of the spin-filtering part (180 s). A total number of 98 cycles of this type have been collected, so that the acquired statistics is twice as large as the one of the spin-filtering measurements.
At the end of the beam time, analysis of the acquired data has started. The analysis is performed by two separate groups in order to cross-check each step, which comprise:
- Calibration of the STT
- Analysis of the “Null”-measurement
- Investigation of systematic errors
- Analysis of the spin-filtering measurements
- Determination of a precise σ_1

Conclusion In the period August to October 2011, the PAX Collaboration has performed a spin-filtering test experiment with protons at the COSY storage ring. All the subsystems of the experimental setup (polarized target, COSY ring and related equipment, beam-polarimeter) worked as expected or even better, like for the vacuum system resulting in beam lifetimes larger than 8000 s. Particularly the new NEG pump system installed below the target chamber was very effective for the achievement of the ideal experimental conditions. A series of spin-filtering cycles has been prepared and successfully accomplished. A careful analysis of the experimental data is ongoing.

2 COSY Operation and Developments

2.1 Beam Time at COSY

For 2011 in total 6888 hours of operation were scheduled. 4760 hours (53.3%) were scheduled for user beam time, 1008 hours (11.3%) were scheduled for dedicated beam dynamic studies, equipment tests for HESR and FAIR related activities, 1120 hours (12.6%) were used for COSY machine development and experimental set-up, see Fig. 34. Maintenance/shutdown duration was 2040 hours (22.9%). The distribution of user hours is listed in Table 4.

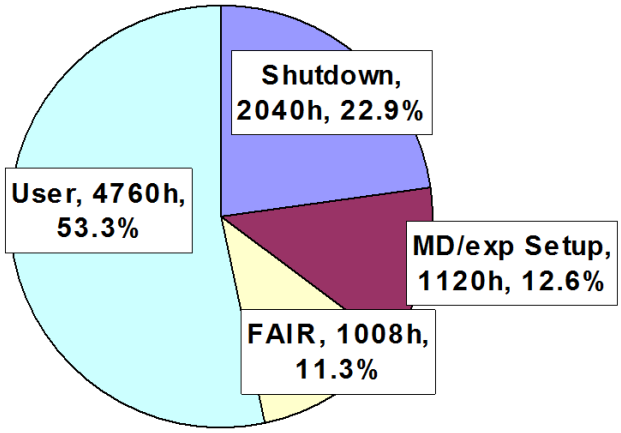

Fig. 34: COSY beam-time statistics in 2011.

Table 4: Overview over COSY user beam time in 2011.

Date	Experiment	Duration	Reaction, experiment #
17.01.–23.01.	EDM	1 week	Studies of the Horiz. Spin Coherence Time, 176.4
07.02.–06.03.	WASA	4 weeks	$pd \rightarrow {}^3HeX$, 208
21.03.–10.04.	ANKE	3 weeks	$pn \rightarrow K^+n\Lambda$, 203
18.04.–24.04.	WASA	1 week	ω-decay in pp, 209
25.04.–01.05.	WASA	1 week	η' in pp, 184.1
23.05.–10.07.	ANKE	7 weeks	PIT, $np \rightarrow (pp)spectator + \pi^-$, 205
05.09.–02.10.	PAX	4 weeks	Filterexperiment PAX, 199.2
24.10.–20.11.	TOF	4 weeks	TOF N^* resonances, 193.2
Total '11		25 weeks	

2.2 Polarization physics with PAX

One of the highlight of the COSY machine operation in 2011 was the successful execution of the polarization build-up measurement for the PAX collaboration. Albeit the beam request for this experiment was very demanding all requirements could successfully be fulfilled. The preparation of the beam time was done in three subsequent machine development weeks, followed by a four week block of data taking. The PAX target consists of a storage cell polarized gas target which is located at the low beta section installed in 2009. The beam size is very small there which allows a narrow storage cell operation yielding a higher target density. As the main goal of the spin filter experiment is to proof and to verify the existence of the polarization build-up of an initially unpolarized beam by interaction with the polarized hydrogen target, which is a very slow process, very long beam lifetimes are essential. Furthermore, high beam intensity is also important since the filtering will be run for several beam lifetimes to get a significant polarization of the beam, and only then the polarization measurement will start. The analyzing powers at 49.3 MeV kinetic energy are known. Therefore the build-up and measurement had to be carried out at this energy. Since the COSY injection is at 45 MeV a small acceleration to 49.3 MeV was set up. The low beta section was in operation already at injection energy and the corresponding four quadrupole magnets were successfully ramped together with the COSY main magnets with beam stored and accelerated for the first time. The beam was electron cooled to achieve a long beam lifetime. The cooler was set up at 45 MeV. After acceleration the high voltage of the electron cooler was adjusted to the experiment energy and the optimization of electron beam steering was carried out. As a result of the required high intensities and strong electron cooling instabilities of the beam occurred visible in strong coherent betatron oscillations. A beam feedback system detecting these oscillations with beam position monitors was applied to suppress the instabilities and the related beam losses with correction kickers (dampers). At 45 MeV the electron cooler has been used to increase the injected intensity by stacking. To reach the high lifetimes the orbit of the COSY beam needed a careful correction. The so called orbit response method for this correction was applied. And last but not least a careful adjustment of the working point of the machine was unavoidable. Systematic effects during the polarization measurements were reduced with a spin flipper which can be used to reverse the polarization of the stored beam. The setup of this device was done with a polarized proton beam from the polarized source of COSY. The machine was switched to polarized beam operation several times during the experiment in order to check the functioning of the spin flipper device. The whole setup of the very complicated experiment was carried out in the foreseen time, and the performance over the four weeks of experiment was exceptional. The intensities at the beginning of the store were always higher than $6 \cdot 10^9$ protons (higher intensities cause instabilities and sudden beam losses in the first few minutes of the store). The beam lifetimes were reproducibly in the order of 8000 s (at lower intensities even longer). The beam was adjusted to the 12 mm size storage cell in the low beta section without any major problems. The low beta section could be successfully ramped from 45 MeV to 49.3 MeV together with the other components of COSY for the first time without affecting the intensity of the stored beam.

2.3 Precise absolute luminosity determination at ANKE/COSY

The ANKE collaboration and the COSY machine crew have jointly developed a very accurate method for determining the absolute luminosity in an experiment at an internal target position. The technique relies on measuring the energy losses due to the electromagnetic interactions of the beam as it passes repeatedly through the thin target and measuring the shift of the revolution frequency by studying the Schottky spectrum. This technique allows one to measure the absolute differential cross section for elastic pp scattering with high precision. How that worked out in a real experiment has been shown at COSY, where the ANKE measurements were conducted using an unpolarised proton beam at eight different beam energies, $T_p = 1.0, 1.6, 1.8, 2.0, 2.2, 2.4, 2.6, 2.8$ GeV, interacting with a hydrogen cluster-jet target (for the cross section results see Sect. 1.2).

In order to extract the cross section for any physical reaction, the absolute value of the luminosity must be determined. Luminosity L relates the cross section σ of a given physical process to its corresponding event rate $R = L \times \sigma$. This shows that, apart from a precise measurement of the reaction, it is necessary to determine the luminosity with high accuracy, which is the process-independent quantity and is completely determined by the number of beam and target particles $L = n_b \cdot n_T$. The measurement of beam intensity (n_B) is a routine procedure for any accelerator and is performed via a high precision Beam Current Transformer (BCT). For the current experiment, the BCT signal was introduced directly in the data stream and recorded together with the detector information, providing the actual beam intensity at any given moment. The target density n_T, is determined via the measurement of the beam-revolution frequency shift caused by the electromagnetic interaction of the beam and target particles. It should be mentioned that this procedure is only valid if the coasting beam is used without cooling (details of this method are discussed in H.J. Stein *et al.. Phys. Rev. ST Accel. Beams* **11** (2008) 052801). This provides the following formula for the target density determination:

$$n_T = \left(\frac{1+\gamma}{\gamma}\right) \frac{1}{\eta} \frac{1}{(\mathrm{d}E/\mathrm{d}x)m} \frac{T_0}{f_0^2} \frac{\mathrm{d}f}{\mathrm{d}t} \qquad (3)$$

Here T_0 and f_0 are the initial values of the beam frequency and energy, and $\gamma = (1-\beta^2)^{-1/2}$ is the Lorentz

factor. All three parameters are precisely measured for every experiment at COSY. Stopping power $\mathrm{d}E/\mathrm{d}x$ and mass m of the target atoms are well known and can be easily obtained *e.g.* from the database of NIST-PML, http://www.nist.gov/pml/data/star. Therefore, in order to deduce absolute values for the target density it is necessary to determine the so-called frequency-slip parameter η and of the beam revolution frequency shift $\mathrm{d}f/\mathrm{d}t$ during the data taking.

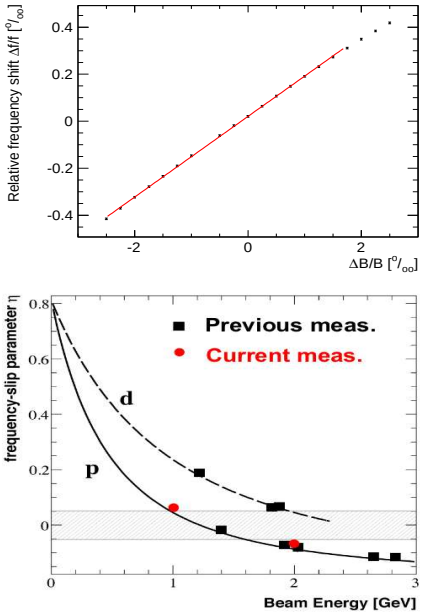

Fig. 35: Upper: Variation of the mean revolution frequency with the field strength in the bending magnets in parts per thousand for 2.0 GeV beam energy. The slope of the fitted straight line yields the value of the momentum compaction factor α from where the η parameter is obtained. Lower: Frequency-slip parameter η as a function of the energy of proton and deuteron beams. The experimental points are the results of ANKE measurements. These are compared with curves corresponding to the predictions of COSY lattice calculations. The shaded area shows the region with $|\eta| < 0.05$ where the error in the energy-loss technique is unacceptably high.

The η parameter can be determined using the following relation:

$$\eta = \frac{1}{\gamma^2} - \alpha, \tag{4}$$

where α is a momentum-compaction factor and can be measured by studying the change of revolution frequency due to change in magnetic field of COSY bending magnets. If the changes are not very large there is a linear relationship between relative revolution frequency shift ($\Delta f/f_0$) and relative change in the field ($\Delta B/B_0$):

$$\frac{\Delta f}{f_0} = \alpha \frac{\Delta B}{B_0} \tag{5}$$

Dedicated COSY cycles were developed to measure the beam revolution frequency while changing the magnetic field in the bending magnets by few parts per thousand. Results of this measurement for 2.0 GeV are presented in Fig. 35, from which the η parameter is determined using Eq. (4). The final value of the frequency-slip parameter for this energy is -0.0700 ± 0.0006. It is seen that for large values of $\Delta B/B_0$ and $\Delta f/f_0$, the relationship is not linear anymore requiring higher order terms in Eq. (5). Fortunately this is only relevant if the frequency shift produced by the target is similarly large, which was avoided by limiting the target density in the experiment. Such settings allow one to determine momentum compaction-factor by fitting only the linear part of the $\Delta B/B_0$ vs $\Delta f/f_0$. This is confirmed by the good agreement between current values of η parameter and theoretical calculations together with our previous measurements. It is important to mention that the η parameter has opposite signs for these two energies, which means that the observed frequency shift during the experiment will have different signs. Figure 36 shows how the Schottky spectra developed during the cycle. Distribution is shifts toward lower values for positive η and moves toward the higher values when η is negative.

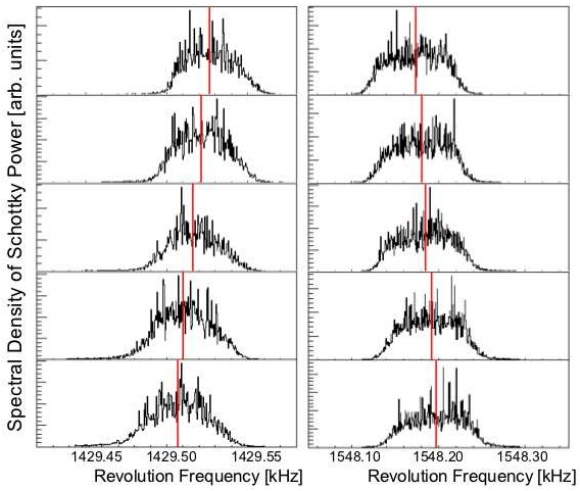

Fig. 36: Schottky power spectra obtained during one 300 s cycle and scaled to harmonic number 1 for 1.0 and 2.0 GeV energy, (left and right column, respectively). Although the data were recorded every 10 seconds, for ease of presentation, only the results from every 70 s are shown, starting from top to bottom. The mean frequencies are indicated by the vertical lines. For a positive η parameter frequency increases through the cycle and *vice versa*

.

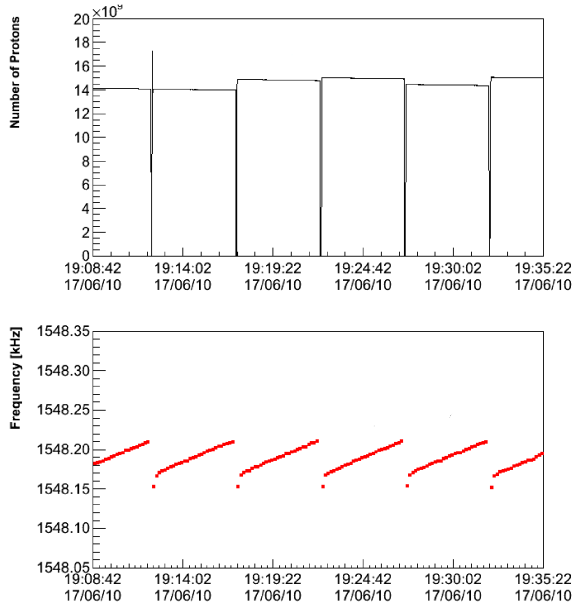

Fig. 37: The BCT particle current n_B, and mean revolution frequency f for a typical machine cycle.

For the final target density determination one has to consider that the observed frequency shift is not only produced by the beam target interaction but also there is a contribution from residual gas in the COSY ring, which should be subtracted. A measurement of this background was performed during special cycles when the ANKE cluster target was on but the beam was steered away from it. In this way it is possible to observe non-target related frequency shifts, which then can be subtracted from the total frequency change (when beam hits the target). During the background measurements, the target has to be switched on, because the target produces additional background in ANKE chamber, which cannot be measured otherwise. The frequency shift caused purely by the target can be presented in this way:

$$\frac{\mathrm{d}f}{\mathrm{d}t}_{target} = \frac{\mathrm{d}f}{\mathrm{d}t}_{total} - \frac{\mathrm{d}f}{\mathrm{d}t}_{bg} \qquad (6)$$

Where $\frac{\mathrm{d}f}{\mathrm{d}t}_{total}$ is the observed frequency shift during the usual measurement and $\frac{\mathrm{d}f}{\mathrm{d}t}_{bg}$ is the frequency shift produced by the residual gas of COSY plus the effect from the ANKE cluster target. Figure 37 shows the typical BCT picture and revolution frequency during the experiment. The target density is determined for each cycle and from that integrated luminosity is deduced. The total accuracy of luminosity determination is roughly 2%, which is mainly defined by the error in the measurement of the η parameter (see Sect. 1.2.5).

2.4 Developments for polarized beams

Another highlight is a new procedure to prevent polarization loss during acceleration of polarized proton beams for a TOF experiment at a beam momentum of 2.7 GeV/c. As demonstrated in the past, electron cooling at COSY injection energy can significantly improve the quality of the extracted beam at the TOF experiment. Unfortunately the strongest imperfection resonance $8 - Q_x/8 - Q_y$ around 2.1 GeV/c leads to a significant polarization loss by additional phase space coupling which was due to the presence of the electron cooler solenoid. As a result the polarization for the experiment was only around 0.6. One setback that was identified is that during these experiments the resonance is encountered in the regular COSY up-ramp. It turned out that in this case no flexibility in fine tuning of the resonance crossing was achievable. In the 2011 TOF beam time the solution was introduced to up an intermediate energy flattop just before the resonances at 2095 MeV/c. At this energy the resonance could then slowly crossed by changing the focusing of the main COSY quadrupoles to increase the horizontal and vertical betatron tunes. This allowed an easy change of the crossing speed. It was now possible to adjust the speed to provide a complete polarization reversal and the polarization after crossing was in the order of 0.75. After crossing the resonance the regular COSY acceleration ramp was continued up to the final momentum.

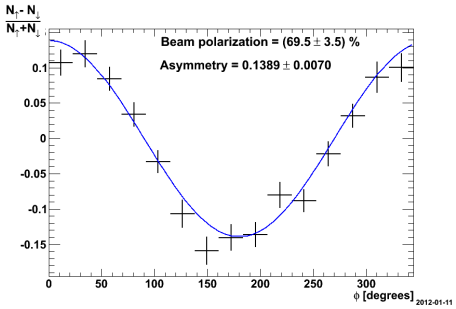

Fig. 38: Asymmetry of elastic scattered protons with beam momentum of 2.7 GeV/c.

Figure 38 shows the asymmetry of elastically scattered protons at 2.7 GeV/c. Both protons are detected with the COSY-TOF spectrometer and the elastic scattering process is separated from multi-pion production by a coplanarity cut and by the calculation of the missing mass. The asymmetry is fitted with a cosine function which gives amplitude of 0.1389 ± 0.0070. Only the angular range in the center-of-mass system of $44 - 56^\circ$ is taken into account, where the proton analyzing power — determined with the SAID Partial-Wave Analysis and weighted with the angular differential cross section — is 0.20. The resulting beam polarization is 69.5% with a statistical error of 3.5%. The slightly reduced polarization at the experiment was caused by a resonance that was crossed just before reaching the final momentum at the reduced ramp rate of the regular COSY acceleration ramp. A complete compensation was therefore not possible.

3 Theoretical Investigations

Introduction

The IKP theory group studies the strong interactions in their various settings — spanning topics in hadron structure and dynamics, the nuclear many-body problem and high-energy Quantum Chromodynamics (QCD). The main focus is on the formulation and application of effective field theories for precision hadron and nuclear physics based on the symmetries of QCD. A shift of focus with more emphasis on high performance computing is presently taking place, spear-headed by the work on nuclear lattice simulations. Within the virtual institute on "Spin and strong QCD" work focuses on applications for physics at COSY and FAIR. Some of the high-lights of these activities are discussed in the following.

3.1 Ab initio calculation of the Hoyle state

Nuclear lattice simulations are a new method to tackle the nuclear many-body problem. They combine the successfully tested few-nucleon forces derived from chiral effective field theory with powerful Monte Carlo methods, that are based on the calculation of the observables on a discretized and finite space-time volume. We have recently completed *ab initio* lattice calculations of the low-energy spectrum of ^{12}C using chiral nuclear EFT. In addition to the ground state and the excited spin-2 state, our calculation finds a resonance with angular momentum zero and positive parity at $-85(3)$ MeV, very close to the ^{4}He+^{8}Be threshold at $-86(2)$ MeV. This is nothing but the Hoyle state. It plays a crucial role in the hydrogen burning of stars heavier than our sun and in the production of carbon and other elements necessary for life. This excited state of ^{12}C was postulated by Hoyle in 1953 as a necessary ingredient for the fusion of three α-particles to produce carbon at stellar temperatures. For this reason, the Hoyle state plays also a very important role in the context of the anthropic principle, although such considerations did not play any role when this state was predicted. The Hoyle state has been an enigma for nuclear structure theory since decades, even the most successful Greens function MC methods based on realistic two- and three-nucleon forces or the no-core-shell-model employing modern interactions have not been able to describe this state. As seen in Fig. 39, the NNLO results for the Hoyle state and spin-2 state are in agreement with the experimental values. While the ground state and spin-2 state have been calculated in other studies, these results are the first *ab initio* calculations of the Hoyle state with an energy close to the phenomenologically important ^{8}Be-alpha threshold. Experimentally the ^{8}Be-alpha threshold is at -84.80 MeV, and the lattice determination at NNLO gives $-86(2)$ MeV. We also note the energy level crossing involving the Hoyle state and the spin-2 state. Note that the orientation bias in our initial state ensemble leads to the splitting of the $J_z = 0$ and $J_z = 2$ components of the spin-2 excited state. The Hoyle state

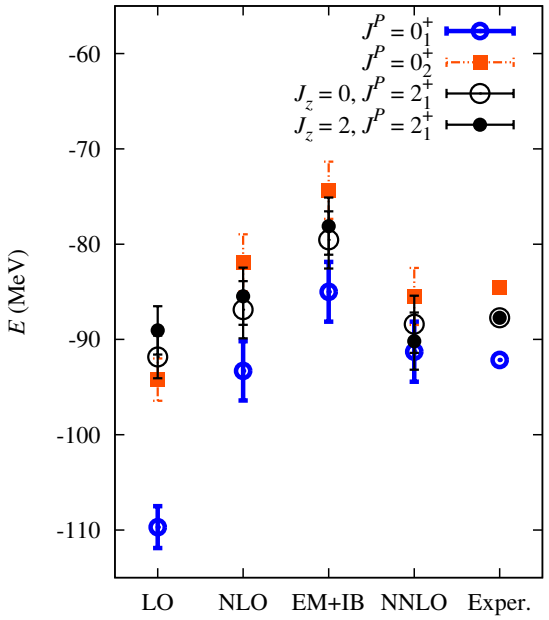

Fig. 39: Spectrum of ^{12}C and comparison with experiment. For each order in chiral EFT labeled on the left. results are shown for the ground state (blue circles). the Hoyle state (red squares) and the $J_z = 0$ (open black circles) and $J_z = 2$ (filled black circles) projections of the lowest-lying spin-2 state. LO: leading order, NLO: isopin-symmetric next-to-leading order, EM+IB: Coulomb and strong isospin-breaking effects at NLO, NNLO: next-to-next-to-leading order.

is lower in energy at LO but higher at NLO. One of the main characteristics of the NLO interactions is to increase the repulsion between nucleons at short distances. This has the effect of decreasing the binding strength of the spinless states relative to higher-spin states. We note the 17 MeV reduction in the ground state binding energy and 12 MeV reduction for the Hoyle state while less than half as much binding correction for the spin-2 state. This degree of freedom in the energy spectrum suggests that at least some fine-tuning of parameters is needed to set the Hoyle state energy near the ^{8}Be+^{4}He threshold. It would be very interesting to understand which fundamental parameters in nature control this fine-tuning. At the most fundamental level there are only a few such parameters, one of the most interesting being the masses of the up and down quarks. Such investigations have already been performed to unravel the quark mass dependence of the deuteron binding energy and of the S-wave nucleon-nucleon scattering lengths. We are presently investigating the ^{12}C spectrum and the closeness of the Hoyle state to the ^{8}Be+^{4}He threshold as a function of the quark masses.

3.2 Finite volume effects in the reconstruction of the $\kappa(800)$ resonance

With the rapid progress in Lattice QCD simulations, the scalar meson resonances start to become into reach. These states have been under intense theoretical investigation as they represent the lightest, yet very broad excited states whose properties and nature are directly connected to chiral symmetry, the fundamental symmetry underlying the strong interactions. The strangeness $S=-1$, $\kappa(800)$ resonance is of particular interest because it does not mix with scalar glueballs and is thus expected to reveal itself with a clear signal.

It is indispensable to estimate the required precision of lattice data that allows for a clear-cut resonance extraction. For this, we have performed an analysis of the error propagation from lattice data to phase shifts and pole position of the light scalar resonances. In the absence of actual lattice data, the lattice levels are generated using Unitarized Chiral Perturbation Theory including next-to-leading-order terms. Fitting just a few low-energy constants to the experimental data, a good description of meson-meson partial waves, including the occuring resonances, can be obtained. The pseudo-lattice data predicted with this solution provide thus a realistic picture of what can be expected in forthcoming lattice simulations. Assigning errors to the pseudo-data, the infinite volume limit with uncertainties on phase shifts and pole positions can be reconstructed. We have developed appropriate extensions of the Lüscher formalism that allow to make this connection in the one- or two-channel case, the latter enabling also the analysis of near-threshold resonances as the $f_0(980)$ or $a_0(980)$. The key lies here in the explicit inclusion of the (model-independent) lowest order chiral interaction V_2 in the potential $V^{\rm fit}$ that is fitted to the pseudo lattice-data stabilizing considerably the extraction. The potential is expanded in powers in the scattering energy (cf. (s^0), (s^0,s^1), $\cdots$ fits shown in Fig. 40). It should be stressed that the current choice of the fit potential is model-independent in the sense that it makes no assumptions on the existence of a resonance. Thus, it is the data themselves that will or not generate resonance poles. For the κ, the reconstructed pole positions are shown in Fig. 40.

Expansions to too low order in s return a false pole position and moreover far too small uncertainty areas. The fit strategy, for the case when the actual pole position is unknown, is thus to expand $V^{\rm fit}$ until the pole position does not change anymore and take the corresponding uncertainty as the final result. In the present case, this would be the area of the (s^0,s^1,s^2) fit as indicated in the figure. The precision of the lattice data to produce the uncertainties shown in Fig. 40 is $\Delta E=2$ MeV (5 MeV for the hatched area) which is rather high. Thus, the model-independent determination of the κ — and, similarly, of the $\sigma(600)$ — is demanding. To put these results into context, the analog analyses of the $\rho(700)$ and the $K^*(892)$ reveal that for these P-wave resonances the extraction of the infinite volume limit is much easier, because the first level lies already in the resonance region, the resonances are narrower, and convergence can already be observed for the (s^0,s^1) fit. In summary, the present method can serve to model-independently extract phase shifts and resonance properties, stabilized by the chiral expansion.

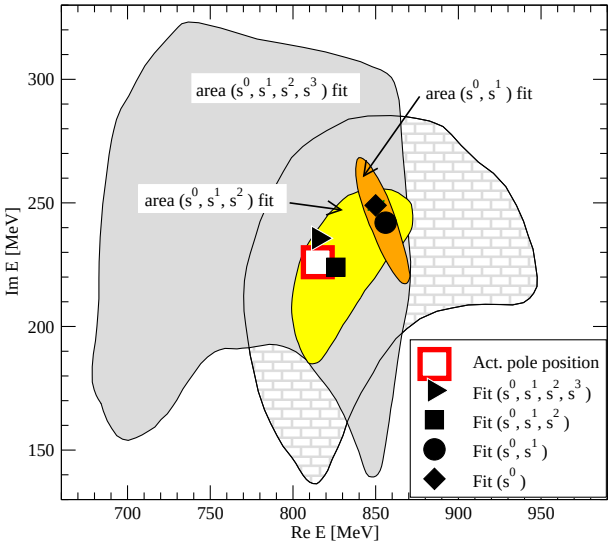

Fig. 40: Pole reconstruction of the $\kappa(800)$. The actual pole position is obtained from a global fit to meson-meson scattering data.

3.3 The H-dibaryon in light of chiral effective field theory

In 1977 Jaffe predicted a deeply bound 6-quark state with strangeness $S=-2$, isospin $I=0$, and $J^P=0^+$ from the bag-model, called the H-dibaryon. Subsequently, many experimental searches for the H-dibaryon were carried out, but so far no convincing signal was found. However, recently evidence for a bound H-dibaryon was claimed based on lattice QCD calculations by the NPLQCD and HAL QCD Collaborations. Extrapolations of the simulations, performed for pion masses $M_\pi \gtrsim 400$ MeV, to the physical mass suggest that the H-dibaryon could be either loosely bound or move into the continuum.

We analyzed various issues related to these lattice results in the framework of chiral effective field theory for the baryon-baryon (BB) interaction at leading order in the Weinberg counting. This scheme has proven successful for the few data on hyperon-nucleon scattering and also for the bounds that exist on the BB interactions with strangeness $S=-2$. One of the occuring low-energy constants, corresponding to the SU(3) flavor-singlet channel, which contributes in the $S=-2$ sector but is not constrained by any presently available data can be fine-tuned to produce a bound H with a given binding energy so that one can examine its properties.

One of the aspects that can be studied in this framework is the quark mass dependence (which is synonymous to the

pion mass dependence because of the Gell-Mann-Oakes-Renner relation) of the binding energy of the H dibaryon. Another important question to be addressed here is how this quark mass dependence is affected when the SU(3) breaking manifested in the masses of the octet baryons is accounted for. In the real world the BB thresholds are not degenerate but they all differ for the relevant $\Lambda\Lambda$, $\Sigma\Sigma$ and ΞN systems.

The results of our study can be summarized as follows:

(1) We find that an assumed loosely bound H dibaryon in the $^1S_0$ partial wave of the coupled $\Lambda\Lambda - \Xi N - \Sigma\Sigma$ system shows a very different behavior than the deuteron, the well-known loosely bound state in the neutron-proton $^3S_1$ channel. In fact, any attraction supplied by the flavor-singlet channel contributes with a much larger weight to the ΞN interaction than to $\Lambda\Lambda$, according to SU(3) flavor symmetry, so that the H-dibaryon should predominantly be a ΞN bound state.

(2) We observe that, for pion masses below 400 MeV, the binding energy of the H is linearly decreasing with decreasing pion mass. In particular, a H binding energy adjusted to the value found by the NPLQCD Collaboration at $M_\pi = 389\,\mathrm{MeV}$ ($E_H = -13.2\,\mathrm{MeV}$), is reduced by 7 MeV at the physical pion mass, cf. the dashed curve in Fig. 41. For larger pion masses, this dependence is weakened. A loosely bound H dibaryon with $E_H = -1.87\,\mathrm{MeV}$ at the physical point shows a very similar pion mass dependence (solid line).

(3) We detect a much more drastic effect caused by the SU(3) breaking related to the values of the three thresholds $\Lambda\Lambda$, $\Sigma\Sigma$ and ΞN. For physical values the binding energy of the H is reduced by as much as 60 MeV as compared to a calculation based on degenerate (*i.e.* SU(3) symmetric) BB thresholds. Translating this observation to the situation of the calculation by the HAL QCD Collaboration, we see that the bound state has disappeared at the physical point. For the case of the NPLQCD calculation, a resonance in the $\Lambda\Lambda$ system might survive.

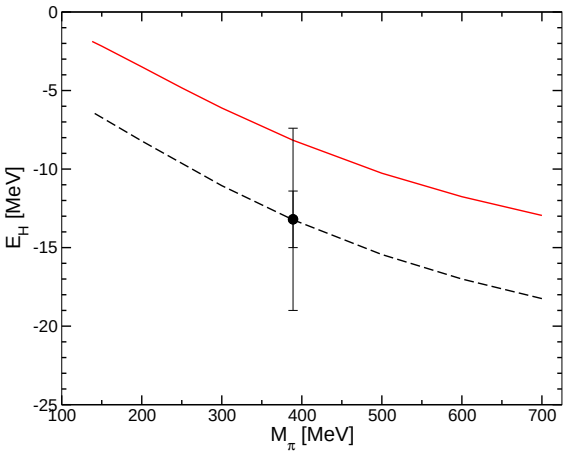

Fig. 41: Dependence of the binding energy of the H-dibaryon on the pion mass M_π. The solid curve correspond to the case where the low-energy constant is fixed such that $E_H = -1.87\,\mathrm{MeV}$ for physical masses while for the dashed curve the constant is fixed to yield $E_H = -13.2\,\mathrm{MeV}$ for $M_\pi = 389$ MeV so that it coincides with the NPLQCD lattice calculation (circle).

3.4 Theoretical analysis of $\eta/\eta' \to \pi\pi\gamma$

Radiative decays are known to be very sensitive tools to explore decay mechanisms. Especially, when studied together with two hadrons as decay products, they allow to adjust the invariant mass of the two-hadron system via a variation of the photon energy without interference of strong three-body final state interactions. We here present a new method to analyze model–independently decays with $\pi\pi\gamma$ final states, where soft bremsstrahlung does not occur and where the pion pair is of invariant mass square below the first *significant* $\pi\pi$ inelasticity. In the (iso)vector case, the latter is given by the $\omega\pi$ threshold. For the η and η' decays studied here, the pion pair appears in an isovector p-wave, and we confine ourselves to only this partial wave in what follows.

The method is based on the observation that the transitions at hand can be split into two parts: a universal one governed by the $\pi\pi$ final-state-interactions and a reaction-specific one, which we assume to be perturbative. The former, which is known to be non-perturbative, especially in the kinematic region relevant for the η' decays, can be related to the pion vector form factor using unitarity and analyticity. The latter is the quantity of interest. We may therefore write for both decays

$$\frac{d\Gamma}{ds_{\pi\pi}} = |A\,P(s_{\pi\pi})\,F_V(s_{\pi\pi})|^2\,\Gamma_0(s_{\pi\pi})\;,$$

where $\Gamma_0(s_{\pi\pi})$ contains known kinematic factors. Here left-hand cuts are suppressed both kinematically as well as chirally. We may therefore expand the function $P(s_{\pi\pi})$ in a Taylor series around $s_{\pi\pi} = 0$ and write for the η decay

$$P(s_{\pi\pi}) = 1 + \alpha s_{\pi\pi} + \mathscr{O}\left(s_{\pi\pi}^2\right)\;,$$

and analogously with α replaced by α' for the η'. Since the pion vector form factor is known to very high accuracy from measurements at KLOE, SND, and BaBar, the only unknowns in the above equations are the normalization factors A and A' and the shape parameters α and α'. An excellent fit can be achieved as can be seen from Figs. 42 and 43 for the η and η' decay, respectively, with

$$\begin{aligned} \alpha &= (1.96 \pm 0.27 \pm 0.02)\mathrm{GeV}^{-1} \quad \text{and} \\ \alpha' &= (1.80 \pm 0.49 \pm 0.04)\mathrm{GeV}^{-1}\;, \end{aligned}$$

where the first (second) uncertainty reflects the statistical uncertainty of the data (originates from the pion vector form factor). One might wonder about the contribution from $\rho - \omega$ mixing: in Fig. 43 the thin green line shows this effect under the assumption that the mixing here comes with the same strength as in the pion vector

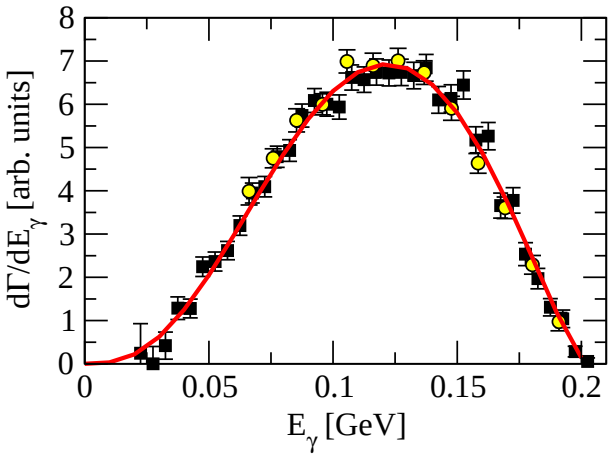

Fig. 42: Fit to the data on $\eta \to \pi^+\pi^-\gamma$.

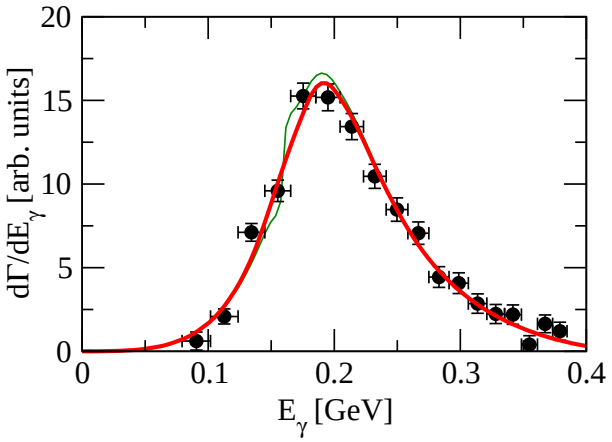

Fig. 43: Fit to the data on $\eta' \to \pi^+\pi^-\gamma$. The thin green line indicates a possible signal from $\rho - \omega$ mixing.

form factor — this might well be a gross overestimation, since the quark model predicts a reduction factor 1/9 between the two reactions. Clearly the data are not yet accurate enough to decide, if $\rho - \omega$ mixing is relevant in the η' decays or not.

In a next step the effective parameters can be matched to one-loop chiral perturbation theory. From this analysis it follows that, when keeping terms leading in N_c only, the slope parameters for the η and the η' decay are to be the same, consistent with our findings. This supports our hypothesis that the function $P(s_{\pi\pi})$ can be treated perturbatively.

To summarize we presented a general parameterization for data for the reactions $\eta\prime/\eta \to \pi\pi\gamma$ in terms of two parameters only. These parameters can be interpreted exploiting the chiral properties of the transition amplitudes. In fact, by invoking large N_c arguments together with chiral Ward identity constraints half of the empirical values for the slope parameters can be related to the pion radius, indicating that only half of their values are truly reaction.

3.5 Exotic Z_b states as hadronic molecules

In addition to the quark-antiquark mesons and triple-quark baryons, it is generally believed that QCD allows the existence of exotic hadrons. However, there are rare appealing evidences for the exotics, mainly because most of the candidates have the same quantum numbers as conventional hadrons and hence difficult to be identified. Therefore, the observation of two charged resonances in the bottomonium mass region, $Z_b^{\pm}(10610)$ and $Z_b^{\pm}(10650)$, by the Belle Collaboration deserves in-depth studies. Both Z_b states were observed in five channels, $\Upsilon(1S,2S,3S)\pi$ and $h_b(1P,2P)\pi$. Their quantum numbers are $I^G(J^P) = 1^+(1^+)$. With Breit-Wigner parameterizations, the masses were reported to be 10607.2 ± 2.0 MeV and 10652.2 ± 1.5 MeV, which marginally coincide with the $B\bar{B}^*$ and $B^*\bar{B}^*$ thresholds, 10604.6 ± 0.6 MeV and 10650.2 ± 0.8 MeV, respectively. Being so close to the $B^{(*)}\bar{B}^*$ thresholds, it is reasonable to assume that both states are S-wave hadronic molecules, *i.e.*, states generated from the interaction between bottom and anti-bottom mesons. We further assume that their masses are below the corresponding thresholds, so that model-independent relation between the renormalized coupling constant $z^{\rm eff}$ and binding energy $\mathscr{E} \equiv M_{Z_b} - M_{B^{(*)}} - M_{B^*}$ can be derived as

$$(z^{\rm eff})^2 = \frac{8\pi}{\mu^2}\sqrt{-2\mu\mathscr{E}},$$

where μ is the reduced mass of the bottom and anti-bottom mesons.

Based on a nonrelativistic effective field theory which has a power counting in terms of the velocity of the intermediate heavy mesons, we calculated the decays of the $\Upsilon(5S)$ into $h_b\pi\pi$ and $h_b(2P)\pi\pi$ through intermediate Z_b states. Being hadronic molecules, the Z_b states should couple to any other fields through intermediate bottom and anti-bottom mesons. However, for the $\Upsilon(5S)Z_b\pi$ vertex, it is found that the one-loop diagrams are highly suppressed. Power counting of two-loop diagrams were performed, and we found that a certain type of two-loop diagram may be of similar size or even larger than the one-loop ones. Without doing explicit two-loop calculations, we approximate the $\Upsilon(5S)Z_b\pi$ vertex by a contact term. Such a contact term can as well originate in a subdominant compact component of the Z_b wave function. Fortunately, the $Z_b h_b \pi$ vertex is dominated by the bottom meson loops, and hence allows a nontrivial test of the hadronic molecular picture.

The decays $\Upsilon(5S) \to h_b\pi^+\pi^-$ and $h_b(2P)\pi^+\pi^-$ are observed to be completely dominated by the two Z_b states. Therefore, we make a fit to the measured invariant mass spectra of $h_b\pi$ and $h_b(2P)\pi$. The best fit, shown in Fig. 44, was obtained with $\chi^2/\text{d.o.f.} = 54.1/22 = 2.45$. In this way, we demonstrated that the data allows the Z_b masses to be smaller than the corresponding bottom meson–anti-bottom meson thresholds. The binding energies resulting from the fit turn out to be very small, espe-

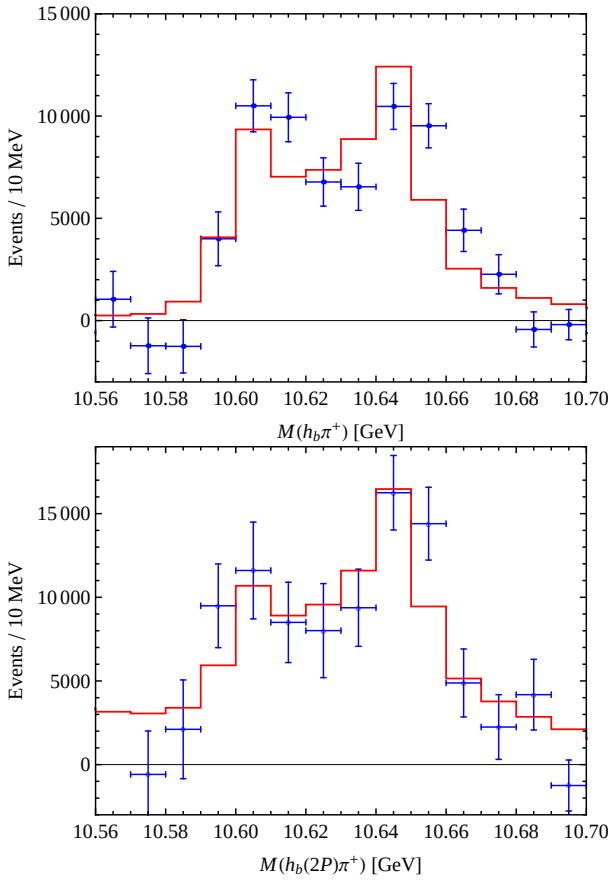

Fig. 44: Comparison of the calculated invariant mass spectra of $h_b\pi^+$ and $h_b(2P)\pi^+$ with the measured missing mass spectra $MM(\pi)$.

cially the one for the higher state Z_b',

$$\mathscr{E}_{Z_b} = -4.7^{+2.2}_{-2.3}\ \text{MeV}, \qquad \mathscr{E}_{Z_b'} = -0.11^{+0.06}_{-0.14}\ \text{MeV}\ .$$

This study gives further crdit to the assunmption that the two Z_b states may be considered as S-wave loosely bound states of the $B^{(*)}\bar{B}^*$, even though the reported masses are lightly above the thresholds. Data with better quality are very welcome in order to make firmer statements.

3.6 Nuclear matter based on chiral few-nucleon forces

A theoretical approach to nuclear matter based on the two- and three-nucleon interaction derived from effective field theory by Epelbaum, Glöckle, and Meißner has been developed, employing non-relativistic many-body theory. Whereas traditional two-nucleon forces have a strongly repulsive core at short distances, the modern chiral interactions incorporate the physics at large momentum scales into the low energy constants and employ universal regulator functions. As a consequence, large momentum transfers between the interacting nucleons are suppressed, a feature which allows to use perturbation theory for nuclear matter. A major effect of the nuclear medium is the blocking of occupied intermediate

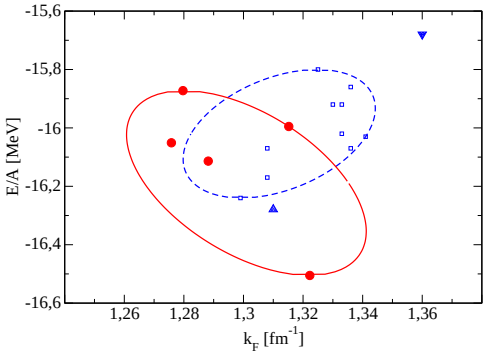

Fig. 45: Saturation points of nuclear matter. Downward triangle (blue): Bethe's estimate, upward triangle (blue): liquid drop model(Möller, Myers, Swiatecki, and Treiner), rectangle (blue): microscopic mean-field approaches, circles (red): present approach.

state due to the Pauli principle. We adopt the expansion scheme proposed by Baker in 1971 which is based on the R-matrix, *i.e.* the solution of the Lippmann-Schwinger integral equation for nucleon-nucleon scattering incorporating Pauli blocking of the intermediate states. The binding energy of nuclear matter is obtained as a perturbative expansion based on the R-matrix and eventually many-body forces. Alternatively, one can use renormalization group techniques to obtain a universal interaction for low momenta, commonly called V_{low-k}. In approaches of this kind, the connection with the counting scheme of effective field theory is not obvious, however. At order NLO, there are no three-body forces and saturation occurs at densities far above the empirical saturation density. In Fig. 45, we show the saturation points of nuclear matter obtained in the present formalism for each of the five two-nucleon interactions obtained at order N^{2}LO by Epelbaum and collaborators (red circles). These interactions employ different cut-offs for the regulator function. The binding energies per particle scatter between -15.8 MeV and -16.6 MeV, while the Fermi momenta are contained in the interval ranging from $k_F = 1.27$ fm^{-1} to $k_F = 1.33$ fm^{-1}. If one wants to reduce this uncertainty, one has to increase the order of the chiral expansion. Microscopic calculations employing empirical interactions need approximately ten parameters to reproduce both the binding energies and the charge distributions of finite nuclei. The interactions which give the minimal chi-squared fits of the known stable nuclei have been used to obtain the saturation points of nuclear matter (blue squares) and an ellipse has been added to guide the eye. By inspection one finds that the saturation points obtained by the present calculation based on the N^{2}LO interaction (circles) overlap with the empirical ones. This is quite an encouraging result, given that we have not performed a fine-tuning of the input parameters.

4 Developments for the HESR

4.1 Beam Dynamics and Operating Cycle

For the HESR lattice an optics setting has been developed with $\gamma_{tr} = 6.2$ which is optimized for accumulation at injection energy (momentum and geometric acceptance, efficient stochastic cooling). This setting is suitable for momenta below injection energy and for momenta above 8 GeV/c. In the momentum range between 3.8 GeV/c and 8 GeV/c a quadrupole setting with $\gamma_{tr} = 13$ will be used. Changing from one setting to the other is possible accepting small tune variations (RF off). At final momentum beam diameters at electron cooler and/or target can be adjusted to the desired values. Presently the correction schemes for orbit deviations and for chromaticity compensation are being revised taking into account recent changes in the dipole and quadrupole magnet design.

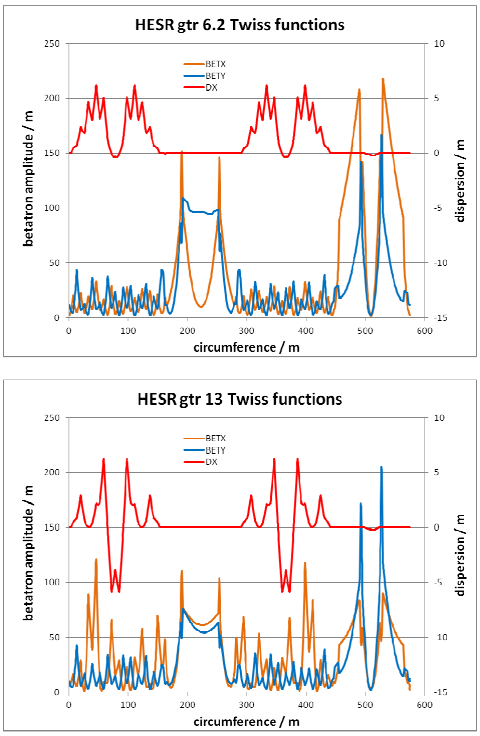

Fig. 46: Twiss functions for HESR for standard optics (top) and for medium momentum optics (bottom). See text for details.

4.2 Injection and Accumulation

At FAIR pbars are produced in the antiproton production target with a rate of some 10^7 $\bar{p}/s$. These particles are then captured and transferred to the collector ring CR with large aperture. Every 10 seconds 10^8 cooled pbars are ready for kicker injection into HESR in which they are accumulated for about 1000 s or 100 injections. Using an RF barrier the circulating particles will be confined to one half of the circumference of HESR, and the fresh pbars will be injected into the empty half of the ring. Afterwards the barrier between both bunches will be lowered thus merging both bunches into one. Longitudinal cooling will limit the momentum spread to acceptable values. The numerical calculations were adapted to the details of the injection kicker magnet design.

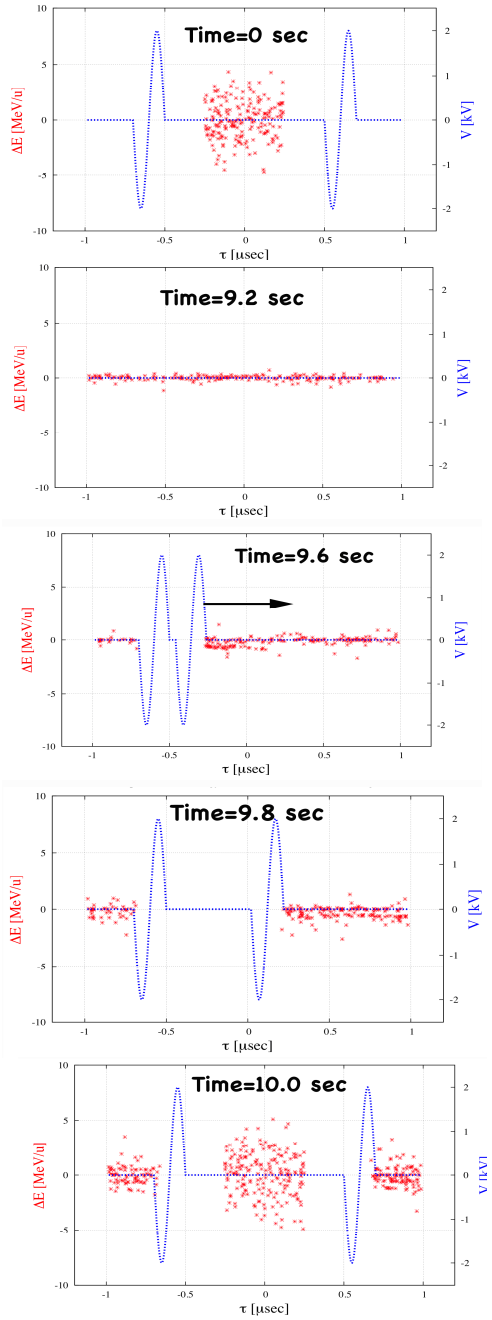

Fig. 47: First cycle of antiproton accumulation with a moving barrier. At $t = 9.5$ s the initially overlapping two barrier pulses are created. One barrier is then moved in the direction as indicated by the arrow. During the barrier motion the beam is compressed to provide new space for injection. The second batch is injected at $t = 10$ s. Barrier shapes and bunch lengths are adapted to the design of the HESR injection equipment.

The kicker current will rise from 0 to about 6000 A within 250 ns and stays constant for 500 ns. Fall time again is 250 ns. The typical timing is sketched in Fig. 47. To gain confidence in the accumulation simulation results (*cf.* H. Stockhorst et al., Status of stochastic cooling predictions at the HESR, Proc. of IPAC11, San Sebastian, Spain) and to prove the reliability of the method a Proof-Of-Principle (POP) experiment has been successfully carried out in collaboration with the GSI Darmstadt (*cf.* M. Steck *et al.*, Demonstration of Longitudinal Stacking in the ESR with Barrier Buckets and Stochastic Cooling, Proc. of COOL11, Alushta, Ukraine).

A possible design for the injection hardware has been developed: (i) injection dipole, (ii) septum magnet, (iii) kicker magnet with power supply. These devices are required for the given injection geometry and particle properties provided by CR. As an example first design drawings for the injection kicker magnet are presented in Fig. 48.

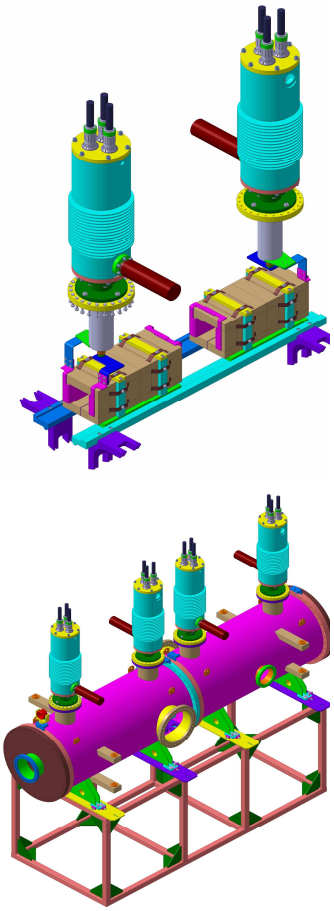

Fig. 48: Possible kicker magnet design: Ferrite magnets, support structure and high voltage feed-through with resistor and capacitance (top), vacuum tank with assembly access and pumping port (bottom). For geodetic purposes both tanks can be treated as one device.

4.3 Magnet Development

Taking into account the Twiss functions of HESR for the revised ion optics and the accumulation task of HESR the iron shapes of dipole and quadrupole magnets were revised. Results from previous estimations of the dynamic aperture of HESR were included. To guarantee good field quality up to 1.7 T a gap in the iron close to the pole face is required, see Fig. 49. Calculations were carried out on the basis of 3D models.

Fig. 49: Quarter of dipole iron yoke with Purcell gap above the beam centre. The white rectangle is the area of the coil. The white quarter of a disc is part of the beam cross section.

Table 5: Calculated integrated multipole coefficients of the bent dipole magnet for 4 excitations.

B / T	0.17	0.42	1.0	1.7
b_1: 2-pole	10000	10000	10000	10000
b_2: 4-pole	1.00	0.50	0.29	0.12
b_3: 6-pole	-0.92	-0.96	-1.09	-1.28
b_4: 8-pole	-0.04	-0.02	-0.01	0.00
b_5: 10-pole	0.12	-0.13	-0.27	-1.27
b_6: 12-pole	0.01	0.01	0.01	0.01
b_7: 14-pole	-0.00	0.00	-0.01	0.02
b_8: 16-pole	0.00	0.00	-0.00	0.00
b_9: 18-pole	-0.01	0.01	-0.01	0.00
b_{10}: 20-pole	0.00	0.01	0.01	0.00

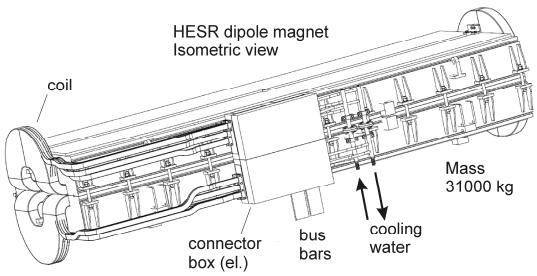

Fig. 50: Cut-out of one of the technical drawings of the HESR dipole magnet showing an isometric view of the assembled magnet.

For the quadrupole magnets an optimization similar to the one for the dipole magnets will be performed. Sex-

tupole and steerer magnets are developed and manufactured in close collaboration with INCDIE ICPE-CA in Bucharest. This institute is coordinating all Romanian involvements into HESR. These involvements cover a substantial amount of the Romanian in-kind contribution to FAIR. For all magnets which are required for HESR operation the details have been specified and technical drawings as a basis for the tendering process have already been prepared.

4.4 RF

Two identical cavities are needed for the accumulation scheme and for acceleration. They will be operated with optimized low level control to allow moving barrier bucket (BB) operation. A frequency range from 0.4 to 10 MHz is sufficient for revolution frequencies between 440 and 520 kHz and operation up to the 20th harmonics. Voltages of $\pm$2500 V are needed during accumulation (BB-frequency: 5 MHz, 1:10 pulsed, moving barrier by 2nd cavity); acceleration can be accomplished with $\pm$1000 V cw dual harmonic operation; during the experiment phase a barrier bucket voltage of $\pm$1000 V cw at 2.5 MHz is sufficient. Per cavity 12 ferrite cores with forced air cooling shall be used. The combination of two cores connected to one amplifier provides the best matching condition for all operation modes and allows the use of semiconductor amplifiers with moderate RF-power. The fabrication of the two 1.2 m long cavities and the special air jet disks is about to start in-house.

4.5 Stochastic cooling

The main system of the HESR stochastic cooling (SC) system will operate in the frequency range from 2–4 GHz (*cf.* H. Stockhorst *et al.*, Stochastic Cooling for the HESR at the FAIR Facility, Proc. of PAC09, Vancouver, Canada). In total, 5 SC-tanks will be installed, each tank housing 64 slot coupler rings and each ring is coupled out by eight electrodes (*cf.* R. Stassen *et al.*, Recent developments for the HESR stochastic cooling system, Proc. of COOL07, Bad Kreuznach, Germany). Two tanks will be used as pickups, each cryogenically cooled by two cold heads on top of the tank. Support bars and rings connect the combiner-boards with the second stage of the cryopumps. Thus the lowest temperature of about 20 K will be found at the Wilkinson resistors which are the main noise sources.
Each pickup will be used to detect the signals of all three cooling planes (horizontal, vertical and longitudinal). The 16:1 combiners join the electrodes in beam direction, while the 2:1 combiners join neighboring electrode-rows to get the upper, lower, right and left signals for the transverse cooling. These combiners are designed as a heat trap for the heat flow coming from the RF lines. The inner part of one pickup tank including all combiner-boards is shown in Fig. 51. The design phase of the pickup tanks is now in the final stage and production is about to start.

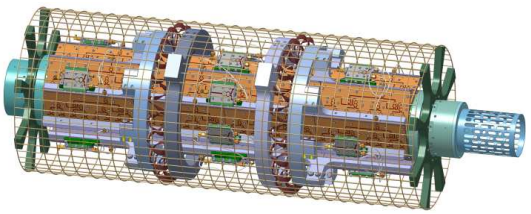

Fig. 51: Inner part of one pickup tank with combiner-boards and support bars for the cryogenic connections.

The kicker-tank layout will be similar to the pickup-tank layout except that no cryogenic cooling system will be installed and the electrode combination within the tank and thus the number of feed troughs will be adjusted according to the RF power needed for the new accumulation scheme (*cf.* T. Katayama *et al.*, Beam accumulation with barrier voltage and stochastic cooling, Proc. of IPAC10, Kyoto, Japan). Three tanks will be installed, one for each cooling plane. Nevertheless all tanks will be fully equipped to ensure that each tank can be used for any cooling plane. This gives a good compromise to meet the necessary phase advance at the different foreseen optics. During accu-mulation all tanks can be used for longitudinal cooling if more RF power is needed. A relay-matrix will be used to switch between the different operating modes. This concept requires an installed RF power of about 250 W for each transverse cooling direction at each tank, or 500 W per tank when used for longitudinal cooling (*cf.* R. Stassen *et al.*, The Stochastic Cooling System of HESR, Proceedings of Cool11, Alushta, Ukraine).

4.6 Vacuum

To characterize the longest section of the HESR beam pipe without pumping ports a test bench has been set up. It images exactly the installations in one typical vacuum "unit cell" between the middle of two neighbouring dipole magnets. Different pumping scenarios can be studied with this installation to determine the optimum pumping power needed in each operating mode. The first result is that in the middle of the 4.2 m long dipole magnet an equilibrium pressure of $7 \cdot 10^{-11}$ mbar has been achieved without special surface treatment. Furthermore, chain clamps from different vendors have been checked whether they could be useful to connect CF flanges of the HESR beam pipe (vacuum tightness under mechanical stress). These chain clamps are necessary because of the tight assembly situation in the HESR arcs.

4.7 PANDA integration

Two dipole magnets have been specified which are required to form the PANDA chicane together with the PANDA dipole magnet which is under the responsibility of the PANDA collaboration. Core parameters of the solenoid to compensate the beam rotation introduced by the PANDA solenoid have been fixed. The associ-

ated tune shift can be compensated by retuning HESR quadrupole magnets. The interaction between the antiproton beam and the residual gas in HESR gives rise to the production of positively charged ions. These ions are trapped in the negative potential well of the antiproton beam. In a dedicated report the adverse effects of ion trapping like tune shifts, tune spreads and coherent instabilities are reviewed (*cf.* F. Hinterberger, Ion Trapping in the High-Energy Storage Ring HESR, JÃ¼l-4343 (2011)). Actions to mobilize and finally remove the trapped ions are discussed there.

4.8 Project Issues

For all devices to be installed in HESR the detailed specifications have been documented. Technical planning is synchronized with the architects on a regular basis. The relevant documents for the radiation protection section of the building permit have been submitted to the authorities. A quality management on the basis of DIN EN ISO 9001 has been implemented and is being synchronized with the one at FAIR. Physics experiments which are severely delayed due to the modularization of the FAIR project are checked whether an earlier start of these experiments at the HESR is possible. In this context investigations to use the HESR for an operation with heavy ions have been launched.

4.9 Day-one experiment at HESR

The conceptual design of the luminosity monitor for the PANDA experiment is based on measuring the differential elastic Antiproton-Proton scattering rate by 4 planes of silicon strip tracking detectors in the forward area. The absolute precision of integrated luminosity is limited by the lack of existing data on this system in the relevant momentum region, therefore a day-one experiment at HESR dedicated to antiproton-proton elastic scattering has been proposed. The goal of the day-one experiment is to measure a wide range of 4-momentum transfer t (0.0008 – 0.1 GeV^2) so that the contribution of the physical differential distribution to the absolute luminosity uncertainty is less than 1%. The polar angle of scattered antiprotons and the energy of recoil protons will be measured at forward angles by tracking detectors and by thick energy detectors near 90°, respectively. The conceptual design of the day-one experiment is finished. Figure 52 shows the sketch of the day-one experiment at HESR. Part of device has been fabricated and the commissioning of them with proton-proton elastic scattering will take place at COSY in the upcoming years.

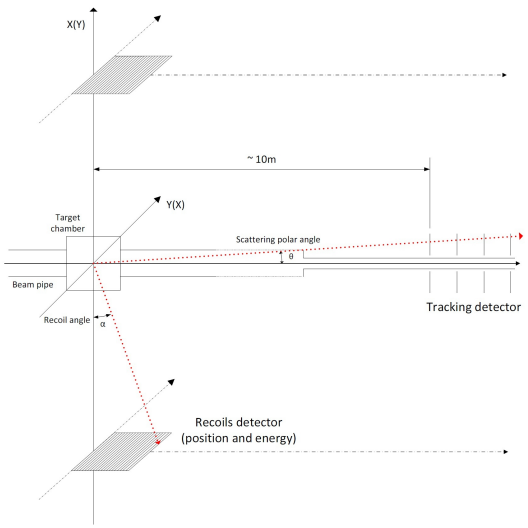

Fig. 52: Sketch of the day-one experiment at HESR.

In order to measure the energy as well as the position of the reoil protons with kinematic enery in the range of 0.4 – 60 MeV, a dedicated detector system consisting of two silicon strip detectors and two germanium strip detectors with dimension of 7.64 cm×5 cm×1 mm (thickness) and 8.04 cm×5 cm×(5/11) mm (thickness), respectively, has been proposed. Both germanium detectors have been fabricated. Figure 53 shows the 5-mm-thick germanium detector picture as well as an alpha soure spectrum observed on the high voltage side of the detector.
Conventional Mesytec electronics have been chosen for the readout of all detectors. Both the preamplifier MPR16 and shaping amplifier MSCF16 have 16 channels, respectively. The 32 channel MADC32 module with VME type will serve as ADC in DAQ system. To verify the perfor-

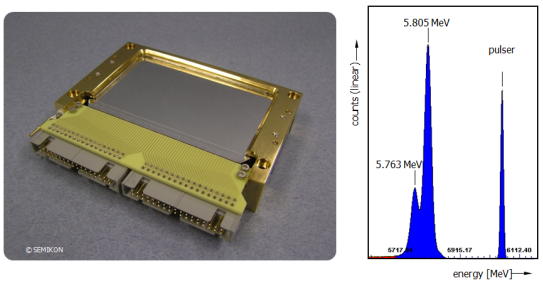

Fig. 53: The fabricated 5mm-thick-Ge detecotr and the alpha source spectrum observed on the high voltage side.

mance of those modules a comparison test based on an Ortec silicon detector with readout by Ortec single channel electronics and Mesytec electronics has been implemented. Test results indicate that the integrated Mesytec electronics is slightly better than single channel electronics. A comparison of alpha source spectra taken from both electronics has been plotted in Figure 54 .

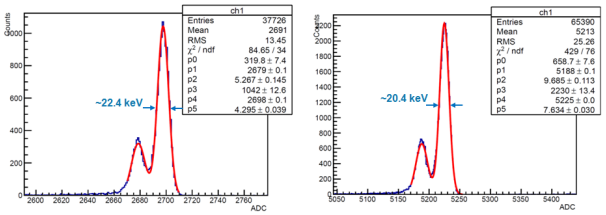

Fig. 54: ^{244}Cm alpha source spectrum with readout of Ortec single channel electronics (left) and Mesytec electronics (right).

In order to commission newly built device at COSY, it is proposed to use the existing cluster target at ANKE. Due to the limited space, a specific detector chamber which will be added to the existing scattering chamber has been designed as shown in Figure 55. The assessment for the proposal tells that the existing target and scattering chamber can be used to commission the day-one detectors.

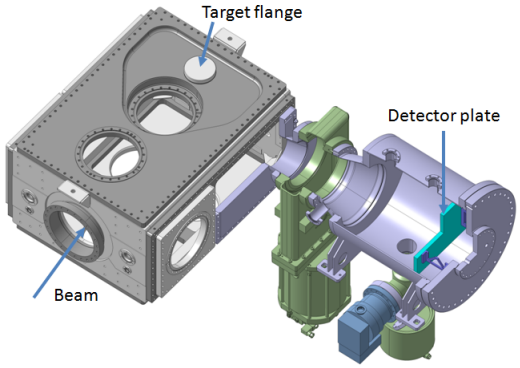

Fig. 55: Detector chamber designed to match the existing ANKE facility.

5 The PANDA Experiment at FAIR

5.1 Introduction

The new Facility for Antiproton and Ion Research (FAIR) will be one of the largest accelerator facilities in the world giving access to a large variety of different experiments to gain new insights into the structure of matter and the evolution of the universe. The construction work of the complex has started with the cutting of the first trees during this fall.

The $\overline{\text{P}}$ANDA experiment is one essential part of FAIR. Its goal is to improve the understanding of Quantum Chromo Dynamics (QCD) in the charmonium energy regime. In this regime many new and unexpected hidden and open charm states were found in the last years. $\overline{\text{P}}$ANDA will be able to measure the new states with unprecedented resolution of the width and the mass and, in addition, will be able to extend the search for new states into the region of high orbital angular momentum.

Essential for all states which decay into charged particles is the precise tracking of those particles to determine their origin and their momentum. For this purpose $\overline{\text{P}}$ANDA uses two different tracking systems in the central detector, a large volume gaseous detector made out of gas filled straw tubes, the Straw Tube Tracker (STT) and a small size silicon pixel and strip detector directly around the interaction point called Micro Vertex Detector (MVD). Both systems are under development in Jülich together with other groups inside the $\overline{\text{P}}$ANDA collaboration.

In addition Jülich is working on a luminosity monitor which measures the Coulomb elastic scattering in the strong interference region. This detector is needed to determine the absolute cross section of states and for the relative normalization of a resonance scan.

5.2 Micro vertex detector

The purpose of the Micro Vertex Detector (MVD) of $\overline{\text{P}}$ANDA is the precise measurement of tracks from charged particles close to the interaction point. With this data it is possible to identify short living particles which decay after a short flight path before they can be measured in a detector system and to determine the momentum of these particles with a very high resolution together with the central tracker. The MVD has four barrel layers with a radial distance from 4 up to 14 cm from the interaction point and six disk layers in the forward direction. Two different detector systems are used inside the MVD. The inner layers are equipped with silicon hybrid pixel detectors, which are able to cope with high track densities and large radiation damages while the outer layers use silicon strip detectors which have less radiation length by a comparable point resolution.

This year two important steps towards the final MVD were done. The first was the successful production of the third prototype (ToPix3) of the future readout ASIC for the pixel detector part. The ToPix3 was designed by the INFN Torino. In comparison of the predecessor the operation speed was tripled, the number of pixels were doubled and the digital functionality largely improved.

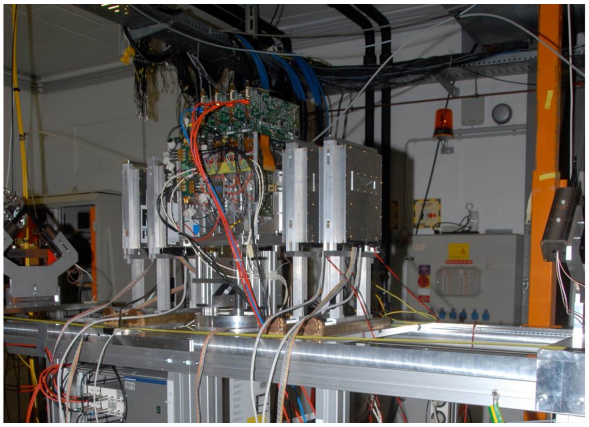

Fig. 56: Photograph of the testbeam setup of the combined pixel - strip testbeam in November 2010. The testbeam was held at the Jessica site of the COSY storage ring in Jülich. In this picture the beam is coming from the left side, flying through two layers of strip detectors, four layers of pixel detectors and at the end again through two layers of strip detectors.

This chip was tested at the COSY accelerator together with prototype strip detectors developed at the HISKP in Bonn. The complete setup consisted out of two scintillator bars at the front for triggering purposes, two layers of strip detectors, four layers of pixel detectors, again two layers of strip detectors and at the end two scintillators (see Fig. 56). Various test were done with different detector setups, variation of the depletion voltage and different incident angles of the beam onto the detectors. All measurements were done with a proton beam of 2.7 GeV/c.

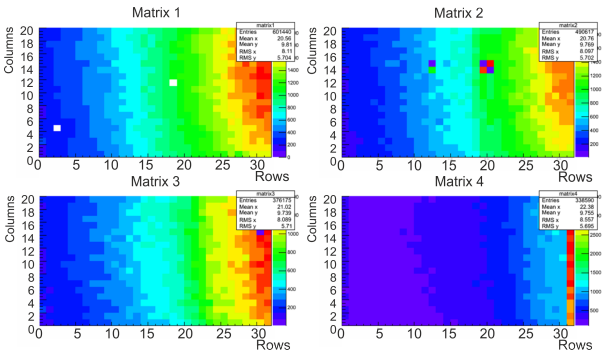

Fig. 57: Scatter plot of the beam profile on the four pixel detector layers.

Figure 57 show as a first result the profile of the beam on the four pixel detector layers. One can nicely see that the beam is a bit off to the right side. On layer 1 two sensor pixels are not connected to the readout electronics, which can be seen by the two white pixels on the first matrix. On matrix 2 four sensor pixels have a short resulting in a characteristic box pattern with two pixels with very high

counts and two pixels with very low counts. The testbeam was very successful with all chips functional. In total several hundred Gigabyte of data could be stored on tape which have to be analyzed within the next year.
The second important step was the finalization of the technical design report (TDR) for the MVD (see Fig. 58. In this document the work of the last eight years of research and development work is summarized. It is the basis for the future production of the MVD and a prerequisite to receive the necessary construction money.

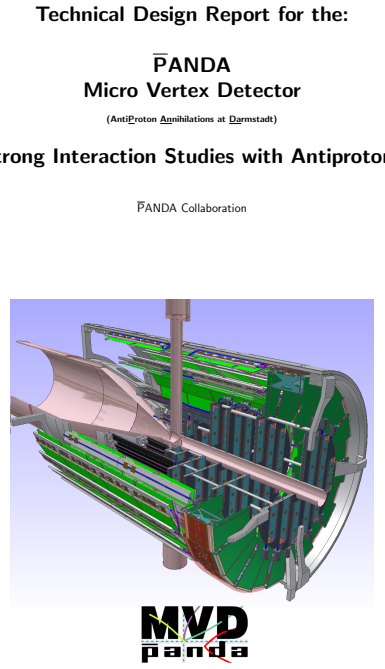

Fig. 58: Title page of the Technical Design Report of the Micro Vertex Detector.

In addition to the detailed description of the hardware of the detector the TDR also contains a comprehensive set of Monte-Carlo simulation studies. They give an estimate of the later performance of the detector once it is build. As an example figure 59 shows the vertex resolution along the beam direction of a J/Ψ meson decaying in lepton pairs. The required resolution is better than 100 μm which is well achieved with 60 μm.
This document was approved by the collaboration and is given officially to the FAIR management where an external referee committee will evaluate it.

5.3 Straw Tube Tracker

A major milestone was reached in September 2011 with the decision of the Straw Tube Tracker as the central tracking detector in the PANDA target spectrometer, taken by the whole PANDA collaboration. During the past years two different options have been developed including dedicated prototype constructions, various beam tests and full simulation and analysis studies: a Time-Projection-Chamber (GEM-TPC) and a Straw Tube Tracker (STT), both with drift time and amplitude readout to measure the trajectory of charged particles and their energy loss for particle identification. Both options were presented for evaluation in a series of technical workshops to an external review committee, consisting of members from CERN, Stanford, Carnegie Mellon University and Vienna University, with expertise in the fields of detector technologies and related analyses methods. Based on the final report of the referees about the qualification of both detectors for the PANDA experiment, finally the whole PANDA collaboration chose the Straw Tube Tracker as the central tracking detector by a clear vote.

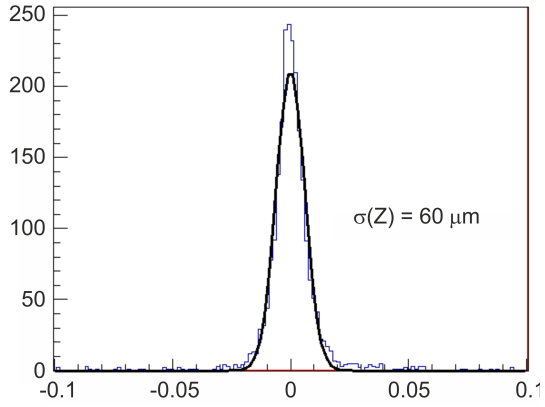

Fig. 59: Vertex resolution of a J/Ψ meson decaying into lepton pairs.

The construction and installation of the PANDA-STT during the years 2012–2015 will be carried out in a joint project of institutions in Italy (Frascati, Pavia, Ferrara), Poland (Cracow), Romania (Bucharest) and Germany (FZ Jülich). The detailed technical design report (cf. Fig. 60) about the STT construction has been submitted to FAIR in April 2012. The final commissioning of the assembled STT including the readout and data-acquisition system will be performed with a proton beam at the COSY accelerator in Jülich. After the completion of these tests the whole detection system will be shipped to the FAIR facility for the installation in the PANDA spectrometer.

The STT consists of about 4600 single straw tubes with a length of 150 cm, diameter of 1 cm and very thin film wall of 27 μm mylar. The tubes are arranged in six sectors of close-packed planar layers, defining a cylindrical detection volume of 150 cm length and 84 cm diameter (see Fig. 61). Note the self-supporting feature of the layout, avoiding a dedicated mechanical frame structure to sustain the total wire tension of 230 kg and tube stretching of 3.5 tons (weight-equivalent) for all straws in the

Technical Design Report for the:

$\overline{\text{P}}$ANDA
Straw Tube Tracker

(AntiProton Annihilations at Darmstadt)

Strong Interaction Studies with Antiprotons

$\overline{\text{P}}$ANDA Collaboration

April 2, 2012

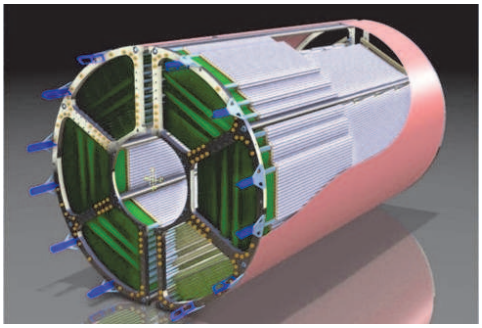

Fig. 60: Title page of the Technical Design Report of the Straw Tube Tracker.

STT detector.

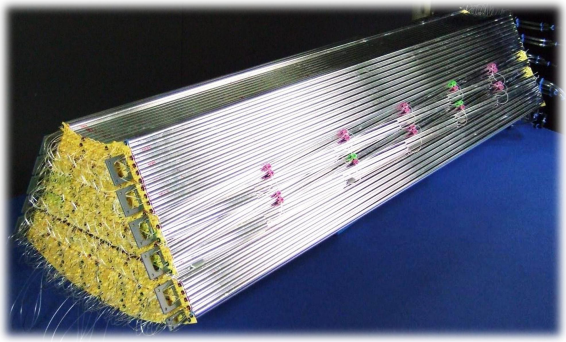

Fig. 61: Full-scale prototype of one straw sector (out of six) of the PANDA-STT. Readout electronics and alignment frame are not shown here.

The tasks of the STT are the spatial reconstruction of charged particle tracks with high resolution in a broad momentum range from about a few 100 MeV/c up to 8 GeV/c, the event recognition by associating single tracks in the STT and information in other detector components together to one event, the measurement of particle momenta by the reconstructed trajectory in the 2 T solenoid magnetic field and the measurement of the specific energy loss (dE/dx) for particle identification (pid). The additional pid information from the STT is needed to separate protons, kaons and pions in the low momentum range below 1 GeV/c. The continuous data-acquisition without a hardware trigger at an interaction rate of about $2{\cdot}10^7$ s^{-1} requires a very fast and efficient track and event reconstruction in real-time to recognize interesting reaction events and start the data storage to disk.

The design and materials of the single straw tubes and the technique of self-supporting planar straw layers have been first developed for the STT in the COSY-TOF experiment and were further optimized for the PANDA-STT. Therefore, the COSY-STT detection system, including calibration and reconstruction methods, is considered to be an ideal test system for the PANDA-STT. The achieved spatial resolution of 140 μm for the 2700 straws of the COSY-STT can be extrapolated to about 100 μm for the PANDA-STT due to the 65 % higher gas and ionization density there. In particular the reliable operation of the STT in the surrounding vacuum of the large COSY-TOF time-of-flight barrel during about three years now is a strong design proof of all used materials and assembly techniques, important for the long-term operation of the PANDA-STT of more than 10 years.

The STT features a high number of 27 layers in radial direction for the track reconstruction, with 19 straw layers oriented in beam direction and four stereo double-layers in the middle section skewed by about $\pm 3^\circ$ relative to the axial layers. The spatial resolutions of the detector, confirmed by prototype measurements and the COSY-STT, are about 150 μm ($\sigma_{r\phi}$) in radial direction and 2–3 mm (σ_z) in beam direction. Together with the very low material budget of about 1.2 % a momentum resolution $\sigma(p)/p$ of 1–2 % will be achieved.

Unique for a straw detector is the additional readout of the signal amplitude for a measurement of the energy loss for particle identification. Test measurements performed at COSY with proton beams at three different momenta (0.6, 1.0, 2.9 GeV/c) obtained energy resolutions $\sigma(E)/E$ of 8$\pm$1 % for proton tracks traversing layers of 16 straws (Fig. 62). An extrapolation of this result to the 27 straw layers in the PANDA-STT yields a very high energy resolution of down to 6 % and a high particle separation power in the region below 1 GeV/c.

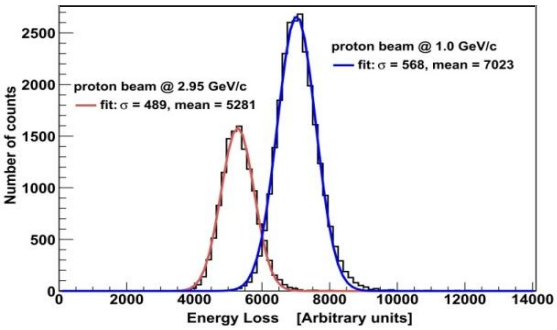

Fig. 62: Measured energy loss for protons with a momentum of 1.0 GeV/c and 2.9 GeV/c after applying a truncated mean cut. The obtained energy resolutions are $\sigma(E)/E \simeq 8\pm1$ % (gaussian fit).

5.4 Physics Performance Benchmark of the PANDA Central Tracker

One task during detector development is the study of the expected performance in a realistic scenario by means of simulations. For the tracking detector, a set of benchmark channels to test the detector's capability to precisely reconstruct charged particle tracks, momenta, masses and secondary vertices has been identified previously.
The results of these benchmark simulations have also been considered for the decision which detector technology (time projection chamber or straw tube tracker) to implement for the PANDA central tracker.
Here, we present the results obtained for the analysis of the reaction

$$\bar{p}p \to \psi(3770) \to D^+D^- \to K^-\pi^+\pi^+K^+\pi^-\pi^- \quad (7)$$

at a beam momentum of 6.5788 MeV/c. It has a typical signature which is common for several channels of the PANDA physics program. Within the scope of this benchmark, its following key features are of particular interest:

- Secondary vertices with a short decay length (312 μm for the charged D mesons),
- A relatively large number of ejectiles (6 for this channel) to be reconstructed in an exclusive analysis,

The majority of the decay particles have a momentum between 0.5 GeV/c and 3 GeV/c. While the kaons are only found in the forward hemisphere, the pions are also ejected at backwards angles due to their lower mass. However, the majority is found within a range between 5° and 60° in both cases. There is a high probability that at least one of the decay particles is strongly forward peaked.
Reconstructing this class of events requires a good interplay of the central tracking detectors MVD and STT as well as additional information from the forward tracking to detect also those particles which are ejected at shallow polar angles below 10°. The secondary vertex resolution is tested by reconstructing the displaced decay vertices of the D-mesons.
For the study of the achievable invariant mass and vertex resolutions, a large sample (10^5) of signal events has been simulated and passed to an analysis chain similar to the procedure which would be used in a real experiment. The detector properties (*e.g.* time resolution of individual straws) have been evaluated with test measurements and implemented in the simulation.
The relevant subdetectors which contribute hits to the reconstructed tracks are MVD, STT and forward GEM. Their track points undergo the full track reconstruction procedure of pattern recognition, track finding and track fitting. In order to exclude any influence of the particle identification on the tracking results, the simulated Monte Carlo true PID information has been used. In addition

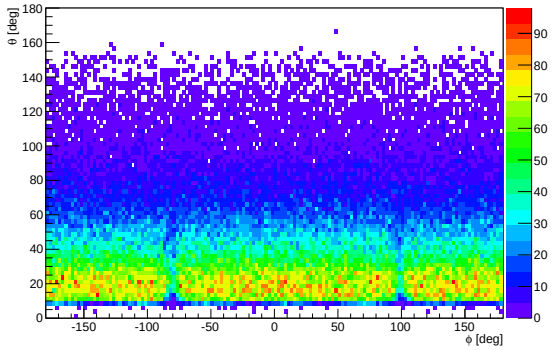

Fig. 63: Polar and azimuthal angle distribution of the reconstructed π^+.

to the pure signal, also mixed events have been analyzed where a physics event is superimposed with generic background events according to the expected event rate of $2 \cdot 10^7$ events per second in PANDA. This results in the tracks of several particle interactions simultaneously being present in the detector which have to be disentangled by the reconstruction software.
In the first step of the analysis all reconstructed track candidates which have at least one STT hit are considered for further processing. The distribution of polar and azimuthal angle of the reconstructed pions which pass the STT volume is shown in Fig. 63. The presence of the target pipe is clearly visible in the plot (slight drop at $\phi = -80°$ and $\phi = 100°$) as well as the $\pm 10°$ shift in the observed ϕ position due to the bending of the oppositely charged particles' tracks in the magnetic field.
The decay particles are then combined to D^+ and D^- meson candidates. A first selection is done by requiring that the reconstructed D masses differ by no more than 750 MeV from the nominal D mass. After that, a vertex fit to the D-meson decay vertices is carried out.
In the case of multiple candidates within one event, the best one is selected based on the χ^2 result from the vertex fit. The mass and vertex position of the events which pass this selection follow a Gaussian distribution around the nominal value.

Table 6: Expected vertex (σ_{xy}, σ_z) and mass (σ_m) resolutions. The columns show the results obtained for different event types and configurations of the reconstruction software. They demonstrate the effect of the cleanup code and the capability of the reconstruction code to process mixed events with virtually no resolution loss.

	Pure signal (w/o cleanup)	Pure signal (w/ cleanup)	Mixed events (w/ cleanup)
σ_{xy}	54.5 μm	55 μm	61 μm
σ_z	104.3 μm	104 μm	109 μm
σ_m	17 MeV	16 MeV	17 MeV

The obtained vertex resolution is in the order of $\sigma_{xy} = 55$ μm in xy-direction and $\sigma_z = 104$ μm in z-direction; the mass resolution is in the order of $\sigma_m = 16$ MeV after the vertex fit. Almost identical results

are obtained for the simulations of signal events which are mixed with background (compare Table 6).

5.5 Determination of the X(3872) width resolution

Despite that many experiments have observed the $X(3872)$ state, its exact nature is still not clear. Several theoretical models were developed to explain its properties. Even if these models have significantly different predictions on the width, their calculation are consistent with the world upper bound: $\Gamma_X < 2.3\,MeV/c^2$. In addition, they also seem to favor the $J^{PC} = 1^{++}$ quantum number assignment for the $X(3872)$ meson.

For $p\bar{p}$ annihilation experiments like $\overline{\text{P}}$ANDA , the most effective method by which the width can be extracted with the higher precision is the resonance scan method. In this method, the measurement precision depends primarily on the knowledge of the beam energy distribution and resolution at each individual nominal center-of-mass energy used. The $\overline{\text{P}}$ANDA experiment, thanks to the excellent quality and intensity of the HESR antiproton beam, is expected to have sufficient resolution to measure the width of $X(3872)$ meson, and thus will provide additional decisive information on its nature.

A resonance scan simulation has been performed in order to estimate the precision on the width measurement with $\overline{\text{P}}$ANDA . It was based on the interpertation of the $X(3872)$ as $\chi_{c1}(2P)$ state decaying to the $J/\psi\pi^+\pi^-$ final state. In this case the cross section line shape consists of a non-relativistic Breit-Wigner and a non-resonant nearly constant physical background. It determines the number of final state events at a given nominal center-of-mass energy. The signal is a Gaussian distribution of the reconstructed 4-particle invariant mass with σ_{SIG} width reflecting the detector resolution in the resonance vicinity region. It is folded with an instrumental background which is modeled by an Argus function according to a signal to background ratio, r_{SB}, value. The parameters used in the simulation are listed in Table 7.

Table 7: Input parameters for the event generator of the simulation.

Parameter	Value
Acceptance × Efficiency	0.3
$\mathscr{L}$	$864\,nb^{-1}/day$
$\delta p/p$	3×10^{-5}
$f_{\mathscr{B}} = \mathscr{B}(J/\psi \to e^+e^-, \mu^+\mu^-)$	0.12
Phys. background cross section	$1.2\,nb$
Number of scan points	10
Scan range around the resonance	$2\,MeV$
Time spent per scan point	$4\,days$
σ_{SIG}	$8.3\,MeV$
c_{ARGUS}	-10

The cross section distribution is reconstructed from the fit to the generated $J/\psi\pi^+\pi^-$ invariant mass spectrum at each considered center-of-mass energy. To obtain the width and the mass of the $X(3872)$ state, the cross section distribution is fitted by the line shape function convoluted with the beam profile. The fit procedure minimized the χ^2-function with respect to the mass and the width of the resonance. An example of a two-dimensional histogram of χ^2 for various scans of mass and width values is shown in Fig. 64.

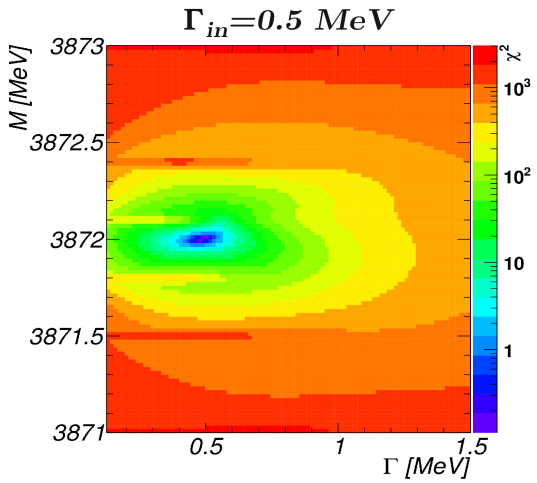

Fig. 64: The χ^2 variation as functions of the mass and the width parameters for $\Gamma_{in} = 0.5\,MeV$ and $r_{SB} = 2$.

The minimization procedure found several local minima with respect to the mass which explains the non-parabolic variation of the projected χ^2-function in the $y-$axis over the considered mass range for these plots. The global minimum corresponds to the reconstructed values of the mass and the width of the $X(3872)$.

The influence of r_{SB} and the finite uncertainty of the luminosity $\Delta\mathscr{L}/\mathscr{L}$ on the measurement were investigated separately. The study considered three different input widths, namely 0.136, 0.5 and $1\,MeV/c^2$. The results are reported in Fig. 65.

As expected, the precision on the width measurement worsens as r_{SB} decreases and the best precision is then achieved for $r_{SB} = 10$ with $\sigma_\Gamma/\Gamma_{in} < 1\%$ for $\Gamma_{in} = 0.5$ and $1\,MeV/c^2$ and $\sigma_\Gamma/\Gamma_{in} \sim 2\%$ for $\Gamma_{in} = 136\,keV/c^2$. To obtain a more realistic model of the instrumental background distribution, further investigation such as a full detector simulation using an adequate event generator is required. Detailed knowledge of the signal to background ratio is needed for a precise measurement of the mass and the width of the $X(3872)$ state since the uncertainty of the luminosity determination for $\Delta\mathscr{L}/\mathscr{L} < 5\%$ does not affect the resolution of the width. Therefore, with the design precision on the luminosity measurement for $\overline{\text{P}}$ANDA ($\Delta\mathscr{L}/\mathscr{L} = 3\%$), the width of $X(3872)$ can be determined with excellent accuracy thus allowing a better understanding of its nature.

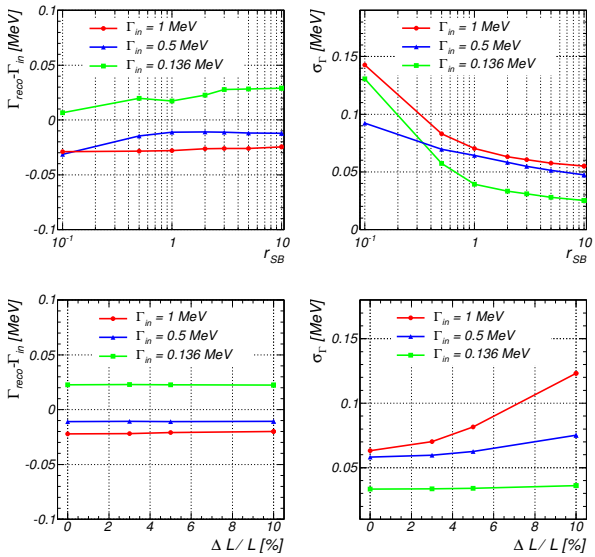

Fig. 65: Variation of the reconstructed width Γ_{reco} and its respective precision σ_Γ as a function of the signal to background ratio r_{SB} with $\Delta\mathscr{L}/\mathscr{L} = 0\%$ (upper) and of the relative uncertainty of the luminosity measurement at each individual scan point $\Delta\mathscr{L}/\mathscr{L}$ with $r_{SB} = 2$ (lower).

6 Further Experimental Activities

6.1 Laser-induced Particle Acceleration

While the development towards laser-induced particle accelerators has seen vast improvements in recent years, it is yet a completely untouched issue whether the laser-generated beams are or can be spin-polarized. Since many high-energy and nuclear-physics experiments require polarized beams it is vital to investigate this possibility. This is a major goal of a joint working group of the IKP, the Jülich Supercomputing Centre and the Institut for Laser and Plasma Physics (ILPP) of Düsseldorf University.

Currently, our experiments are carried out at the ARC-turus laser facility of the ILPP, that operates at a pulse energy of a few J, reaching a pulse power of up to 300 TW and a focus intensity of approx. 10^{20} W/cm^2. As a first step, the technique to measure the polarization of the laser accelerated beams has been established (see also last year's Annual Report). For commissioning of the set-up, it has been employed to few-MeV protons accelerated in foil targets, where no polarization built-up is expected. As a side-product the differential Si(p,p')Si cross section — *i.e.* an observable that is typically measured at conventional particle accelerators — has been obtained, see Sect. 6.1.1. The laser data are in very good agreement with the ones from the Cologne Tandem-accelerator. Preparations to employ the method to laser-accelerated protons and ions from (polarized) gas targets are under way, see Sect. 6.1.2.

In the long run it is planned to install a laser-based facility — offering peak powers even in the PW regime — at FZJ. Such a facility would not only allow to continue our polarization studies with beams of few 10 MeV kinetic energies. The intention rather is to implement a multi-purpose user facility for research with various kinds of photon and particle beams, see Sect. 6.1.3.

6.1.1 Experiments with laser-produced protons from foil targets

For the first polarization studies, the titan-sapphire laser (PULSAR-100 by Amplitude Technologies) of the ARC-turus laser laboratory was directed on on a gold foil target of 3 μm thickness. The energy that was delivered on the target amounts to approx. 1.2 J, the intensity profie at the focus point was of Gaussian shape with a FWHM of 7 μm. Protons are accelerated by the Target Normal Sheath Acceleration (TNSA) mechanisms from carbon-hydride impurities at the back side of the foil. Their energy spectrum, which is measured with the help of a spectrometer dipole magnet, is depicted in Fig. 66

The protons have a wide energy spectrum and emission angles of up to $\sim 20°$. To measure the degree of polarization of this proton beam, secondary elastic proton scattering off nuclei with known cross sections and analyzing powers is utilized. The apparatus, described in more detail in last years Annual Report, selects protons with

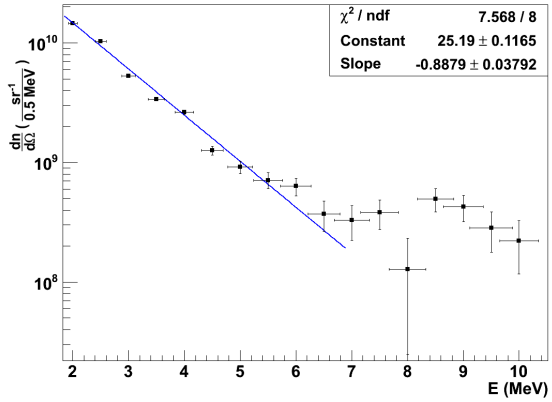

Fig. 66: Energy spectrum of the protons from our experiment with foil targets at ILPP.

energies 3.2 ± 0.2 MeV under an adjustable emission angle with an acceptance of roughly 1° and directs them on a silicon foil with 24 μm thickness. Behind this foil the ϑ, ϕ angular distributions of the scattered protons are measured. Due to the very short proton-pulse lengths the detectors are hit more or less simultaneously. Therefore, CR-39 track-detectors, that have no dead time and do not respond to the EMP of the laser, have been used.

Figure 67 shows the measured differential cross section $d\sigma/d\Omega(\vartheta)$ of the Si(p,p')Si reaction. The data is an average over ten laser shots, corresponding to a total beam-time of merely few 100 fs. The excellent agreement with the results from literature not only gives us confidence in the reliability of the method and the extracted differential distributions, but also suggests a high potential of laser-accelerated beams for hadron physics.

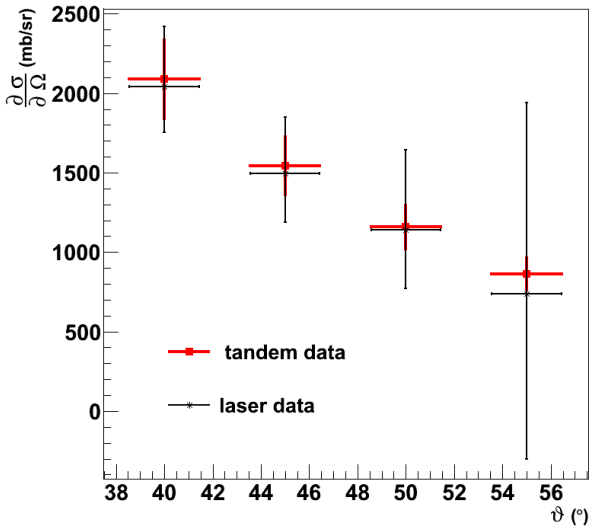

Fig. 67: Measured cross section of the Si(p,p')Si scattering in dependence of the scattering angle. The data from our experiment with laser-produced protons with energies 3.2 ± 0.2 MeV (black points) are compared to the results from measurements at the Cologne Tandem (red) at 3.1 MeV.

A preliminary analysis of the proton scattering distributions yields no significant asymmetries in the azimuthal angle ϕ and thus indicates that the polarization of the laser-generated proton beams is compatible with zero. Thus, as a next step it is planned to use target configurations promising significant beam polarizations. Here, pre-polarized ^{3}He gas seems to be promising since it can be obtained and stored over few days in suitable quantities and maintains its polarization over several days at room temperature.

6.1.2 Simulations of gas targets

Major challenges of a polarization measurement with a gas target is that the ions have to be accelerated from an underdense gas target to kinetic energies of at least few MeV. That has so far only been achieved in a single measurement at the VULCAN laser facility in 2006, where the pulse energies are much bigger than at ARCturus. In order to investigated the feasibility of such experriments at at the ILPP, we have perforemed corresponding simulation calculations with the EPOCH code.
EPOCH is a Particle-in-Cell code (PiC) which runs on PCs as well as on the JUROPA supercomputer of FZJ. As a first step, PC simulations were carried out in order to reproduce the data from VULCAN as well as the corresponding simulations from that group which can be found in the paper by Willingale *et al.*, *PRL* **96**(2006) 245002. From the latter it has been concluded that ion acceleration in gas targets, like in thin foils, is driven by TNSA. This requieres that the laser pulse penetrates the gas jet and thus pushes out electrons at the rear side of the generated plasma which, in turn, generate the strong quasi-static electric fields for ion acceleration.
Since our EPOCH simulations show godd agreement with the VULCAN results, we adapted them to the boundary conditions typically found at the ILPP. As an example Fig. 68 shows the result of such a JUROPA simulation.

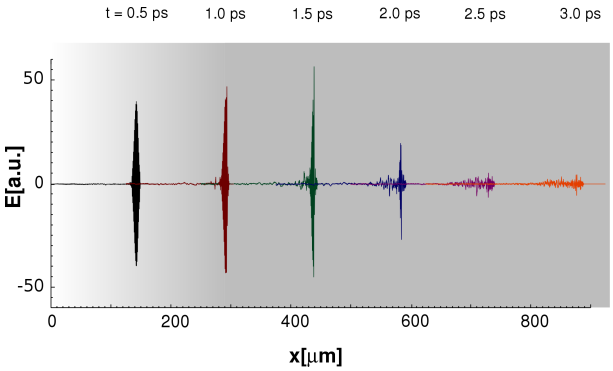

Fig. 68: Electric field strenght of the laser pulse while propagating through a helium gas jet. The density distribution of the gas jet is indicated by the greyish background shading. The propagating pulses are shown for different times after the focus point.

It is seen that the laser pulse is completely absorbed after propagating roughly 500 μm through the gas jet. Under these condiditions helium ions of only a few keV kinetic energy are to be expected which is in line with the result of a first test measurement. This suggests that for the upcoming experiment shorter gas jets or longer laser pulses have to be used.

6.1.3 Towards a PW-laser centre at FZJ

It has been proposed by a consortium of the Peter Grünberg Institut PGI-6, the Institut für Kernphysik, the Institute for Advanced Simulation JSC/IAS, the Institut für Energie- und Klimaforschung IEK-5 (all FZJ), the Universities Düsseldorf, Dortmund and Münster, the Fraunhofer Institut für Lasertechnik, Laser & Laseroptik, Aachen, as well as ITEP and MPEI Moscow, Russia, to install and operate a Petawatt-scale laser facility at the FZJ next to the COSY accelerator hall that enables research with short-pulsed photon and particle beams, see Fig. 69.

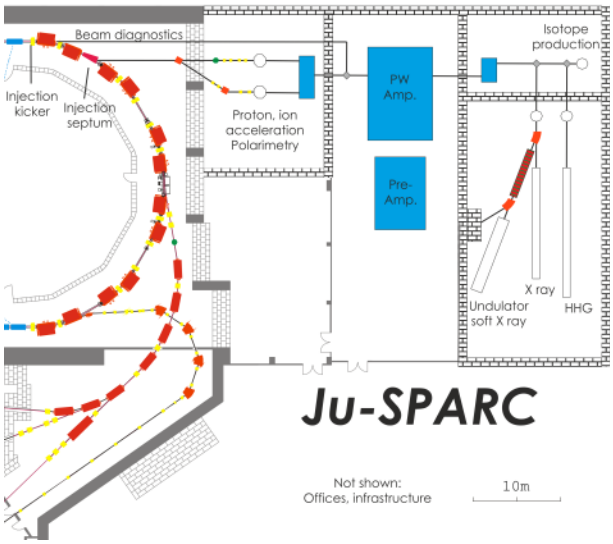

Fig. 69: Floor plan of the proposed JuSPARC laser facility next to the COSY accelerator hall (l.h.s.).

The Jülich Short-pulse Particle Acceleration and Radiation Center (JuSPARC) will be the first multi-purpose facility of its kind, accommodating local and regional research teams from a wide range of disciplines including materials science, structural biology, accelerator technology, plasma and nuclear physics. The heart of JuSPARC will comprise a turn-key PW-laser system with a pulse length of few 10 fs and a repetition rate of about 5 Hz, augmented by adjoining target areas dedicated to short-pulse hadron, electron beam or X-ray applications, respectively. Research at JuSPARC will mainly be targeted at:

Use of short-pulse synchrotron radiation in the hard and soft X-ray range: A key challenge of condensed-matter physics today lies in the understanding of electronically correlated materials on the nanoscale. This demands a time-resolved investigation on the level of electronic time-scales, *i.e.* 1–100 fs. It is thus planned to create a femtosecond pulsed X-ray facility as a major part of JuSPARC.

Beam-diagnostics studies: Future high-energy electron-positron colliders pose stringent demands on the control of the transversal beam dimensions and location. Expected beam diameters range from 500 nm to 10 μm — such accuracies require novel beam diagnostics tools. A recent development is the "laser-wire technique", based on Thomson scattering of laser light off the stored electrons. Electron beams require laser powers ranging from MW to GW. For protons, due to the much smaller Thompson-scattering cross section, the laser pulse must be significantly more intense. A new application of this technique could thus be achieved with a PW laser and the circulating COSY beam. Exploitation of the spin-dependent part of the Thompson scattering opens the possibility for time- and position-sensitive beam-polarization diagnostics with unprecedented accuracy. This may be of importance for planned EDM experiments at storage rings.

Generation of polarized particle beams in laser-induced plasmas: As described above, IKP-2 has developed a method to measure the degree of polarization of laser-induced proton and light ion beams: Preliminary experiments are underway to determine optimal parameters for building polarized beam sources, in particular for ^{3}He ions. Such a development could be useful for the planned EDM studies and complement work on a polarized ^{3}He source for RHIC at BNL.

Research on new acceleration mechanisms to increase the acceleration efficiency and quality of multi-MeV proton beams: In order to inject laser-generated beams into the COSY ring (at a proton energy of 40 MeV), both the beam divergence and the momentum spread must be significantly reduced. Their transversal phase space is very small (typically below 1 πmm mrad) and a compact, strongly focusing magnetic system (e.g. quadrupole magnets) can effectively catch these beams. Momentum selection can be achieved with dipole magnets. A prototype magnetic quadrupole doublet has been designed at the IKP and is now being tested. Due to the short pulse lengths the longitudinal phase-space volume is also small, despite the strong energy variation of the accelerated particles. It is therefore possible to achieve almost mono-energetic beams with a momentum spread that matches the COSY acceptance threshold. In a first step, such feasibility studies will be performed at JuSPARC with the goal to later use the facility as an injector for COSY.

Frozen pellets targets (which require proper triggering of the laser pulses) are ideally suited to realize continuously operating sources for laser-accelerated particles. A new generation of such targets is being built at the IKP in collaboration with ITEP and at MPEI. Another type of cryogenic targets, so-called cluster-jet targets, has been built at the University of Münster and is routinely used for internal target experiments at COSY.

Feasibility studies on laser-driven nuclear spallation and isotope production: In principle, laser-induced fusion reactions can create neutron fluxes of up to 10^{19} n/s. For example, an Al-H composite target irradiated by a PW laser beam would produce protons with energies of the order of 10 MeV, their spectrum resembling that of evaporating protons from spallation processes. Interactions of these protons in a secondary target would lead to neutrons in the MeV range. Another possible field of applications for laser-accelerated protons is the production of radioactive isotopes for Positron-Emission Tomography (PET). PET requires short-lived isotopes like ^{11}C, ^{13}N, ^{15}O and ^{18}F, which are typically produced at cyclotrons. Further progress of the PET technology is currently hindered by limitations of the accelerator size and necessary shielding. A possible development stimulus seems possible by the use of laser-generated proton beams with energies of a few 10 MeV. At present, laser-based approaches cannot yet be regarded as replacements for conventional accelerators. However, anticipated improvements in intensity, size and price could make this route viable in the near future.
Within the JuSPARC project, IKP would be responsible for items 2 – 5. For all mentioned applications it will require major efforts to make the step from single-shot laboratory experiments to a continuously operating facility that makes full use of the laser repetition rate.

A Councils

A.1 Hadron and Accelerator Physics Program Advisory Council

Prof. Mei Bai	Brookhaven National Laboratory, U.S.A.	
Prof. K.-T. Brinkmann	University Bonn	
Prof. M. Garçon	CEA-Saclay, FR	
Prof. A. Jankowiak	Helmholtz Zentrum Berlin	
Prof. K. Jungmann	KVI Groningen, NL	
Prof. K.-H. Kampert	University Wuppertal	
Prof. S. Paul	TU München	Chairperson
Prof. K. Peters	GSI Darmstadt	
Prof. D.-O. Riska	University Helsinki, FI	
Prof. C. Roberts	Argonne National Laboratory, U.S.A.	
Prof. S. Vigdor	Brookhaven National Laboratory, U.S.A.	

A.2 COSY Program Advisory Committee

Prof. M. Anselmino	L'Universita di Torino, IT	
Prof. D. Barber	DESY Hamburg	
Prof. E. Epelbaum	Universität Bochum	
Prof. M. Garçon	CEA-Saclay, F	Chairperson
Prof. N. Kaiser	TU München	
Prof. B. Kämpfer	FZ Dresden-Rossendorf	
Prof. O. Kester	GSI Darmstadt	
Prof. T. Kishimoto	RCNP Osaka, J	
Prof. A.K. Opper	George Washington University, USA	
Prof. P. Salabura	Jagellonian University Cracow, PL	
Prof. U. Thoma	Universität Bonn	
Prof. W. Weise	DESY, Hamburg	
Prof. H. Wilschut	KVI Groningen, NL	

B Publications

1. Experiment

1. **ABC Effect in Basic Double-Pionic Fusion — Observation of a new resonance?**
   P. Adlarson *et al.* [WASA-at-COSY Collaboration],
   Phys. Rev. Lett. **106**, 242302 (2011) [arXiv:1104.0123 [nucl-ex]]

2. **Adiabatic Cooling of Antiprotons**
   G. Gabrielse *et al.*,
   Phys. Rev. Lett. **106**, 073002 (2011)

3. **Measurement of the in-medium ϕ-meson width in proton-nucleus collisions**
   A. Polyanskiy *et al.*,
   Phys. Lett. B **695**, 74 (2011) [arXiv:1008.0232 [nucl-ex]]

4. **The Measurement of the $pp->K^+n\Sigma^+$ reaction near threshold**
   Y. Valdau and C. Wilkin,
   Phys. Lett. B **696**, 23 (2011) [arXiv:1008.3465 [nucl-ex]].

5. **Pionic deuterium**
   T. Strauch *et al.*,
   Eur. Phys. J. A **47**, 88 (2011) [arXiv:1011.2415 [nucl-ex]]

6. **Reaction $pp \to pp\pi\pi\pi$ as a background for hadronic decays of the η' meson**
   M.J. Zielinski, P. Moskal, A. Kupsc,
   Eur. Phys. J. A **47**, 93 (2011) [arXiv:1107.4278 [hep-ex]]

7. **Exclusive measurement of the $pp \to nn\pi^+\pi^+$ reaction at 1.1 GeV**
   T. Skorodko *et al.*,
   Eur. Phys. J. A **47**,108 (2011) [arXiv:1012.1463 [nucl-ex]]

8. **Investigation of γ-ray fold distributions in $N \leq 82$ Gd, Eu and Sm nuclei: Observation of a double-humped fold distribution**
   R.M. Lieder *et al.*,
   Eur. Phys. J. A **47**, 115 (2011)

9. **Comparison of inclusive K^+ production in proton-proton and proton-neutron collisions**
   Y. Valdau *et al.*,
   Phys. Rev. C **84**, 055207 (2011) [arXiv:1109.0176 [nucl-ex]]

10. **Photoproduction of neutral pions off protons**
    V. Crede *et al.*,
    Phys. Rev. C **84**, 055203 (2011) [arXiv:1107.2151 [nucl-ex]]

11. **Upper limits for a narrow resonance in the reaction $p+p \to K^+ + (\Lambda p)$**
    A. Budzanowski *et al.* [COSY-HIRES Collaboration],
    Phys. Rev. D **84**, 032002 (2011) [arXiv:1105.2281 [hep-ex]].

12. **The Institut für Kernphysik at Forschungszentrum Jülich**
    M. Büscher, A. Lehrach, F. Goldenbaum
    Nucl. Phys. News, Vol. **21**, Issue 1, p.5 (2011)

13. **Pumped helium system for cooling positron and electron traps to 1.2 K**
    J. Wrubel *et al.* [ATRAP Collaboration],
    Nucl. Instrum. Meth. A **640**, 232 (2011).

14. **The CAD model of the PANDA Micro-Vertex-Detector in physics simulations**
    S. Bianco *et al.*,
    Nucl. Instrum. Meth. A **654**, 630 (2011)

15. **A high rate, low radiation length Micro-Vertex-Detector for the PANDA experiment**
    T. Stockmanns, for the PANDA, Kollab.
    Nucl. Instrum. Meth. A **650**, 64 (2011)

16. **Pumped helium system for cooling positron and electron traps to 1.2 K**
J. Wrubel *et al.*,
Nucl. Instrum. Meth. A **640**, 232 (2011)

17. **An alternative for polarized antiproton beams**
D. Grzonka *et al.*,
Hyperfine Interactions (2011)

18. **Results from the IAEA Benchmark of Spallation Models**
S. Leray *et al.*,
J. Korean Phys. Soc. **59**, 791 (2011)

2. Theory

19. **Self-consistent calculations of the strength function and radiative neutron capture cross section for stable and unstable tin isotopes**
A. Avdeenkov, S. Goriely, S. Kamerdzhiev, S. Krewald
Phys. Rev. C **83**, 064316 (2011) [arXiv:1108.1717 [nucl-th]]

20. **Three-body $D\bar{D}\pi$ dynamics for the X(3872)**
V. Baru, A.A. Filin, C. Hanhart, Y.S. Kalashnikova, A.E. Kudryavtsev, A.V. Nefediev
Phys. Rev. D **84**, 074029 (2011) [arXiv:1108.5644 [hep-ph]]

21. **Precision calculation of the π^-d scattering length and its impact on threshold πN scattering**
V. Baru, C. Hanhart, M. Hoferichter, B. Kubis, A. Nogga, D. Phillips
Phys. Lett. B **694**, 473 (2011) [arXiv:1003.4444 [nucl-th]]

22. **Precision calculation of threshold π^-d scattering, πN scattering lengths, and the GMO sum rule**
V. Baru, C. Hanhart, M. Hoferichter, B. Kubis, A. Nogga, D.R. Phillips
Nucl. Phys. A **872**, 69 (2011) [arXiv:1107.5509 [nucl-th]]

23. **Heavy quarkonium: progress, puzzles, and opportunities**
N. Brambilla *et al.*
Eur. Phys. J. C **71**, 1534 (2011) [arXiv:1010.5827 [hep-ph]]

24. **Isospin splittings of doubly heavy baryons**
S.J. Brodsky, F.-K. Guo, C. Hanhart, U.-G. Meißner
Phys. Lett. B **698**, 251 (2011) [arXiv:1101.1983 [hep-ph]]

25. **Relevance of complex branch points for partial wave analysis**
S. Ceci, M. Döring, C. Hanhart, S. Krewald, U.-G. Meißner, A. Svarc
Phys. Rev. C **84**, 015205 (2011) [arXiv:1104.3490 [nucl-th]]

26. **Light meson mass dependence of the positive parity heavy-strange mesons**
M. Cleven, F.-K. Guo, C. Hanhart, U.-G. Meißner
Eur. Phys. J. A **47**, 19 (2011) [arXiv:1009.3804 [hep-ph]]

27. **Bound state nature of the exotic Z_b states**
M. Cleven, F.-K. Guo, C. Hanhart, U.-G. Meißner
Eur. Phys. J. A **47**, 120 (2011) [arXiv:1107.0254 [hep-ph]]

28. **Kaon-nucleon scattering lengths from kaonic deuterium experiments revisited**
M. Döring, U.-G. Meißner
Phys. Lett. B **704**, 663 (2011) [arXiv:1108.5912 [nucl-th]]

29. **Unitarized Chiral Perturbation Theory in a finite volume: Scalar meson sector**
M. Döring, U.-G. Meißner, E. Oset, A. Rusetsky
Eur. Phys. J. A **47**, 139 (2011) [arXiv:1107.3988 [hep-lat]]

30. **Dynamical coupled-channel approaches on a momentum lattice**
M. Döring, J. Haidenbauer, U.-G. Meißner, A. Rusetsky
Eur. Phys. J. A **47**, 163 (2011) [arXiv:1108.0676 [hep-lat]]

31. **The reaction $\pi^+ p \to K^+\Sigma^+$ in a unitary coupled-channels model**
M. Döring, C. Hanhart, F. Huang, S. Krewald, U.-G. Meißner and D. Ronchen
Nucl. Phys. A **851**, 58 (2011) [arXiv:1009.3781 [nucl-th]]

32. **When hadrons become unstable: a novel type of non-analyticity in chiral extrapolations**
F.-K. Guo, C. Hanhart, F. J. Llanes-Estrada, U.-G. Meißner
Phys. Lett. B **703**, 510 (2011) [arXiv:1105.3366 [hep-lat]]

33. **Effect of charmed meson loops on charmonium transitions**
F.-K. Guo, C. Hanhart, G. Li, G., U.-G. Meißner, Q. Zhao
Phys. Rev. D **83**, 034013 (2011) [arXiv:1008.3632 [hep-ph]]

34. **To bind or not to bind: The H-dibaryon in light of chiral effective field theory**
J. Haidenbauer, U.-G. Meißner
Phys. Lett. B **706**, 100 (2011) [arXiv:1109.3590 [hep-ph]]

35. **DN interaction from meson exchange**
J. Haidenbauer, G. Krein, U.-G. Meißner, L. Tolos
Eur. Phys. J. A **47**, 18 (2011) [arXiv:1008.3794 [nucl-th]]

36. **Two and three-body structure of the Y (4660)**
P. Hagen, H.-W. Hammer, C. Hanhart
Phys. Lett. B **696**, 103 (2011) [arXiv:1007.1126 [hep-ph]]

37. **Interplay of quark and meson degrees of freedom in a near-threshold resonance: multi-channel case**
C. Hanhart, Y.S. Kalashnikova, A.V. Nefediev
Eur. Phys. J. A **47**, 101 (2011) [arXiv:1106.1185 [hep-ph]]

38. **Improved nuclear matter calculations from chiral low- momentum interactions**
K. Hebeler, S.K. Bogner, R.J. Furnstahl, A. Nogga, A. Schwenk
Phys. Rev. C **83**, 031301 (2011) [arXiv:1012.3381 [nucl-th]]

39. **Towards a high precision calculation for the pion-nucleus scattering lengths**
S. Liebig, V. Baru, F. Ballout, C. Hanhart, A. Nogga
Eur. Phys. J. A **47**, 69 (2011) [arXiv:1003.3826 [nucl-th]]

40. **Chiral perturbation theory calculation for $pn \to d\pi\pi$ at threshold**
B. Liu, V. Baru, J. Haidenbauer, C. Hanhart
Eur. Phys. J. A **47**, 12 (2011) [arXiv:1007.1382 [nucl-th]]

41. **Chiral Symmetry, Nuclear Forces and All That**
U.-G. Meißner
Festschrift in Honor of Gerald E. Brown, World Scientific, ISBN-13 978-981-4329-08-8, p.345 (2011) [arXiv:1011.1343 [nucl-th]]

42. **Three Nucleon Force Effects in Intermediate Energy Deuteron Analyzing Powers for dp Elastic Scattering**
K. Sekiguchi *et al.*
Phys. Rev. C **83**, 061001 (2011) [arXiv:1106.0180 [nucl-ex]]

43. **Triton with long-range chiral N(3)LO three-nucleon forces**
R. Skibinski *et al.*
Phys. Rev. C **84**, 054005 (2011) [arXiv:1107.5163 [nucl-th]]

44. **The Tucson-Melbourne Three-Nucleon Force in the automatized Partial Wave Decomposition**
R. Skibinski *et al.*
Eur. Phys. J. A **47**, 1 (2011) [arXiv:1101.2150 [nucl-th]]

45. **Migdal and his Theory in Jülich**
J. Speth, F. Grümmer and S. Krewald
Phys. At. Nucl. **74**, 1125 (2011)

46. **Theory of Finite Fermi Systems — The Stony-Brook Jülich Interaction**
J. Speth, S. Krewald, F. Grümmer
Festschrift in Honor of Gerald E. Brown, World Scientific, ISBN-13 978-981-4329-08-8, p.433 (2011)

47. **Effects of density dependence of the effective pairing interaction on the first 2^+ excitations and quadrupole moments of odd nuclei**
S.V. Tolokonnikov, S. Kamerdzhiev, D. Voytenkov, S. Krewald and E.E. Saperstein
Phys. Rev. C **84**, 064324 (2011) [arXiv:1107.4232 [nucl-th]]

48. **Antiproton scattering off ^{3}He and ^{4}He nuclei at low and intermediate energies**
Yu.N. Uzikov, J. Haidenbauer, B.A. Prmantayeva
Phys. Rev. C **84**, 054011 (2011) [arXiv:1107.3906 [nucl-th]]

3. Accelerator (including conference proceedings)

49. **Investigation of various electron ring concepts for the ENC with regard to depolarising effects**
O. Boldt *et al.*
J. Phys. Conf. Ser. **295**, 012157 (2011)

50. **Correcting systematic errors in high-sensitivity deuteron polarization measurements**
N.P.M. Brantjes *et al.*
Nucl. Instrum. Meth. A **664**, 49 (2011)

51. **Particle acceleration in laser-induced relativistic plasmas: a novel approach for polarized sources?**
M. Büscher *et al.*
J. Phys. Conf. Ser. **295**, 012151 (2011)

52. **Progress of the 2 MeV Electron Cooler Development for COSY-Jülich/HESR**
J. Dietrich *et al.*
Proc. of IPAC 2011; San Sebastian, Spain; 05.–09.09.2011; pp. 3427–3429

53. **Status of the 2 MeV Electron Cooler for COSY/HESR**
J. Dietrich *et al.*
Proc. of The Intern. Workshop on Beam Cooling & Related Topics; Alushta, Ukraine; 12.–16.09.2011; pp. 15–18

54. **Status of the 2 MeV Electron Cooler for COSY-Jülich/HESR**
J. Dietrich *et al.*
Proc. of PAC11; New York, USA; 28.03.– 01.04.2011; pp. 1918–1920

55. **Progress with the Scintillation Profile Monitor at COSY**
J. Dietrich, V. Kamerdzhiev, F. Klehr, K. Reimers
Proc. of DIPAC2011; Hamburg, Germany; 16.–18.05.2011; pp. 164–166

56. **Simulation of High-Energy Electron Cooling at COSY with BETACOOL Code**
J. Dietrich, L. Mao
Proc. of The Intern. Workshop on Beam Cooling & Related Topics; Alushta, Ukraine; 12.–16.09.2011; pp. 15–18

57. **Ionisation Profile Monitors-IPM at GSI**
T. Giacomini, P. Forck, J. Dietrich, D.A. Liakin, J.G. De Villiers
Proc. of DIPAC2011; Hamburg, Germany; 16.–18.05.2011; pp. 419–421

58. **Performance of the Scintillation Profile Monitor in the COSY Synchrotron**
V. Kamerdzhiev, J. Dietrich, K. Reimers
Proc. of IPAC 2011; San Sebastian, Spain; 05.–09.09.2011; pp. 1201–1202

59. **Performance and Perspectives of Hadron Storage Rings**
A. Lehrach
Proc. of Science series by SISSA Trieste, PoS (STORI11); **066** (2011)

60. **The polarized electron-nucleon collider project ENC at GSI/FAIR**
A. Lehrach *et al.*
J. Phys. Conf. Ser. **295**, 012156 (2011)

61. **Status and future plans of polarized beams at COSY**
B. Lorentz *et al.*
J. Phys. Conf. Ser. **295**, 02146 (2011)

62. **The High-Energy Storage Ring (HESR)**
R. Maier for the HESR Consortium
Proc. of 2011 Particle Accelerator Conference; New York, NY, USA; 28.03.–01.04.2011

63. **Closed Orbit Correction in 2MeV Electron Cooler section at COSY**
L. Mao *et al.*
Proc. of The Intern. Workshop on Beam Cooling & Related Topics; Alushta, Ukraine; 12.–16.09.2011; pp. 92–94

64. **Beam Cooling at HESR in the FAIR Project**
D. Prasuhn, J. Dietrich, R. Maier, R. Stassen, H. Stockhorst
Proc. of The Intern. Workshop on Beam Cooling & Related Topics; Alushta, Ukraine; 12.–16.09.2011

65. **The Spin Aberration of Polarized Beam in Electrostatic Rings**
Yu. Senichev, A. Lehrach, R. Maier, D. Zyuzin
Proc. of IPAC 2011; San Sebastian, Spain; 05.–09.09.2011

66. **The Stochastic Cooling System of HESR**
R.Stassen *et al.*
Proc. of The Intern. Workshop on Beam Cooling & Related Topics; Alushta, Ukraine; 12.–16.09.2011

67. **Status of stochastic cooling predictions at the HESR**
H. Stockhorst, R. Maier, D. Prasuhn and R. Stassen, T. Katayama
Proc. of IPAC2011; San Sebastian, Spain; 04.–09.09.2011

68. **Konzept einer gasgekühlten beschleunigergetriebenen Transmutationsanlage**
B. Thomauske *et al.*
Synthese Report, Aachen, März 2011, Aachen Nuclear Safety Reports (ANSR) Volume 1.; 978-3-941277-11-3

69. **Electron Beam Diagnostics in Electron Cooling Devices**
T. Weibach, K. Aulenbacher, J. Dietrich
Proc. of DIPAC2011; Hamburg, Germany; 16.–18.05.2011; pp. 158–160

70. **Optical Electron Beam Diagnostics for Relativistic Electron Cooling Devices**
T. Weibach, K. Aulenbacher, J. Dietrich
Proc. of The Intern. Workshop on Beam Cooling & Related Topics; Alushta, Ukraine; 12.–16.09.2011; pp. 121–124

C Talks and Colloquia

1. M. Büscher
   High Intensity Lasers Meet Conventional Accelerators
   Physikalisches Kolloquium
   Univ. Düsseldorf, Germany, 13.01.2011

2. M. Büscher
   Status of the Target TDR
   Plenary talk at the PANDA collaboration meeting
   GSI Darmstadt, Germany, 17.03.2011

3. J. Dietrich
   Progress with the 2 MeV Electron Cooler for COSY-Jülich/HESR
   Invited talk at the HICforFAIR Workshop of the
   Institut für Angewandte Physik der J.W.Goethe-Universität Frankfurt/Main
   Riezlern, Austria, 06.03.2011

4. J. Dietrich
   Status 2 MeV Electron Cooler for COSY-Jülich/HESR
   31th HESR Consortium Meeting
   Mainz, Germany, 12.04.2011

5. J. Dietrich
   The new 2 MeV Electron Cooler for COSY-Jülich/HESR
   39th COSY-PAC Meeting
   Jülich, Germany, 09.05.2011

6. J. Dietrich
   The new 2 MeV Electron Cooler for COSY-Jülich/HESR
   Seminar talk
   BINP Novosibirsk, Russia, 27.05.2011

7. J. Dietrich
   The new 2 MeV Electron Cooler for COSY-Jülich/HESR
   Seminar talk
   JINR Dubna, Russia, 10.06.2011

8. J. Dietrich
   Status of the 2 MeV Electron Cooler for COSY/HESR
   Invited talk at COOL11
   Alushta, Ukraine, 12.09.2011

9. J. Dietrich
   Der 2 MeV Elektronkühler für COSY
   MAMI-Seminar, Institut für Kernphysik, Universität Mainz
   Mainz, Germany, 15.12.2011

10. R. Engels
    Modern Targets for Particle Physics and Beyond
    Seminar
    Kurchatov Institute, Moscow, Russia, 24.05.2011

11. R. Engels
    Modern Targets for Particle Physics and Beyond
    Seminar
    Budger Institute, Novosibirsk, Russia, 27.05.2011

12. R. Engels
    Extra Physics with an Atomic Beam Source and a Lamb-Shift Polarimeter
    XIV International Workshop on Polarized Sources, Targets and Polarimetry
    St. Petersburg, Russia, 14.09.2011

13. A. Gillitzer
Antiproton-nucleus collisions with PANDA
International Workshop on “In-Medium Effects in Hadronic and Partonic Systems”
Obergurgl, Austria, 21.–25.02.2011

14. A. Gillitzer
Antiproton-Nucleus Collisions at PANDA
ECT* Workshop on “Short Range Correlations in Nuclei and Hard QCD Phenomena”
Trento, Italy, 14.–18.11.2011

15. A. Gillitzer
Baryon Spectroscopy with PANDA
ECT* Workshop on “Amplitude Analysis in Hadron Spectroscopy”
Trento, Italy, 14.–28.01.2011

16. A. Gillitzer
Status of COSY-TOF and the ppK-study
LEANNIS Meeting
Heidelberg, Germany, 01.07.2011

17. A. Gillitzer
Strong Interaction Physics with PANDA: Selected Topics
Swedish FAIR (SFAIR) Meeting
Lund, Sweden, 09.–10.11.2011

18. D. Gotta
Pionic Hydrogen and Deuterium
International Conference on Exotic Atoms (EXA11)
Vienna, Austria, 05.–09.09.2011

19. D. Grzonka
An alternative for polarized antiproton beams
10th International Conference on Low Energy Antiproton Physics (LEAP 2011)
Vancouver, Canada, 27.04.–03.05.2011

20. D. Grzonka
Physics with Antimatter at FLAIR and AD/CERN
Seminar talk, Jagiellonian University
Cracow, Poland, 13.12.2011

21. D. Grzonka
Status of Meson Physics at COSY
PrimeNet Meeting
Uppsala, Sweden, 05.12.2011

22. J. Haidenbauer
Baryon-baryon interactions with strangeness in effective field theory
Seminar at Institut für Theoretische Physik II
Ruhr-Universität Bochum, Germany, 13.01.2011

23. J. Haidenbauer
Hyperon-nucleon and hyperon-hyperon interactions in chiral effective field theory
474. WE-Heraeus-Seminar — Strong Interactions: From Methods to Structures
Bad Honnef, Germany, 12.–16.02.2011

24. J. Haidenbauer
Charm production in antiproton-proton collisions
17th CBM Collaboration Meeting and Symposium on Charm, Dileptons and Deconfinement
Dresden, Germany, 04.–08.04.2011

25. J. Haidenbauer
The antinucleon-nucleon interaction: From LEAR to FAIR
Seminar at Institut für Theoretische Physik I
Universität Gießen, Germany, 07.07.2011

26. J. Haidenbauer
Hyperon-nucleon and hyperon-hyperon interactions in chiral effective field theory
The Fifth Asia-Pacific Conference on Few-Body Problems in Physics 2011 (APFB11)
Seoul, South Korea, 22.–26.08.2011

27. J. Haidenbauer
YN and YY meson-exchange models
ECT* Workshop Strange Hadronic Matter
Trento, Italy, 26.–30.09.2011

28. C. Hanhart
Extracting Weak Phases from Dalitz Plots and CP Studies
Workshop on Amplitude Analysis in Hadron Spectroscopy
Trento, Italy, 24.–28.01.2011

29. C. Hanhart
How to identify hadronic molecules
Workshop on Strong interactions: From methods to structures
Bad Honnef, Germany, 12.–16.02.2011

30. C. Hanhart
Perspectives in Hadron Physics
Theoretische Teilchenphysik und Kosmologie
Aachen, Germany, 14.04.2011

31. C. Hanhart
Theoretical issues in Dalitz plot analysis
Workshop Physics at LHCb Bad Honnef, Germany, 26.–29.04.2011

32. C. Hanhart
Perspectives in Hadron Physics
Seminar at Institut für Teilchenphysik
Siegen, Germany, 30.05.2011

33. C. Hanhart
Electric dipole moments for light nuclei in EFT
485. WE-Heraeus-Seminar — Search for Electric Dipole Moments (EDMs) at Storage Rings
Bad Honnef, Germany, 03.–05.07.2011

34. C. Hanhart
Light quark effects on charmonium properties
KVI Groningen, The Netherlands, 04.10.2011

35. M. Hartmann
Kaon pair production in pp, pd, dd and pA collisions at COSY
XLIX International Winter Meeting on Nuclear Physics BORMIO2011
Bormio, Italy, 24.–28.01.2011

36. M. Hartmann
Kaon pair production in pp, pd, dd and pA collisions at COSY
XLII. Arbeitstreffen Kernphysik
Schleching, Germany, 24.02.–03.03.2011

37. M. Hartmann
Measurement of the in-medium ϕ-meson width in proton-nucleus collisions
17th CBM Collaboration Meeting and Symposium on Charm, Dileptons and Deconfinement
Dresden, Germany, 04.–08.04.2011

38. M. Hartmann
Momentum dependence of hadronic production of the ϕ-meson and its width in nuclear matter
International Conference on Exotic Atoms and Related Topics
Vienna, Austria, 05.–09.09.2011

39. A. Holler
Particle Acceleration in Laser-Induced Relativistic Plasmas — A Novel Approach for Polarized Sources?
XIV International Workshop on Polarized Sources, Targets and Polarimetry
St. Petersburg, Russia, 12.–16.09.2011

40. A. Kacharava
Internal Experiments at COSY-Jülich
STORI 2011 — 8th International Conference on Nuclear Physics at Storage Rings
Frascati, Italy, 09.–14.10.2011

41. S. Krewald
Effective Field Theory Approach to Nuclear Matter
International School of Nuclear Physics in Erice, 33rd Course From Quarks and Gluons to Hadrons and Nuclei
Erice, Italy, 16.–24.09.2011

42. S. Krewald
Overview: Phenomenological approaches to $N^\star$ extraction
The 8th International Workshop on the Physics of Excited Nucleons(NSTAR 2011)
Newport News, USA, 13.–20.05.2011

43. S. Krewald
Recent Developments in the Jülich model
Sixth International Workshop on Pion-Nucleon Partial-Wave Analysis and the Interpretation of Baryon Resonances
George Washington University, USA, 23.–27.05.2011

44. S. Krewald
Theory of Baryon Resonances
28th Students' Workshop on Electromagnetic Interactions
Bosen(Saar), Germany, 04.–09.09.2011

45. A. Lehrach
EDM Storage Ring at Jülich
Search for Electric Dipole Moments (EDMs) at Storage Rings
485. WE-Heraeus-Seminar — Search for Electric Dipole Moments (EDMs) at Storage Rings
Bad Honnef, Germany, 04.–06.07.2011

46. A. Lehrach
Performance and Perspectives of Hadron Storage Rings
STORI 2011 — 8th International Conference on Nuclear Physics at Storage Rings
Frascati, Italy, 09.–14.10.2011

47. U.-G. Meißner
Ab initio calculation of the Hoyle state
Workhop on Nuclear Many-Body Open Quantum Systems: Continuum and correlations in light nuclei
Trento, Italy, 06.–10.06.2011

48. U.-G. Meißner
Theory of the nucleon EDM — new insights
485. WE-Heraeus-Seminar — Search for Electric Dipole Moments (EDMs) at Storage Rings
Bad Honnef, Germany, 04.–06.07.2011

49. U.-G. Meißner
Theory of Nuclear Forces
Lectures at the course Temas actuales en Fisica nuclear
Universidad Internacional del Mar, Aguiles, Spain, 07.2011

50. U.-G. Meißner
Two-photon corrections from dispersion relations
Workshop on Radiative Corrections
MIT, Cambridge, USA, 30.07.2011

51. U.-G. Meißner
Ab initio calculation of the Hoyle state
Rutherford Centennial Conference on Nuclear Physics
Manchester, United Kingdom, 08.–12.08.2011

52. U.-G. Meißner
Theory of kaonic deuterium in view of SIDDHARTA
International Conference on Exotic Atoms and Related Topics (EXA2011)
Austrian Academy of Sciences, Vienna, Austria, 05.–09.09.2011

53. U.-G. Meißner
Das Anthrophische prinzip – oder – Physik mit dem Supercomputer
Workshop on "Normativität und Ethik"
Universität Bonn, Germany, 10.2011

54. U.-G. Meißner
Theorie: Herausforderung & Perspektiven
KHuK Jahrestagung 2011
Bad Honnef, Germany, 08.–09.12.2011

55. M. Mertens
Measuring the Width of the $D^{\star}_{s0}(2317)$ with the PANDA Detector
XLII. Arbeitstreffen Kernphysik
Schleching, Germany, 24.02.–03.03.2011

56. M. Mertens
An efficient threshold and noise extraction algorithm suitable for FPGAs
DPG spring meeting
Münster, Germany 21.–25.03.2011

57. M. Mertens
Determination of the $D^{\star}_{s0}(2317)$ width with the PANDA Detector
International Conference on Exotic Atoms (EXA11)
Vienna, Austria, 05.–09.09.2011

58. N. Nikolaev
Precursor Experiments to Search for Permanent Electric Dipole Moments (EDMs) of Protons and Deuterons at COSY
Advanced XIV Workshop on High Energy Spin Physics
Dubna, Russia, 20.–24.09.2011

59. A. Nogga
Subleading chiral few-nucleon forces
Workshop on "Perspectives of the Ab Initio No-Core Shell Mode"
TRIUMF, Vancouver, Canada, 10.02.2011

60. A. Nogga
No-core shell model calculations from chiral-eft-based interactions
FUSTIPEN Topical Meeting on Effective field theories for nuclear structure studies
Caen, France, 03.03.2011

61. A. Nogga
Basics of group theory for quantum systems
Lecture at the Lecture series of the Espace de Structure NuclÃ©aire Theorique
Saclay, France, 12.09.2011

62. W. Oelert
AD performance and its extension towards ELENA
10th International Conference on Low Energy Antiproton Physics (LEAP 2011)
Vancouver, Canada, 27.04.–01.05.2011

63. W. Oelert
Prospects for antiproton physics, my perspective
10th International Conference on Low Energy Antiproton Physics (LEAP 2011)
Vancouver, Canada, 27.04.–01.05.2011

64. W. Oelert
Antimaterie — die geheimnisvolle Materie aus Antiteilchen - I
Theresien-Gymnasium Ansbach
Ansbach, Germany, 14.07.2011

65. W. Oelert
Antimaterie - die geheimnisvolle Materie aus Antiteilchen - II
Theresien-Gymnasium Ansbach
Ansbach, Germany, 15.07.2011

66. W. Oelert
ELENA — An Upgrade to the Antiproton Decelerator at CERN
FLAIR Meeting
Liverpool, Great Britain, 21.–22.02.2011

67. W. Oelert
ELENA — 100 keV Antiprotonen am CERN/AD
DPG spring meeting
Münster, Germany, 20.–25.03.2011

68. W. Oelert
From hot to cold anti-hydrogen
Workshop on Cold Antimatter and High Precision Physics (Pbar-11)
Matsue, Japan, 28.–30.11.2011

69. W. Oelert
On our way to Anti-hydrogen at Rest
Workshop on Anti-matter and Gravitation
Paris, France, 10.–11.10.2011

70. A. Polyanskiy
Measurement of the in-medium ϕ-meson width in proton-nucleus collisions
XIV International Conference on Hadron Spectroscopy
Munich, Germany, 13.–17.06.2011

71. A. Polyanskiy
ϕ-meson production on nuclei and in-medium ϕ-meson width
STORI 2011 — 8th International Conference on Nuclear Physics at Storage Rings
Frascati, Italy, 09.–14.10.2011

72. J. Ritman
Cracow-Jülich Cooperation
Foundation for Polish Science review of the international PhD program in applied nuclear physics and innovative technologies
Cracow, Poland, 29.11.2011

73. J. Ritman
Presentation of the MESON conference series
IUPAP C-12 Commission meeting
MIT, Boston, USA, 25.07.2011

74. J. Ritman
Status of PANDA
8th International Workshop on Heavy Quarkonium 2011
GSI Darmstadt, Germany, 05.10.2011

75. S. Schadmand
Asking mother nature questions about hadron physics
Seminar, IIT Indore
Indore, India, 08.11.2011

76. S. Schadmand
Hadron Physics via Meson Decays
5th DAE-BRNS Workshop on Hadron Physics
BARC Mumbai, India, 31.10.–04.11.2011

77. S. Schadmand
ω conversion decays with WASA-at-COSY
Meeting on Conversion Decays of Baryon Resonances
Warsaw, Poland, 10.–11.04.2011

78. S. Schadmand
PANDA at FAIR
Symposium on India-PANDA program
BARC Mumbai, India, 02.11.2011

79. S. Schadmand
Produktion und Zerfälle von Mesonen in hadronischen Reaktionen
Seminar, II. Physikalisches Institut
Univ. Gießen, Germany 14.04.2011

80. S. Schadmand
The Facility for Antiproton and Ion Research
The 4th Workshop of the APS Topical Group on Hadronic Physics (GHP2011)
Anaheim, CA, USA, 27.–29.04.2011

81. S. Schadmand
WASA Detector at COSY
Meeting on Conversion Decays of Baryon Resonances
Warsaw, Poland, 10.–11.04.2011

82. S. Schadmand
What are decaying mesons trying to tell us?
Seminar Florida State University, Tallahassee
Tallahassee, USA, 03.05.2011

83. O. Schult
Wie wollen wir leben? — Gedanken eines Physikers
24. Todestag von Joseph Kardinal Höffner im Diözesanrat der Katholiken im Erzbistum Köln
Maternushaus, Köln, Germany, 16.10.2011

84. R. Stassen
The new HESR RF-System
Physik und Technik von Beschleunigern
TU Darmstadt, Germany, 11.07.2011

85. H. Ströher
Plans at COSY
EDM Meeting Brookhaven National Laboratory
Upton, New York, USA, 14.–15.03.2011

86. H. Ströher
News from COSY
NSTAR 2011 — The 8th International Workshop on the Physics of Excited Nucleons
Newport News, Virginia, USA, 17.–20.05.2011

87. H. Ströher
Experimental Summary
485. WE-Heraeus-Seminar — Search for Electric Dipole Moments (EDMs) at Storage Rings
Bad Honnef, Germany, 04.–06.07.2011

88. H. Ströher
The road towards Polarized Antiprotons
STORI 2011 — 8th International Conference on Nuclear Physics at Storage Rings
Frascati, Italy, 09.–14.10.2011

89. H. Ströher
Frontiers of Science
Seminar at Tbilisi State University
Tbilisi, Georgia, 05.–09.12.2011

90. P. Wintz
Status of STT Hardware Developments
Workshop: Special Technical Board
GSI Darmstadt, Germany, 01.–02.02.2011

91. P. Wintz
Status of the hardware developments and achievements for the STT
XXXVI. PANDA Collaboration Meeting
GSI Darmstadt, Germany, 14.–18.03.2011

92. P. Wintz
STT Hardware Status
Workshop: 2nd PANDA Central Tracker Review Meeting
GSI Darmstadt, Germany, 21.–22.06.2011

93. P. Wintz
STT Prototype Results
Workshop: 2nd PANDA Central Tracker Review Meeting
GSI Darmstadt, Germany, 21.–22.06.2011

94. P. Wintz
STT Reconstruction Without T_0 Knowledge
Workshop: 3rd PANDA Central Tracker Review Meeting via EVO
GSI Darmstadt, Germany, 09.08.2011

95. P. Wintz
The Tracking System In The PANDA Apparatus
13th ICATPP Conference on Advanced Technology and Particle Physics
Como, Italy, 03.–07.10.2011

96. A. Wirzba
Introductory talk: Rare eta decays and tests of fundamental symmetries
PrimeNet Workshop
Jülich, Germany, 26.–28.09.2011

97. A. Wirzba
Rare eta meson decays and tests of fundamental symmetries
Ruhr-Universität Bochum, Germany, 30.06.2011

98. A. Wirzba
Theory summary
485. WE-Heraeus-Seminar — Search for Electric Dipole Moments (EDMs) at Storage Rings
Bad Honnef, Germany, 04.–06.07.2011

D Diploma and Ph.D. Theses

1. Bachelor, Master, Diploma

1. S. Henssler,
   Programmierung eines Eingabeassistenten für das Softwaresystem PANDA-Root,
   Bachelorarbeit, FH Aachen, Campus Jülich

2. N. Hohn,
   Messung und Anpassung der Abkühlkurve des Fokaldetektors für das Kristallspektrometer am IKP/FZJ,
   Bachelorarbeit, RWTH Aachen

3. R. Mitter,
   Optimierung und Automatisierung eines Pellet-Tracking-Systems,
   Bachelorarbeit, FH Aachen

4. A. Seyen,
   Interferometrische Vermessung des Dichteprofils zweier Gasdüsen für die Injektion eines Gasjets in eine Vakuumkammer,
   Bachelorarbeit, FH Koblenz, Rhein-Ahr-Campus Remagen

5. M. Zurek,
   Determination of the neutron detection efficiency in the WASA-at-COSY detector setup,
   Bachelorarbeit, Jagiellonian University Cracow, Poland

6. D. Pohl
   Silizium-Pixel-Auslesechips fÃ¼r den PANDA Mikro Vertex Detektor 2011,
   Masterarbeit, Ruhr-Universität Bochum

7. T. Bednarski,
   Feasibility study of measuring CP symmetry violation via $\eta \to 4\pi$ decay using WASA-at-COSY detector,
   Diplomarbeit, Jagiellonian University Cracow, Poland

8. I. Engin,
   Preparations for the polarization measurement of ^{3}He ions from laser-induced plasmas,
   Diplomarbeit, RWTH Aachen

9. M. Jabua,
   Readout upgrade for the focal plane detector of the Jülich Bragg spectrometer,
   Diplomarbeit, Georgian Technical University — Faculty of Informatics and Control Systems

10. A. Lasar,
    Optimierung und Kalibrierung eines Spin-Filters für das BOB-Experiment,
    Diplomarbeit, FH Aachen, Campus Jülich

11. S. Schlemmer,
    Optimierung der Quenchkammer eines Lambshift-Polarimeters durch ein Spiegelsystem zum Einfang der induzierten Ly-a Photonen,
    Diplomarbeit, FH Gelsenkirchen

12. F. Stollenwerg,
    Model-independent approach to $\eta \to \pi^+\pi^-\gamma$ and $\eta' \to \pi^+\pi^-\gamma$,
    Diplomarbeit, Universität Bonn

2. Ph.D.

13. H. Bhatt
Study of a rare decay $\eta \to e^+e^-\gamma$ using WASA-at-COSY,
IIT Bombay, India

14. C. Böhme
Untersuchung zur Profilmessung von Hadronenstrahlen mittels Restgasfluoreszenz und -ionisation,
TU Dortmund

15. E. Borodina
Online system for data monitoring, visualisation and control at the COSY-TOF experiment,
Moscow State Institute of Electronics and Mathematics, Russia

16. B.-R. Jany,
Leading modes of the $3\pi^0$ production in proton-proton collisions at incident proton momentum 3.35 GeV/c,
Jagiellonian University, Cracow, Poland

17. W. Krzemien
Search of the eta-mesic ^{4}He with the WASA-at-COSY detector,
Jagiellonian University, Cracow, Poland

18. P. Podkopal
Investigations of the reaction $dd \to {}^3He n\pi^0$ at 350 MeV beam energy with WASA-at-COSY,
Jagiellonian University, Cracow, Poland

19. A. Pricking
Double pionic fusion to ^{4}He — Kinematically complete measurements over the energy region of the ABC effect,
Universität Tübingen

20. N. Raab
Development of a method to measure the polarization of laser-accelerated protons,
Universität zu Köln

21. T.H. Randriamalala
Conceptual Design of the PANDA Luminosity Monitor and Reconstruction Strategy to Measure the Width of the X(3872) State,
Ruhr-Universität Bochum

22. M. Röder
Final state interactions and polarization observables in the reaction $\vec{p}p \to pK^+\Lambda$ close to threshold,
Ruhr-Universität Bochum

23. A. Winnemöller
Analyse des verbotenen η-Meson Zerfalls $\eta \to \pi^0e^+e^-$ am Experimentaufbau WASA-at-COSY,
Universität Münster

24. L. Yurev
Study of the decay $\eta \to e^+e^-e^+e^-$ with WASA-at-COSY,
Universität zu Köln

E Awards & Offers for Professorships

C. Hanhart: Member of the Particle Data Group

S. Krewald: Editorial Board of Physical Review C for the period 2011 – 2013

F Funded Projects

Project	Responsible	Partner Institute	Funded by
Virtual Institute Spin and Strong QCD	U.-G. Meißner	GSI, Univ.'s Bern, Bonn, Ferrara, Cracow, Torino	HGF
Development of a high energy electron cooler	J. Dietrich	TU Dortmund; BINP Novosibirsk, JINR Dubna (Russia)	HGF
Förderung Nachwuchs-Austausch China	J. Dietrich		HGF/CSC
CARE BENE Network	R. Tölle		
DIRAC Phase 1	R. Tölle		EU/FP6
Project FAIR	R. Toelle	GSI	EU/FP7
HESR — Magnet Dipole	R. Toelle		
IFMIF-EVEDA project - Work program	R. Toelle		CEA
HadronPhysics 2	D. Grzonka		EU/FP7
POLPBAR ERC Advanced Grant	H. Ströher		EU/FP7
Scalar Mesons	M. Büscher	ITEP, INR Moscow (Russia)	DFG
Pellet Target	M. Büscher	ITEP, MPEI Moscow (Russia)	DFG
Laser applications of a pellet target	M. Büscher	ITEP, MPEI Moscow (Russia), Univ. Düsseldorf	DFG
Systematic study of higher charmonia	C. Hanhart	ITEP Moscow (Russia)	DFG
Polarized Nuclear Fusion	R. Engels	PNPI Gatchina (Russia)	DFG
Molecular polarized target	R. Engels	PNPI Gatchina (Russia)	DFG
Studies of pion production	A. Kacharava	JINR Dubna (Russia)	DFG
PAX/COSY	F. Rathmann		DFG
Response function of short-lived isotopes	S. Krewald		DFG
Broken Symmetries	H. Machner	Univ. Helsinki (Finland)	DAAD
Extra Dimensions in Flavor Physics	U.-G. Meißner		DAAD
Bilat. Zusammenarbeit mit Georgien	A. Kacharava		BMBF/WTZ
Deexcitation mechanisms and reaction kinetics in exotic atoms	D. Gotta		BMBF/WTZ
Polarisationseffekte in der $\bar{p}d$ Streuung	J. Haidenbauer		BMBF/WTZ
Modeling of Polarized Beam Dynamics	A. Lehrach		BMBF/WTZ
Baryon Resonance Analysis	U.-G. Meißner	JLAB (U.S.A.)	JLAB
QCD dynamics in vector meson diffractive production	N. Nikolaev	JINR Dubna (Russia)	Heisenberg-Landau Grant

G JCHP-FFE Projects

Project	Institute	Responsible
PD Dr. A. Khoukaz	Westfälische Wilhelms-Universität Münster	Mesonenproduktion in Nukleon-Nukleon- und Nukleon-Kern-Stößen an COSY
Prof. Dr. K. Nakayama	University of Georgia	Unified analysis of meson production in hadron- and photon-induced reactions in the resonance engergy region
Prof. Dr. A. Vasilyev	PNPI Gatchina	Development, commissioning and operation of components for the COSY Experiments WASA and ANKE and spin-filtering studies at COSY as preparation for the PAX experiment in the framework of the FAIR project at GSI
Prof. Dr. V. Koptev	PNPI Gatchina	Silicon Tracking Telescope for ANKE
Prof. Dr. H. Freiesleben	TU Dresden	COSY-TOF detector
Prof. Dr. B. Kämpfer	Forschungszentrum Dresden-Rossendorf	Silicon Tracking Telescopes for ANKE and PAX
Prof. Dr. M. Nioradze	Tbilisi State University	np systemstudy with pol. beams and pol. Targets at ANKE, and Maintenance and development of the tracking detectors for WASA(ANKE) and analysis of data from double pol. Experiments
Prof. Dr. U. Thoma	HISKP Universität Bonn	Partialwellenanalyse von Daten aus proton-induzierten Reaktionen
Prof. Dr. H. Clement	Universität Tübingen	Experimente an COSY-TOF
Prof. V. Afanasyev	Moscow State University	Development of online software tools for COSY-TOF
Prof. Dr. O. Willi	Universität Düsseldorf	Measurements of the degree of polarization of laser accelerated protons
Prof. Dr. Y. Kiselev	ITEP Moscow	Phi meson production in pN and pA Reactions
Dr. A. Schäfer	Universität Regensburg	Baryon-Resonanzen, g_A und die effektive Restaurierung der chiralen Symmetrie
PD Dr. A. Rusetsky	HISKP Universität Bonn	Inelastic baryon resonances from lattice QCD
Prof. Dr. P. Moskal	Jagellonian University Krakow	Investigations of the CP symmetry with WASA at COSY
Prof. Dr. B. Kamys	Jagellonian University Krakow	Strangeness Production with WASA-at-COSY
PD M. Jezabek	Polish Academy of Sciences	Development of the PID method based on the dE/dx measurement for the Straw Tube Tracker
Dr. H. Calen	Uppsala University	A pellet tracking system for PANDA and for WASA
Prof. D. U. Wiedner	Ruhr-Universität Bochum	Entwicklung eines innovativen, kompakten Monitorsystems für einen elektromagnetischen Kristallkalorimeter und Ent-wicklung von Software-Werk-zeugen zur Teilchenidenti-fikation mit elektromagne-tischen Kristallkalorimetern

Prof. Dr. T. Weis	TU Dortmund	Development of a Fast Orbit Feedback System for the HESR and Beam Tests at COSY
Prof. Dr. U. Wiedner	Ruhr-Universität Bochum	Measurement of $\eta \to \pi^+\pi^-e^+e^-$ with WASA-at-COSY
Prof. Dr. P. Moskal	Jagellonian University Krakow	Dalitz Decays of Mesons with WASA-at-COSY
Prof. H. Gao	Duke University, USA	Investigation of φ-proton correlation and Bound State from Productions from Proton-Proton and Proton-Nucleus Reaction
Prof. Dr. P. Moskal	Jagellonian University Krakow	η meson production with polarized proton beam
Prof. A. Roy	Indian Institute of Technology Indore, India	Radiative Decays of the omega Meson with WASA-at-COSY
Prof. Dr. A. Magiera	Jagellonian University Krakow	Investigations of Charge Symmetry Breaking in the $dd \to {}^4He^0$
Prof. Dr. E. Steffens	Universität Erlangen-Nürnberg	Spin-Experiment an ANKE
Prof. Dr. H. Clement	Universität Tübingen	Installation and Commissioning of a DIRC at the WASA Detector as well as experiments with WASA-at-COSY
Prof. Dr. W. Eyrich	Universität Erlangen-Nürnberg	Vorbereitung und Durchführung von Experimenten an COSY-TOF und WASA
Prof. A. Gerasimov	ITEP Moscow	Development of a Frozen-Pellet Target
Prof. Dr. W. Kühn	Universität Giessen	FPGA-Based Trigger System for WASA
Prof. Dr. M. Düren	Justus-Liebig-Universität Gießen	Development of a DIRC Cherenkov detector for WASA
Dr. P. Lenisa	Università degli Studi di Ferrara	Spin-filtering studies in storage rings
Prof. Dr. A. Kulikov	JINR Dubna	Experiments with ANKE, WASA and PAX and FAIR
Prof. Dr. A. Kulikov	JINR Dubna	Particle identification with straw detectors
Prof. Dr. K. Brinkmann	HISKP Universität Bonn	Prototyping for PANDA at COSY

H Conferences (co-)organized by the IKP

H.1 485. WE-Heraeus Seminar "Search for Electric Dipole Moments (EDMs) at Storage Rings"

Between July 3 and 6, 2011, a Seminar, entitled "Search for Electric Dipole Moments (EDMs) at Storage Rings", which was sponsored by the Wilhelm und Else Heraeus Foundation and organized by H. Ströher and F. Rathmann, was held at Physikzentrum in Bad Honnef. Particle EDMs are a fascinating research project, because a non-vanishing EDM would point to physics beyond the standard model of particle physics and possibly lead to an understanding of the matter-antimatter asymmetry in our universe. Up to now, no finite EDMs have been found, and only extremely small upper limits ($d < 10^{-27}$ e cm) have been deduced.

In 30 plenary talks and a round table discussion, the scientific and technological aspects of EDM searches have been covered, putting special emphasis on the new idea to use charged polarized particles (p, d, ^{3}He) in storage rings. Such a project, called JEDI (Jülich Electric Dipole Moment Investigations), is pursued at IKP in three stages: (i) preparatory test measurements at the conventional storage ring COSY, (ii) a first direct determination of pEDM and dEDM in a precursor experiment with COSY, and (iii) a dedicated EDM storage ring for an ultimate precision measurement, aiming at a sensitivity of 10^{-29} e cm or better.

Fig. 70: Participants of the 485. WE-Heraeus Seminar in front of the Physikzentrum.

Attracting 89 participants from all over the world, the Physikzentrum was close to its limit of capacity. A follow-up workshop is planned for 2012 at ECT* (Trento, Italy).

H.2 Workshop on Amplitude Analysis in Hadron Spectroscopy

From Januray 24th to 28th a theory workshop on Amplitude Analyses took place at the ETC* in Trento organized by A. Szczepaniak (Indiana University), C. Hanhart (IKP), M. Pennington (Jefferson Laboratory), E. Santopinto (INFN, Genova) and U. Wiedner (Ruhr University Bochum). The near 50 international particiants had intense discussions on various issues in amplitude analysis. Main points of discussion were:

1. On the theoretical side the focus is on the construction of amplitudes, which can be used with as little model dependence as possible, to be used to study multi-hadron final states. This rests on the development of analytical parameterizations constrained by model-independent features such as unitarity, crossing symmetry, and where appropriate, gauge invariance, and chiral symmetry.

2. Standards need to be identified and methods developed to quantify the theoretical uncertainties encoded in such amplitudes. A discussion in this direction should be initiated at a future workshop.

3. A key to making the theoretical and phenomenological efforts directly applicable to experiment is to develop a common interface with easy access and utility. This includes the use of a common language to avoid misunderstandings in the interpretation of data. It is therefore essential to discuss how to implement the amplitudes (mentioned in point 1) within data analysis software packages, and how to disseminate the results interactively.

4. Finally the resonance parameters need to be compared with predictions of QCD and the feasibility of accurate non-perturbative QCD studies in the resonance region has to be evaluated.

The discussion made clear that there is a desire that the availability of data needs to be improved. However, the appropriate compromise between "open access" and the current situation is still to be found.
Talks are available online under http://www.ectstar.eu/.

H.3 School on Amplitude Analysis in Modern Physics from hadron spectroscopy to CP phases

From August 1st to 5th, 2011 a school on amplitude analysis was held at the Physikzentrum Bad Honnef, Germany. It was organized by an international team including S. Schadmand and C. Hanhart from the IKP. The aim

of the school was to bring together graduate students and more senior scientists interested in amplitude analyses — the announcement found very good resonance in the community and we could welcome more than 70 participants. The tools and techniques required for the interpretation of modern precision data, both from future hadron spectroscopy experiments, and from searches for CP violation in heavy meson decays were discussed. The methods provided will be of great importance to fully exploit the rich data samples already available at BaBar, Belle, BES-II/III, COMPASS, CLEO, KLOE and WASA as well as those expected from Belle2, GlueX, LHCb, PANDA and SuperB. The agenda included lecture courses on the topics of dispersion theory (by J.R. Pelaez, Madrid), CP violation in the Standard Model (Th. Mannel, Siegen), phenomenological tools (T. Gershon, Warwick), and precision experiments/data analysis (K. Peters, Darmstadt). A second school of the same kind will be organized in 2012 in the US by the Thomas Jefferson Laboratory.

Fig. 71: Participants of the School on Amplitude Analysis in front of the Physikzentrum.

The presentations are available via http://www2.fz-juelich.de/ikp/workshops/LesNabis/program.shtml.

H.4 Georgian-German Science Bridge

The cooperation between Georgian universities (Georgian Technical University (GTU) and Ivane Javakhishvili Tbilisi State University (TSU)) and Forschungszentrum Jülich (FZJ) has been further strengthened during a visit of an FZJ delegation (headed by Sebastian Schmidt, member of the FZJ board of management) to Tbilisi in December 2011. This was a follow-up meeting of the visit of TSU-rector Alexander Kvitashvili to FZJ and a discussion with the Board-of-Management Chairman Achim Bachem in April 2011.
During the Tbilisi-meeting a number of student and doctoral exchange programs between IKP and GTU/TSU as well as between Shota-Rustaveli National Science Foundation (SRNSF) and FZJ have been signed, which will become effective in 2012.

Fig. 72: During several meetings at FZJ and in Tbilisi the cooperation between FZJ and Georgian universities has been strengthened.

The kick-off event represents a further step towards the Georgian-German Science Bridge, initiated in 2010 by IKP with a Memorandum-of-Understanding between Georgian institutions and FZJ, which not only includes scientific personnel and equipment exchanges, but also common bi-annual workshops (http://www2.fz-juelich.de/ikp/cgswhp/).

I Teaching Positions

Institute	Name	University
IKP-1	PD Dr. A. Gillitzer	Bonn
	PD Dr. F. Goldenbaum	Wuppertal
	Prof. Dr. J. Ritman	Bochum
	PD Dr. S. Schadmand	Köln
	Dr. T. Stockmanns	Bochum
IKP-2	PD Dr. M. Büscher	Köln
	Prof. Dr. D. Gotta	Köln
	PD Dr. F. Rathmann	Erlangen-Nürnberg
	Prof. Dr. H. Ströher	Köln
IKP-3/IAS-4	Univ. Doz. Dr. J. Haidenbauer	Graz
	PD Dr. C. Hanhart	Bonn
	Prof. Dr. S. Krewald	Bonn
	Prof. Dr. U.-G. Meißner	Bonn
	Prof. Dr. N.N. Nikolaev	Moscow
	Dr. A. Nogga	Bonn
	PD Dr. A. Wirzba	Bonn
IKP-4	Prof. Dr. Dr. h.c. J. Dietrich	Dortmund
	PD Dr. A. Lehrach	Bonn
	Prof. Dr. R. Maier	Bonn

J Personnel

J.1 Scientific Staff

M. Azis Hessan (IKP-2) (until 31 October 2011)
Dr. V. Baru (IKP-3) (until 31 March 2011)
Dr. U. Bechstedt (IKP-4)
Dr. K. Bongardt (IKP-4)
DI N. Bongers (IKP-4)
DI R. Brings (IKP-4)
Y. Bsaisou (IKP-3)
PD Dr. M. Büscher (IKP-2)
M. Cleven (IKP-3)
F.U. Dahmen (IKP-4)
DP D. Deermann (IKP-1) (since 4 August 2011)
Prof. Dr.Dr.h.c. J. Dietrich (IKP-4)
DI N. Dolfus (IKP-TA)
R. Dzhygadlo (IKP-1) (until 31 December 2011)
Dr. R. Engels (IKP-2)
I. Engin (IKP-2) (until 31 August 2011)
S. Esch (IKP-1)
DI F.-J. Etzkorn (IKP-4)
Dr. O. Felden (IKP-TA)
M. Gaißer (IKP-2)
Dr. W. Gast (IKP-1)
Dr. R. Gebel (IKP-4)
PD Dr. A. Gillitzer (IKP-1)
PD Dr. F. Goldenbaum (IKP-1)
Prof. Dr. D. Gotta (IKP-2)
Dr. F. Grümmer (IAS-4)
Dr. D. Grzonka (IKP-1)
DI W. Günther (IKP-4)
Univ. Doz. Dr. J. Haidenbauer (IAS-4)
PD Dr. C. Hanhart (IAS-4)
Dr. M. Hartmann (IKP-2)
Dr. V. Hejny (IKP-2)
DI K. Henn (IKP-4)
DP A. Herten (IKP-1) (since 17 October 2011)
DP A. Holler (IKP-4) (since 1 March 2011)
Dr. V. Kamerdjiev (IKP-4)
Dr. A. Kacharava (IKP-2)
DP St. Kölling (IKP-3) (until 30 April 2011)
Prof. Dr. S. Krewald (IAS-4)
PD Dr. A. Lehrach (IKP-4)
DP D. Lersch (IKP-1) (since 1 March 2011)
DP S. Liebig (IKP-3)
Dr. B. Lorentz (IKP-4)
Prof. Dr. R. Maier (IKP-4)
Prof. Dr. U.-G. Meißner (IKP-3/IAS-4)
DP M. Mertens (IKP-1)
Dr. S. Merzliakov (IKP-2)
DP S. Mikirtychiants (IKP-2)
DP D. Minossi (IKP-3) (until 15 June 2011)
Prof. Dr. N.N. Nikolaev (IKP-3)
Dr. A. Nogga (IAS-4)
Prof. Dr. W. Oelert (IKP-1)
DP D. Oellers (IKP-2)
Dr. H. Ohm (IKP-2)
DI N. Paul (IKP-1)
Dr. D. Prasuhn (IKP-4)
DP N. Raab (IKP-4) (until 31 December 2011)
DP T. Randriamalala (IKP-1) (since 1 August 2011)
PD Dr. F. Rathmann (IKP-2)
DP M. Retzlaff (IKP-4)
DI A. Richert (IKP-4)
Prof. Dr. J. Ritman (IKP-1)
Dr. E. Roderburg (IKP-1)
DP M. Röder (IKP-1)
DI J. Sarkadi (IKP-TA)
PD Dr. S. Schadmand (IKP-1)
Dr. R. Schleichert (IKP-2)
DI G. Schug (IKP-4)
Dr. Th. Sefzick (IKP-TA)
Prof. Dr. Y. Senichev (IKP-4)
DI M. Simon (IKP-4)
Dr. R. Stassen (IKP-4)
Dr. H. Stockhorst (IKP-4)
Dr. T. Stockmanns (IKP-1)

Prof. Dr.Dr.h.c. H. Ströher (IKP-2)

DP T. Tolba (IKP-1) (until 31 July 2011)

Dr. R. Tölle (IKP-4)

DI T. Vashegyi (IKP-4)

DP Chr. Weidemann (IKP-2) (until 31 August 2011)

Dr. P. Wintz (IKP-1)

PD Dr. A. Wirzba (IAS-4)

DI J.-D. Witt (IKP-4)

DP P. Wurm (IKP-2)

Dr. H. Xu (IKP-1)

Dr. E. Zaplatin (IKP-4)

DP D. Zyuzin (IKP-4) (since 1 February 2011)

J.2 Technical and Administrative Staff

J. Artz (IKP-TA) (until 31 May 2011)

C. Berchem (IKP-TA)

M. Böhnke (IKP-4)

J. Borsch (IKP-TA) (until 31 December 2011)

P. Brittner (IKP-4)

J. But (IKP-TA)

W. Classen (IKP-4)

M. Comuth-Werner (IKP-TA)

B. Dahmen (IKP-4)

C. Deliege (IKP-4)

G. D'Orsaneo (IKP-2)

R. Dosdall (IKP-1)

J. Elis (IKP-2) (until 30 September 2011)

R. Enge (IKP-4) (until 31 March 2011)

P. Erben (IKP-2)

B. Erkes (IKP-4)

K. Esser (IKP-TA)

H.-W. Firmenich (IKP-TA)

J. Göbbels (IKP-TA)

V. Gupta (IKP-2) (since 18 April 2011)

H. Hadamek (IKP-TA) (until 28 February 2011)

R. Hecker (IKP-4)

S. Henssler (IKP-1) (until 31 August 2011)

E. Heßler (IKP-TA)

N. Hohn (IKP-2) (until 14 August 2011)

M. Holona (IKP-TA)

M. Jabua (IKP-2) (until 15 July 2011)

A. Kieven (IKP-4)

M. Kremer (IKP-TA)

G. Krol (IKP-4)

V. Kau (IKP-TA)

M. Küven (IKP-4)

S. Lambertz (IKP-4) (1 August 2011 until 31 December 2011)

K.-G. Langenberg (IKP-4)

A. Lasar (IKP-2) (until 31 August 2011)

L. Magallanes-Hernandez (IKP-4) (since 1 October 2011)

H. Metz-Nellen (IKP-TA)

S. Müller (IKP-TA)

R. Nellen (IKP-TA)

C. Oslender (IKP-TA)

D.-L. Pohl (IKP-1) (until 28 February 2011)

H. Pütz (IKP-4)

K. Reimers (IKP-4)

G. Roes (IKP-TA)

N. Rotert (IKP-4)

D. Ruhrig (IKP-4)

F. Scheiba (IKP-4)

H. Schiffer (IKP-TA)

S. Schlemmer (IKP-2) (until 12 August 2011)

J. Schmitz (IKP-4)

D. Schönfelder (IKP-2) (until 30 November 2011)

F. Schultheiß (IKP-TA)

A. Seyen (IKP-2) (until 16 September 2011)

H. Singer (IKP-4) (until 31 March 2011)

D. Spölgen (IKP-2)

G. Sterzenbach (IKP-1)

J. Strehl (IKP-TA)

J. Uehlemann (IKP-1)

H. Zens (IKP-4)

IKP-1 = Experimental Hadron Structure
IKP-2 = Experimental Hadron Dynamics
IKP-3 = Theoretical Nuclear Physics
IKP-4 = Large-Scale Nuclear Physics Equipment
IKP-TA = Technical Services and Administration
IAS-4 = Theory of the Strong Interactions

K Further Contributions

(articles available on-line: http://www2.fz-juelich.de/ikp/publications/AR2011/en/contents.shtml)

1. Experimental Hadron Physics

   1.1 Analysing powers for $dp \to pp_s\Delta^0$ reaction at $T_d = 1.6$, 1.8, and 2.27 GeV

   1.2 Mechanisms of the $^1S_0$ diproton formation for the $dp \to pp_s N\pi$ reaction in the Δ isobar region

   1.3 Axx measurements for the $pn \to pp_s\pi^-$ reaction at $T_d = 706$ MeV at ANKE

   1.4 Forward cross section energy dependence of the $pp \to pp_s\pi^0$ reaction at COSY energies

   1.5 Investigation of the ^{3}He+η final state in polarized dp-collisions at ANKE

   1.6 The η meson mass determination with ANKE at COSY

   1.7 Preliminary analysis of the $\eta \to \pi^+\pi^-\pi^0$ decay

   1.8 Study of the $\eta \to \pi^+\pi^-\pi^0$ decay in pp collisions with the WASA-at-COSY

   1.9 Analysis of the $pp \to pp\eta \to \pi^+\pi^-\pi^0$ reaction from 2008 data

   1.10 Studies of the $\eta \to e^+e^-\gamma$ decay in pd reactions measured with WASA-at-COSY

   1.11 Extraction of the $\eta \to \pi^+\pi^-e^+e^-$ Branching Ratio with WASA at COSY

   1.12 Background determination with ROOT-SNIP for $pp \to pp\eta$ reactions

   1.13 Measurement of the double Dalitz decay $\eta \to e^+e^-e^+e^-$ with WASA-at-COSY

   1.14 Study of the polarization degree for the $\vec{p}p \to pp\eta$ measurement with WASA

   1.15 Status of the search for $(^4$He-$\eta)_{bs}$ by means of the WASA-at-COSY facility

   1.16 Towards a Measurement of the $\omega - \pi$ Transition Form Factor

   1.17 The first studies of the K^+ production in pn interactions at ANKE

   1.18 Dalitz plot analysis to extract $N^\star$-resonances, cusp and FSI contributions to the $pp \to pK^+\Lambda$ reaction

   1.19 Neutron Detection with the COSY-TOF detector — studied with the reaction $pp \to pn\pi^+$ at $\varepsilon = 652$ MeV

   1.20 Analysis of the $pp \to nK^+\Sigma^+$ reaction from COSY-TOF data

   1.21 Σ Cusp in the $pp \to \Lambda pK^+$ Reaction

   1.22 Emission of Intermediate Mass Fragments from p+C Collisions at Proton Beam Energies 1.2 – 2.5 GeV

2. Developments for the Experimental Facilities

   2.1 Measurement of the nuclear polarization in H_2 and D_2 molecules after recombination of polarized hydrogen or deuterium atoms

   2.2 Polarized Internal Gas Target of ANKE at COSY: hardware upgrade status

   2.3 Time calibration of WASA-at-COSY Forward Detector

   2.4 A DIRC for WASA-at-COSY — extended prototype tests

   2.5 Development of a Pellet Tracking System for PANDA and WASA

   2.6 Measurement of pellet beam parameters at UPTS

3. Theoretical Physics (see Sect. B for links to published papers)

4. Accelerator Division

   4.1 Closed Orbit Correction in 2 MeV Electron Cooler Section at COSY

   4.2 Performance report of COSY Injector Cyclotron, Ion Sources and Polarimeter

   4.3 Magnets, Alignment and New Installations

   4.4 Radiation Protection

4.5 Status of the 2 MeV Electron Cooler for COSY/HESR

5. Preparations for FAIR

5.1 The HESR Injection System

5.2 Error Estimation for the Trapezoidal Sensors of the PANDA Micro Vertex Detector

5.3 Particle identification with straw tubes for the PANDA experiment

5.4 Determination of the resolution of a silicon strip tracking station

5.5 Analysis and Improvement of Early-Stage Track Reconstruction at the PANDA Micro Vertex Detector

5.6 An alternative approach to produce polarized antiproton beams

6. Technical Developments

6.1 Electronics Laboratory